NUREG/CR-4802
EGG-2486
January 1987

An Evaluation of TRAC-PF1/MOD1 Computer Code Performance During Posttest Simulations of Semiscale Mod-2C Feedwater Line Break Transients

Douglas G. Hall
John C. Watkins

F O R M A L R E P O R T

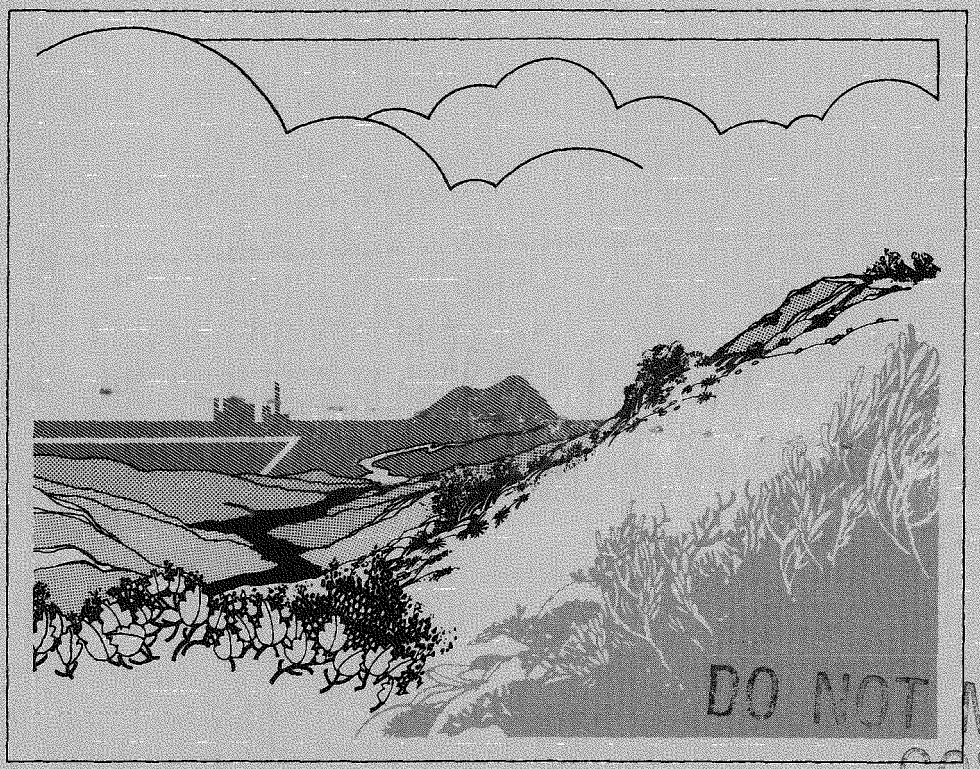

EG&G Idaho

Work performed under DOE Contract No. DE-AC07-76ID01570

for the ***U.S. Nuclear Regulatory Commission***

Idaho National Engineering Laboratory

Managed by the U.S. Department of Energy

Available from

Superintendent of Documents
U.S. Government Printing Office
Post Office Box 37082
Washington, D.C. 20013-7982

and

National Technical Information Service
Springfield, VA 22161

DISCLAIMER

NUREG/CR-4802
EGG-2486
Distribution Category: R2

AN EVALUATION OF TRAC-PF1/MOD1 COMPUTER CODE PERFORMANCE DURING POSTTEST SIMULATIONS OF SEMISCALE MOD-2C FEEDWATER LINE BREAK TRANSIENTS

Douglas G. Hall
John C. Watkins

NUREG/CR--4802

TI87 006042

Published January 1987

EG&G Idaho, Inc.
Idaho Falls, Idaho 83415

Prepared for the
Division of Accident Evaluation
Office of Nuclear Regulatory Research
U.S. Nuclear Regulatory Commission
Washington, D.C. 20555
Under DOE Contract No. DE-AC07-76ID01570
FIN No. A6038

ABSTRACT

This report documents an evaluation of the TRAC-PF1/MOD1 reactor safety analysis computer code during computer simulations of feedwater line break transients. The experimental data base for the evaluation included the results of three bottom feedwater line break tests performed in the Semiscale Mod-2C test facility. The tests modeled 14.3% (S-FS-7), 50% (S-FS-11), and 100% (S-FS-6B) breaks. The test facility and the TRAC-PF1/MOD1 model used in the calculations are described. Evaluations of the accuracy of the calculations are presented in the form of comparisons of measured and calculated histories of selected parameters associated with the primary and secondary systems. In addition to evaluating the accuracy of the code calculations, the computational performance of the code during the simulations was assessed. A conclusion was reached that the code is capable of making feedwater line break transient calculations efficiently, but there is room for significant improvements in the simulations that were performed. Recommendations are made for follow-on investigations to determine how to improve future feedwater line break calculations and for code improvements to make the code easier to use.

EXECUTIVE SUMMARY

An evaluation of the TRAC-PF1/MOD1 reactor safety analysis code was performed during the computer simulations of three Semiscale bottom feedwater break tests. The objectives of this evaluation were to modify an existing system model to produce a model of the Semiscale Mod-2C system, perform and evaluate the results of simulations of the Semiscale tests, evaluate code computational performance, and determine improvements in system modeling and the code for future analyses.

The system model was produced by modifying a similar model used by Sandia National Laboratory in making earlier Semiscale feedwater line and steam line break transient calculations. Numerous modifications were made to the model to make it conform to the Semiscale Mod-2C system. In addition to modifying the code input data to correspond to the later system configuration, the component numbering was changed and the input deck was extensively annotated to make the deck easier to use in this and subsequent analyses.

Steady-state calculations were performed to initialize the calculated system conditions to the conditions that existed before each of the tests. These calculations produced conditions that were in close agreement with the measured test initial conditions, including the primary-to-secondary heat transfer rates and primary and secondary temperatures in the broken loop steam generator, which were of particular interest.

Computer simulations were performed for the system blowdowns in Semiscale tests S-FS-6B, S-FS-7, and S-FS-11, which modeled 100%, 14.3%, and 50% bottom feedwater line breaks, respectively, in a Combustion Engineering System 80 pressurized water reactor. Evaluation of the code's calculational performance was based on its ability to predict the broken loop steam generator response to a loss of secondary inventory, pressurization of the primary system due to loss of heat sink, and the general system response to automated actions of the plant protection system. An attempt was made to continue the simulation of test S-FS-11 into the recovery phase, which included stabilizing the system at specified conditions and refilling the broken loop secondary system. This portion of the simulation was terminated prematurely due to the prediction of an unrealistic heatup of the primary system that precluded meeting the subcooling criterion for completion of the stabilization part of the recovery phase.

Comparisons of the results of the simulations to test data showed that the accuracy varied during different parts of the blowdown. The calculated results coincided with the test results from the start of the transient until shortly after the SCRAM signal occurred. The calculated results paralleled the test data during the period between when the SCRAM and safety injection system (SIS) signals occurred. Then, the calculated results differed significantly from the test results between the time the SIS signal occurred and the end of the blowdown. These differences ultimately led to the simulation of the recovery phase of test S-FS-11 being terminated prematurely.

Evaluations of the code's ability to predict the response of the broken loop steam generator during loss of secondary inventory showed mixed results. The calculations produced histories of break flow rate, primary-to-secondary heat transfer, and primary heat transfer coefficients that were in reasonably good agreement with the data. Other parameters, such as local secondary heat transfer coefficients and local primary side heat fluxes, did not show good agreement. The evaluation was complicated by the influence of other parts of the system, where the responses were not adequately predicted.

A number of confirmed and suspected reasons for the differences between the simulation and test results were identified: (a) omission of a portion of the steam line to each of the steam generators from the code models of the secondary systems; (b) errors in simulating primary-to-secondary heat transfer, particularly in the intact loop steam generator; and (c) errors in calculating crossover line flow contributed to the discrepancies between the calculated and measured results between the times of the SCRAM and SIS signals. The primary-to-secondary heat transfer problem is suspected to be due to simplifications in modeling the U-tubes and intact loop secondary system. Calculation of the crossover line flow could be improved by more accurate modeling of the flow path resistance and minimum area. The discrepancies that occurred after the SIS signal were the result of errors in simulating primary-to-secondary heat transfer in the

intact loop steam generator, perhaps due to errors in simulating energy transfer between the structure of the primary system and the primary fluid, and heat loss to the environment, which was not modeled.

The computational performance of the code was evaluated during the simulations. The simulations were performed with computational efficiency and at reasonable cost. The most difficult of the simulations was performed with a total central processing unit (CPU) to simulated time ratio of 5.42 at a cost of about $700 for a 620 s simulation performed on a Cray computer costing $500 per hour.

The code was evaluated on ease of use. Improvements were identified that could improve the user's efficiency in performing calculations and performing analyses using the calculated results. These improvements were in the areas of model input data, code output data, input checking, and code restarting.

ACKNOWLEDGMENTS

The authors wish to gratefully acknowledge the contributions of the following people that were made during the course of this project and in producing the final report: T. Chen for a large share of the modifications to the TRAC-PF1/MOD1 model to make it applicable to the Semiscale Mod-2C configuration, annotation of the input deck, and early input checking and steady-state calculations; N. S. Larson for computer plotting and data processing; T. J. Boucher for consultations on various aspects of the Semiscale FS test series; J. E. Tolli and G. A. Jayne for computer software support; and B. Spenser for word processing associated with producing the final draft of the report.

CONTENTS

FIGURES

TABLES

AN EVALUATION OF TRAC-PF1/MOD1 COMPUTER CODE PERFORMANCE DURING POSTTEST SIMULATIONS OF SEMISCALE MOD-2C FEEDWATER LINE BREAK TRANSIENTS

1. INTRODUCTION

The U.S. Nuclear Regulatory Commission has funded the development and assessment of the advanced reactor systems analysis computer code, TRAC-PF1/MOD1.[1] The code was developed by Los Alamos National Laboratory and is used to predict and analyze the thermal-hydraulic response of pressurized water reactors (PWRs) to postulated system failures and abnormal operational transients. It features two-fluid, nonequilibrium hydrodynamics modeling with flow regime dependent constitutive equations and offers features that allow it to be used to model a large number of the systems in a PWR.

The work reported in this document had several objectives. The first was to modify a TRAC-PF1/MOD1 model of the Semiscale system, used by Sandia National Laboratory to simulate earlier Semiscale feedwater line and steam line break tests, to make it conform to the Semiscale Mod-2C configuration. The intent was to produce a model with good fidelity that was well annotated to make it easy to use. The second was to perform simulations of three Semiscale feedwater line break tests and evaluate the performance of the code in simulating general system responses during the transients, with the broken loop steam generator response being of particular interest. Two other objectives were to evaluate the computational performance of the code during the simulations and identify areas of possible improvements to the code that would increase user efficiency in performing simulations and subsequent analyses using the simulated results.

The data base for the simulation evaluations consisted of the experimental results of three feedwater line break tests, each simulating a different sized break, conducted in the Semiscale Facility at the Idaho National Engineering Laboratory (INEL). These tests were S-FS-6B (a repeat of the first 600 s of the 100% feedwater line break test S-FS-6 to obtain heat transfer data not obtained during that test), S-FS-7 (a 14.3% feedwater line break), and S-FS-11 (a 50% feedwater line break). The test initial conditions and compounding failures, automatic responses of the plant protection system, and operational procedures were based on those used in the Combustion Engineering System 80 Final Safety Analysis Report calculations.[2] The detailed procedures are contained in the Experiment Operating Specification for the Semiscale Feedwater and Steam Line (FS) Break test series[3] and the associated Appendixes.[4,5]

This report presents a description of the TRAC-PF1/MOD1 model of the Semiscale Mod-2C system that was produced, evaluations of the transient simulations and the code computational performance during those simulations, and recommendations for further study and improvements to the code. Sections 2, 3, and 4 of the report provide background information for the results that are presented in subsequent sections. A description of the Semiscale Mod-2C facility is given in Section 2. A description of the TRAC-PF1/MOD1 model of the Semiscale Mod-2C system is presented in Section 3. The events in the blowdown and recovery phases of the tests are provided in Section 4. Section 5 presents the results of the TRAC-PF1/MOD1 steady-state calculations. Also included in Section 5 is an evaluation of the TRAC-PF1/MOD1 calculation of primary-to-secondary heat transfer in the broken loop steam generator at steady-state conditions. Sections 6, 7, and 8 present evaluations of the simulations of the three tests. Results of an evaluation of the computational performance of this code during the simulations and users experience in performing the simulation and subsequent analyses using the simulation results are given in Section 9. Conclusions of the evaluations are presented in Section 10. Recommendations for improving the quality of the simulations, further studies, and improvements to increase the ease of using the code and code output data are listed in Section 11.

2. SYSTEM DESCRIPTION

The Semiscale Mod-2C system (see Figure 1) is a two-loop, pressurized water reactor (PWR) simulator located at the Idaho National Engineering Laboratory (INEL). The Mod-2C system is modeled after a Westinghouse 3411 MW, four-loop PWR with the primary coolant system volume and core power scaled by a factor of 2 MW/3411 MW. The scaling philosophy followed throughout the design preserves important first-order effects of a loss-of-coolant accident (LOCA). Most notable are the 1:1 elevation scaling and the liquid distributions throughout the Semiscale system.

The Mod-2C system consists of an intact loop, broken loop, and pressure vessel. The intact loop simulates the three unaffected loops of a four-loop PWR. The broken loop simulates the remaining loop where the loss of primary or secondary coolant occurs. The intact loop has a steam generator, pressurizer, pump and associated piping. The broken loop has a steam generator, pump, break simulator and associated piping. Each steam generator has an associated secondary system with connections for feedwater, auxiliary feedwater, and steam discharge. In addition, the two steam generators can be cross connected, simulating the main steam header in a PWR. During part of the Feedwater and Steam Line (FS) break test series, a break in a bottom feedwater line downstream of the check valve was simulated with the broken loop steam generator. Other subsystems include an emergency core cooling system, external heat loss makeup system, leakage makeup system, and noncondensible gas injection system.

The steam generators are two-pass tube and shell design heat exchangers. The elevations of the steam generator nozzles, plena, and tubes are similar to those in a PWR. The downcomer, riser, and steam dome, however, are shorter and the steam drying equipment is simpler and less efficient. The intact loop steam generator contains two short, two medium, and two long tubes. The broken loop steam generator contains one short and one long tube (see Figure 2). The installed tubes represent the range of bend elevations found in a typical PWR steam generator. Primary fluid flows through vertical, inverted U-shaped tubes while secondary coolant passes through the shell side. For the Type II intact loop steam generator, a centrifugal separator at the top of the riser directs the two-phase mixture from the riser to the steam dome wall. For the new Type III broken loop steam generator, the three stages of separation of a PWR generator are simulated with a flow deflector (swirl vane simulator), Fronde Number scaled gravity separation section, and an off-the-shelf centripetal separator. The separation systems increase the quality of the exit steam and increases the liquid supply to the downcomer for recirculation flow. For the FS series feedwater line break tests, feedwater entered the steam generators at the bottom of the downcomer. Auxiliary feedwater entered the downcomers at approximately the elevation of the top of the U-tubes.

The pressurizer is attached to the intact loop hot leg and operates in a manner similar to its counterpart in a large PWR. The surge line hydraulic resistance is scaled to provide representative PWR flow rates. The only major difference is that the pressurizer spray system was not used during these tests.

The reactor vessel (see Figure 3) contains an upper head, upper plenum, electrically heated core, lower plenum, and external downcomer. The upper head region occupies the top 25% of the length of the pressure vessel. The upper plenum extends from the upper core support plate to the top of the heated core region. Two nozzles extend from the upper plenum and provide connection points for the hot leg piping. The flow path from the core to the hot leg nozzles is quite tortuous. In addition to a flow measurement assembly, a simulated control rod guide tube and two simulated core support columns obstruct the flow path. Also, a short set of vertical tubes create a horizontal flow restriction at the hot leg elevation. This flow restriction duplicates that in a PWR.

The core extends downward from the heater rod ground hub to the top of the mixer box. The 25-rod electrically heated core is enclosed in a square housing with no coolant bypass. The peripheral rods are powered separately from the 9 central rods (2 of the 16 peripheral rods are not powered). This allows a simulated radial profile, although a flat radial profile was used during the FS test series. The heater rods have a symmetric chopped-cosine axial power distribution with a peak-to-average power ratio of 1.59.

The lower plenum consists of an annulus and a lower head region, which serves to distribute the flow from the downcomer around the vessel periphery. Coolant flow from the downcomer changes direction within the lower head, turning up into the core housing. A simulated lower core plate provides a significant reduction in coolant flow area.

The external downcomer annulus assembly contains the cold leg nozzles and provides an annular inlet geometry similar to that in a PWR. The lower end of the assembly contains a transition section that funnels the flow into the downcomer pipe. The external downcomer annulus connects to the vessel upper head and

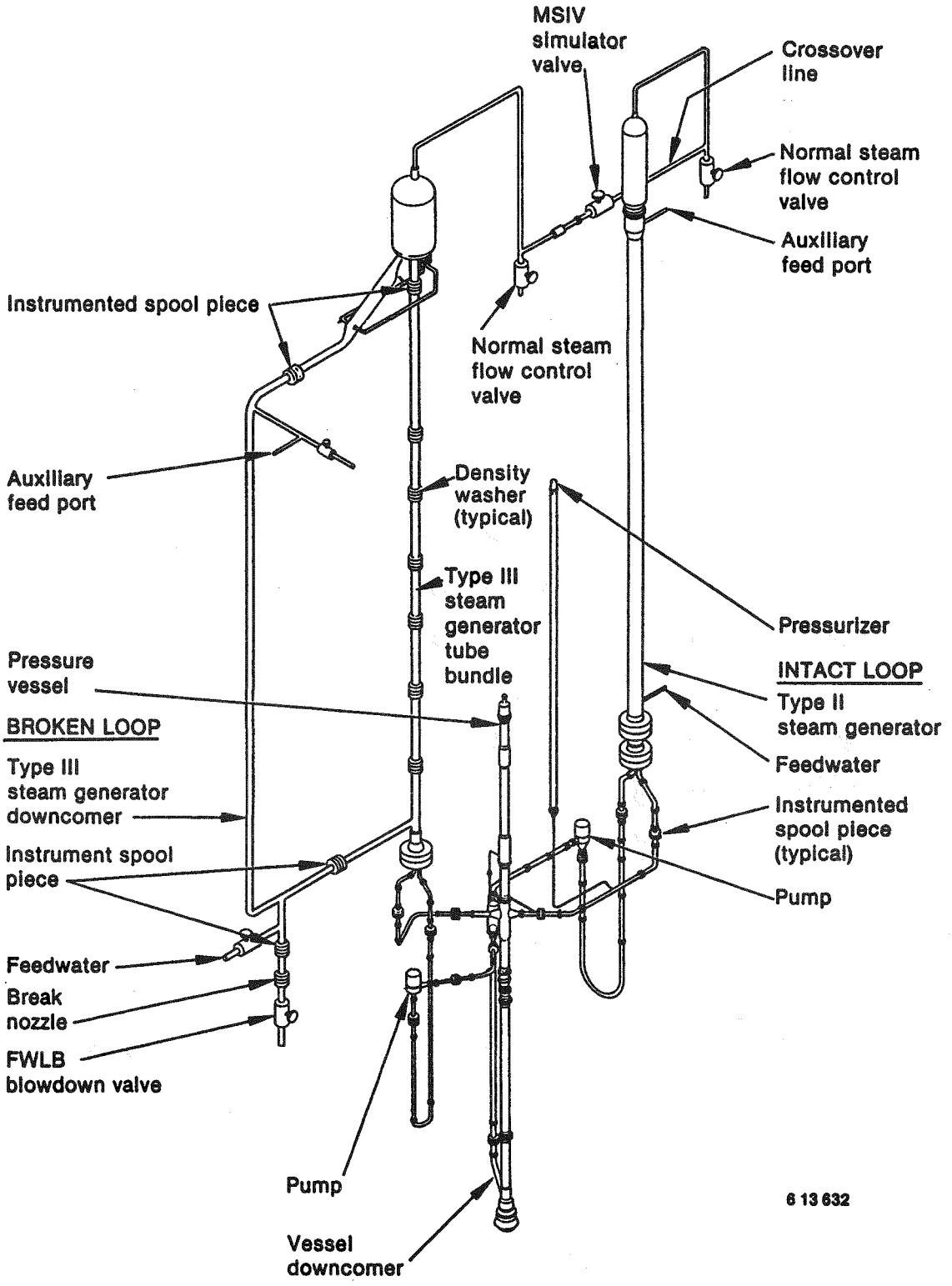

Figure 1. Semiscale-Mod-2C system as configured for the FS test series.

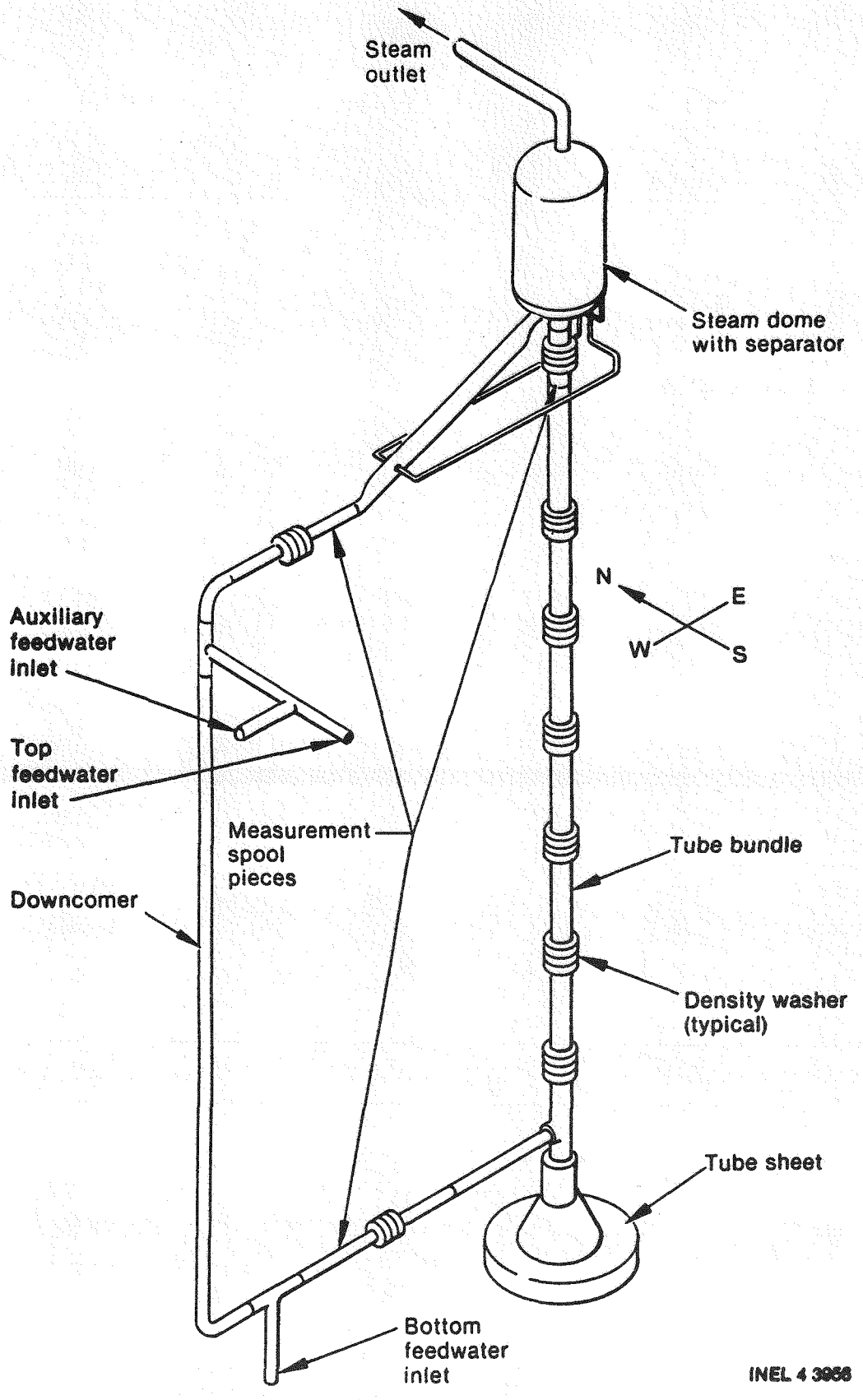

Figure 2. Semiscale Type III broken loop steam generator.

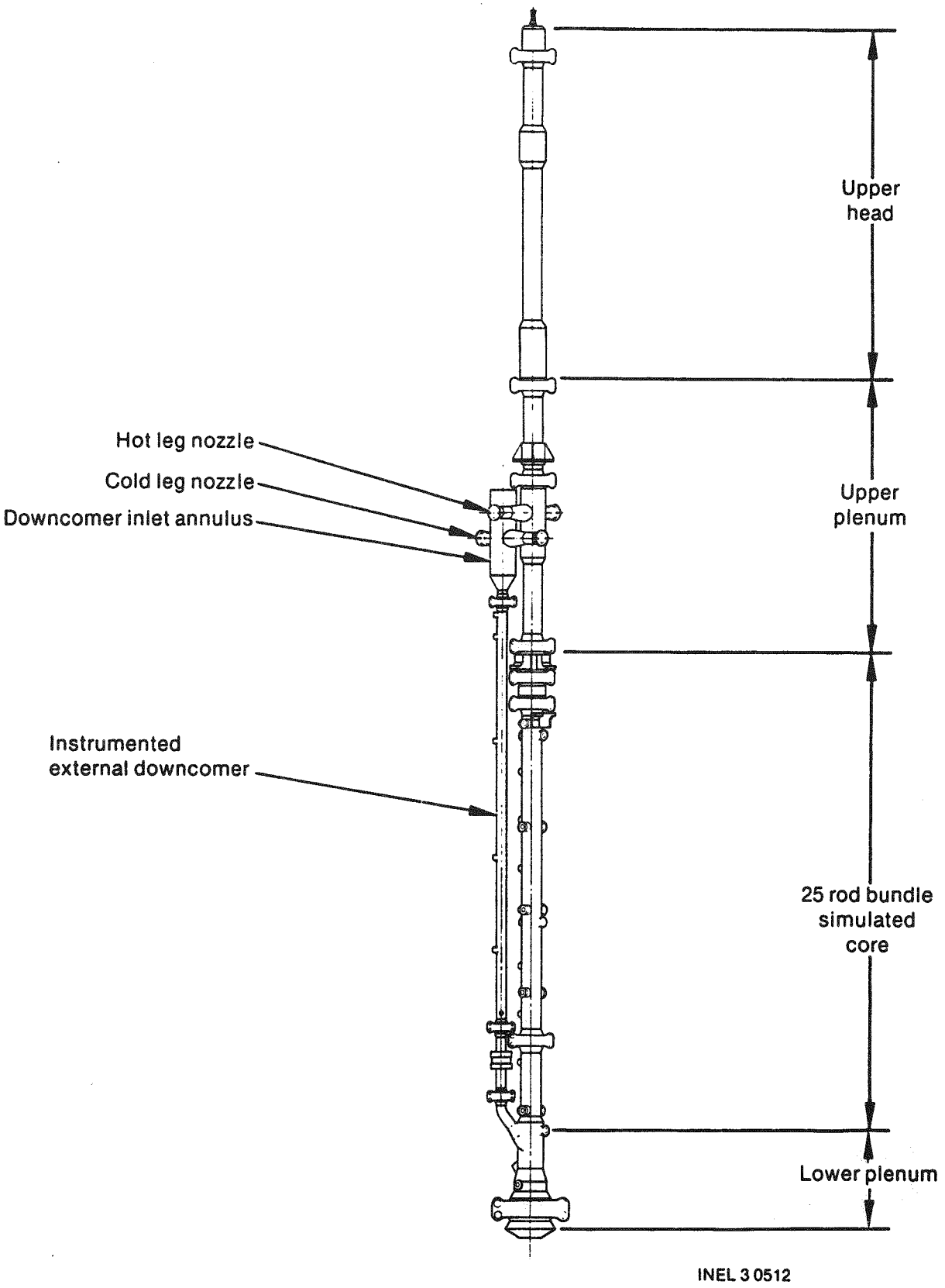

Figure 3. Semiscale Mod-2C pressure vessel.

simulates the bypass flow path in a PWR. This bypass flow amounted to about 2.4% of the total flow for the feedwater line break tests.

An extensive network of instruments measure primary and secondary parameters. Primary system measurements include metal and fluid temperatures, absolute and differential pressures, densities, and volumetric flow rates, including the volumetric flow rate at the broken loop steam generator U-tube exits. Intact loop Type II steam generator measurements include metal and fluid temperatures, absolute and differential pressures, and steam and feedwater flow rate measurements. Broken loop Type III steam generator measurements include normalized primary fluid, U-tube outside wall metal and secondary fluid temperatures, absolute and differential pressures, densities (upper and lower downcomer, tube bundle, and riser), mass flow rate measurements (upper and lower downcomer, and riser) and steam, feedwater, and crossover line flow rate measurements. Condensing systems measure effluent from the steam generator atmospheric dump valves and the break simulator. During these tests, the break simulator was attached to the broken loop steam generator bottom feedwater line and contained instruments for measuring pressure, temperature, density, and mass flow. Redundant mass flow measurements were obtained from the condensing system.

3. TRAC-PF1/MOD1 MODEL DESCRIPTION

The base model was derived largely from a model prepared by Sandia National Laboratories (SNL).[6] Before the Feedwater and Steam Line (FS) break test series, extensive modifications were performed to the Semiscale facility. Table 1 details the major alterations to the Semiscale facility to assemble the Mod-2C configuration and that were subsequently made to the TRAC-PF1/MOD1 model.

Figure 4 depicts the TRAC-PF1/MOD1 nodalization used for the S-FS-6B, S-FS-7, and S-FS-11 transient calculations. There were 41 components, containing a total of 225 cells, used to model the primary and secondary systems. In addition, a total of 175 heat slabs were included (139 heat slabs were associated with 1-D components, and 36 were associated with the 3-D vessel). Two heater rods were simulated in the reactor vessel. A detailed distribution of cells and heat slabs in the model is summarized in Table 2. Appendix A contains a complete listing of the S-FS-11 model. This model is typical of the S-FS-6B and the S-FS-7 models as well.

The 3-D vessel component contains 1 radial ring, 2 unequal azimuthal sectors, and 17 axial levels. Three levels represent the lower plenum, six represent the core, and four each represent the upper plenum and the upper head. Figure 5 contains a nodalization of the vessel. The azimuthal sectors are such that the vessel flow area and volume are split 2:1 between the intact and broken loops, respectively. The sector containing the support column represents two-thirds of the flow area and volume. The sector containing the guide tube represents one-third of the flow area and volume. A pipe component connecting the lowest upper plenum level with the next to the lowest upper head level models the support column. Two tee components with four connections to the vessel were used to model the guide tube. These connections include the top of the upper head level and the bottom, second, and top upper plenum levels. The hot legs connect to the third upper plenum level. The cold legs connect to the downcomer, which in turn connects to the second lower plenum level. The downcomer and the bypass line were both modeled with tee components.

During the test, the core power was augmented by 22 kW to make up for heat losses to the environment uncompensated for by the external heaters. Most of the external heaters are located on primary piping and components. Therefore, most of the environmental heat losses occur in the steam generators. The TRAC-PF1/MOD1 model of the Semiscale Mod-2C facility includes adiabatic boundaries for all components. Consequently, environmental heat losses in the steam generators were not modeled and the 22 kW power augmentation was removed from the indicated core power for these calculations.

The steam generator was modeled entirely with 1-D components. A single primary side U-tube was used to model either the two or six inverted U-tubes in the broken or intact loop steam generator, respectively. The secondary side of each steam generator contained sufficient components to model the downcomer, riser, and steam discharge line. Connected to the secondary side of each steam generator were feedwater, auxiliary feedwater, steam discharge, and steam cross-connect lines. In addition, the broken loop steam generator contained components to simulate the bottom feedwater line break.

Most of the heat slabs associated with the 1-D components contained three radial nodes. However, heat slabs representing the U-tubes and various steam generator secondary structures had five radial nodes each. The majority of the 3-D vessel heat slabs used the lumped parameter model and had only one node.

The single-phase homologous performance curves for the intact and broken loop pumps were based on Semiscale data. The two-phase head and torque multiplier and difference curves for the broken loop pump were also based on Semiscale data. Data from the broken loop pump was substituted for data not available for the intact loop pump.

Modifications to the base Sandia model, to represent the Semiscale Mod-2C configuration, were derived largely from RELAP5/MOD2 input models. Most parameters were directly convertible between the RELAP5 and TRAC-PF1/MOD1 models, the exception being loss coefficients. Guidelines for converting loss coefficients comes from the Primarkreislaufe (PKL) natural circulation and the Babcock and Wilcox (B&W) once through steam generator (OTSG) separate effects tests. When converting RELAP5 loss coefficients for use in TRAC-PF1/MOD1, loss coefficients representing pipe bends were not changed. Loss coefficients representing pipe tees are not included because the TRAC-PF1/MOD1 tee component calculates the losses due to momentum effects, whereas the RELAP5 branch components do not.

Table 1. Summary of changes to the TRAC-PF1/MOD1 Semiscale model

	Model Change	Reason For Change
1.	Replaced the broken loop steam generator	Type III steam generator installed before the FS test series.
2.	Renodalized the intact loop steam generator	Nodalization was simplified and made consistent with the broken loop steam generator nodalization. Also corrected errors in the heat slabs and added the volume of the tube sheet to the model.
3.	Added the crossover line	Was not part of the Mod-2A configuration.
4.	Replaced the pressurizer	The pressurizer was replaced in going to the Mod-2B configuration (before Mod-2C).
5.	Modified the vessel upper head	Flow paths in the upper head were changed when going to the Mod-2B configuration.
6.	Modified the BLSG break spool piece	BLSG break piping changed when the new steam generator was installed.
7.	Modified the intact loop pump suction	Piping was changed from 3 in. to 2-1/2 in. and configuration changed when pump was changed for the Mod-2B configuration.
8.	Replaced the intact loop pump model	Intact loop pump was replaced when going to the Mod-2B configuration.
9.	Revised the broken loop pump characteristics	Pump characteristics were modified using the results of Semiscale pump testing.
10.	Modified the vessel model	Nodalization simplified to be consistent with RELAP5 model. Minor errors were also corrected.
11.	Added HPIS to the broken loop	Was not included in the SNL model.
12.	Initial conditions, pump coast down curve, and power decay curve changed	These items are test specific.
13.	Trips modified for blowdown	These items are test specific.

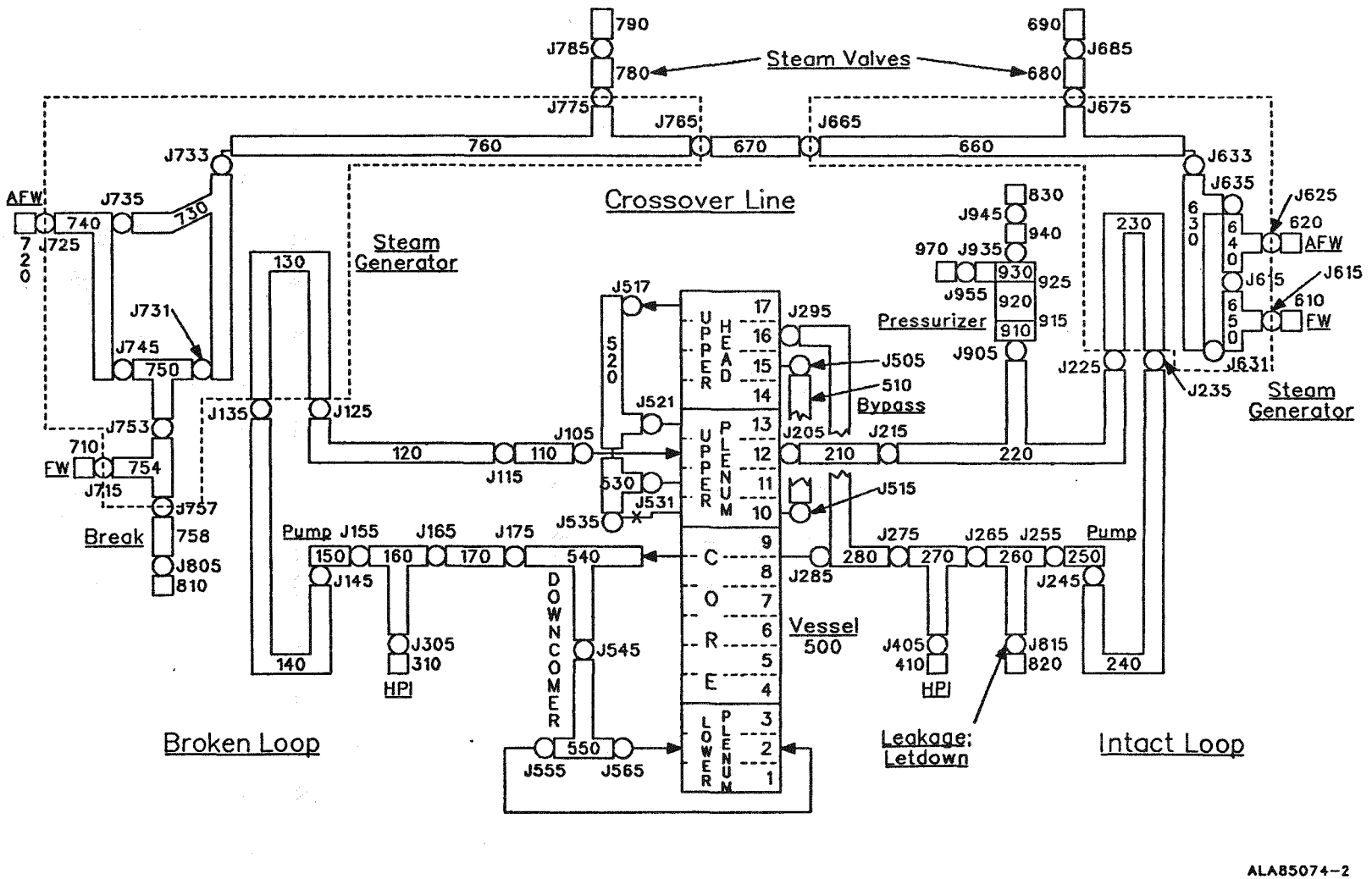

Figure 4. TRAC-PF1/MOD1 nodalization for modeling the Semiscale Mod-2C system.

Table 2. Nodalization summary of the TRAC-PF1/MOD1 Semiscale model

	1-D Fluid Cells	3-D Fluid Cells	Heat Slabs	Breaks And Fills
Intact Loop				
Hot leg	10		10	
U-tubes	16		12	
Pump suction	8		8	
Pump	2		2	
Cold leg	6		6	
HPIS	2		1	1
Leakage	2		1	1
Steam generator secondary	25		19	
Steam discharge	3			1
Feedwater	1			1
Auxiliary feedwater	1			1
Pressurizer				
Vessel	10		10	
Surge line	3		3	
Relief valve/pressure control	4			2
Broken Loop				
Hot leg	8		8	
U-tubes	16		12	
Pump suction	8		8	
Pump	2		2	
Cold leg	4		4	
HPIS	2		1	1
Steam generator secondary	28		19	
Feedwater break	3			1
Steam discharge	3			1
Feedwater	1			1
Auxiliary feedwater	1			1
Crossover line	2			
Reactor Vessel				
Downcomer	12		12	
Lower plenum		6	6	
Core		12	14	
Upper plenum		8	8	
Upper head		8	8	
Support columns	1			
Bypass line	1		1	
Guide tube	6			
Input Model Totals	191	34	175	12

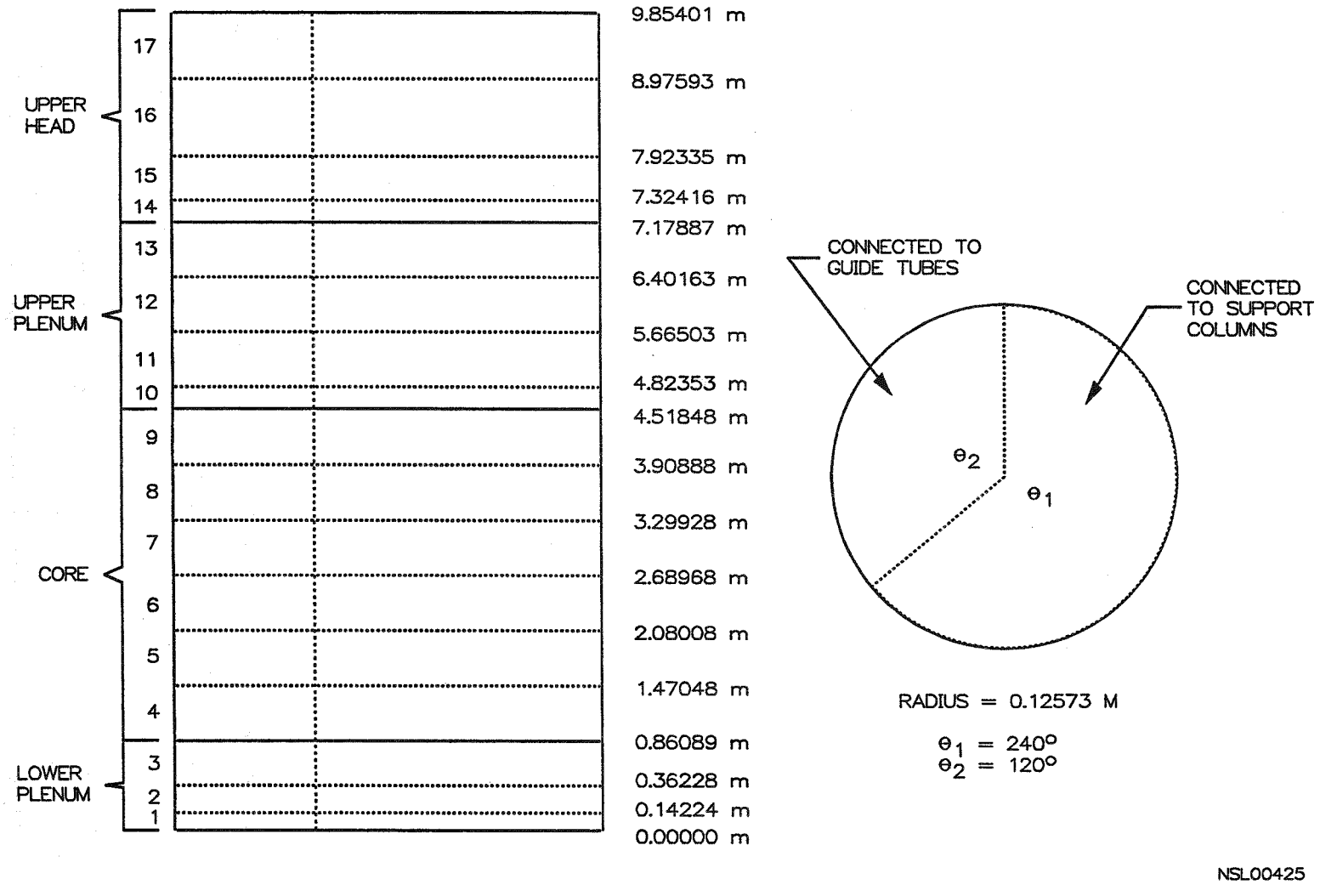

Figure 5. TRAC-PF1/MOD1 nodalization for modeling the Semiscale pressure vessel.

4. FEEDWATER LINE BREAK TRANSIENT DESCRIPTION

The results of three Semiscale bottom feedwater line break tests, designated S-FS-6B, S-FS-7, and S-FS-11, formed the experimental data base for the simulation evaluations reported in this document. The initial conditions and sequence of events for the blowdown (initial) phase of these tests were essentially the same. The principal difference in the tests was the break size. The tests simulated 14.3% (S-FS-7), 50% (S-FS-11), and 100% (S-FS-6B) bottom feedwater line breaks downstream of the feedwater line check valve. Test S-FS-6B was a repeat of the first 600 s of test S-FS-6 to obtain heat transfer data not obtained during that test.

The scenario for the blowdown phase of the transient, as specified in the appendixes to the Experiment Operating Specification (EOS),[4,5] was as follows. A break in a feedwater line occurred that rendered the main feedwater system inoperable such that all feedwater flow was discontinued at break initiation. The check valve in the affected steam generator main steam line was assumed to fail resulting in a communication path between the affected and unaffected steam generators until main steam isolation valve closure. Reactor trip (SCRAM) and turbine trip signals were generated by a high pressurizer pressure signal. Delays associated with transducer response time, rod drop times, and closure of the turbine stop valves were simulated by delaying initiation of the core power decay and closure of the main steam flow control valves. A loss of offsite power was assumed to occur at SCRAM resulting in a coast down of the primary coolant pumps with a simulated delay for transformer decay time.

Low pressure in the affected loop steam generator secondary was assumed to generate a safety injection system (SIS) actuation signal. Main steam isolation valve closure was simulated to occur when the SIS signal occurred by closing the valve in the crossover line flow path connecting the two steam generators. High pressure injection system (HPIS) flow and auxiliary feedwater flows were assumed to be available 25 s after the SIS signal. This delay accounted for diesel startup and sequencing after loss of offsite power. The safety injection capacities were based on the assumption that only one train of HPIS flow is available and the auxiliary feedwater injection rates were representative to the extent possible of the injection rate used in Combustion Engineering FSAR calculations. The blowdown phase of the transient was considered complete at the greater of 4 s after the SIS signal or a representative time for failure identification, which was considered to be 600 s.

Part of the recovery phase of test S-FS-11 was simulated using TRAC-PF1/MOD1. The recovery phase of the transient had two parts, as specified in the EOS appendix.[5] The recovery involved simulating operator actions to stabilize the plant at conditions necessary for plant cooldown to begin followed by refilling the affected loop steam generator secondary. The operator actions simulated during the stabilization part included:

- Terminating auxiliary feedwater to the affected steam generator
- Terminating HPIS flow after the auxiliary feedwater to the affected loop steam generator was terminated and the primary subcooled margin was $\geq$ 27.8 K (50°F) and the pressurizer liquid level was $\geq$ 235 cm (92.5 in.)
- Initiating normal charging and letdown to establish and maintain the pressurizer level between 235 (92.5) and 255 cm (100.4 in.)
- Using the pressurizer warmup internal heaters at half of their full power setting to maintain the primary system subcooled margin between 27.8 (50) and 33.3 K (60°F)
- Reestablishing and maintaining the unaffected steam generator downcomer level between 910 (358.3) and 1000 cm (393.7 in.) with auxiliary feedwater
- Cycling the unaffected steam generator atmospheric dump valve to maintain a secondary pressure of $\leq$ 6.98 MPa (1000 psig).

This part of the recovery was considered to be complete when the pressurizer liquid level, unaffected steam generator downcomer liquid level and secondary pressure, and the primary subcooled margin were being maintained at specified conditions and the core was acceptably cool.

The refill part of the transient included the same type of operations performed during the stabilization phase along with refilling the affected loop steam generator using auxiliary feedwater. The primary coolant pumps were also restarted to ensure a measurable amount of primary circulation flow. This portion of the transient was not simulated using TRAC-PF1/MOD1 because of difficulties encountered during the stabilization part of the recovery phase, which will be discussed in Section 8.

5. STEADY-STATE RESULTS

Steady-state TRAC-PF1/MOD1 calculations were made for each of the Semiscale tests that were simulated to match the test initial conditions reported in the Quick Look Reports for each of the tests.[7-9] (Initial conditions for test S-FS-6 were modified to values for S-FS-6B, which were obtained from the Semiscale Project Group because a Quick Look Report was not published for the rerun of the first 600 s of test S-FS-6.) Measured and calculated values of initial condition key parameters are compared in Table 3. Nearly all of the TRAC-PF1/MOD1 steady-state values are in excellent agreement with their measured counterparts. Notable exceptions are the loop-to-loop temperature differences and some steam generator secondary masses. The differences in calculated cold leg temperatures from one loop to the other are within the measurement uncertainty of the difference between the measured temperatures. Consultation with the Semiscale Project Group during the analysis phase of the evaluation indicated that the initial secondary mass of the broken loop steam generator may have been as much as 10 kg (22.0 lbm) and 7 kg (15.4 lbm) lower than initially reported for tests S-FS-6B and S-FS-7, respectively. The difference between calculated and measured initial secondary mass, if they existed, surprisingly did not appear to have a major effect on the system transient response.

Several controllers were used in the TRAC-PF1/MOD1 steady-state calculations to match the test initial conditions. These included controllers on the primary coolant pumps to obtain specified circulation flows in each of the loops and controllers on the feedwater to each of the steam generators to obtain the specified amount of secondary mass. The primary pressure was fixed at the test initial condition during the steady-state calculation by the PRIZER component, which was part of the pressurizer model. The secondary pressures were fixed by steam receiver BREAK components downstream of the steam control valves during the steady-state calculations for tests S-FS-6B and S-FS-7. These break components were also used to define the time-dependent secondary pressures until the steam control valves were closed during the transient for these two tests. Controllers were added to the steam control valves for the S-FS-11 steady-state calculation. The valves were modulated to obtain the specified secondary pressures during the steady-state calculation. For the transient calculation, the valves were left in the position they assumed to obtain the specified secondary pressure.

Primary-to-secondary heat transfer in the broken loop steam generator was an item of major interest in this evaluation task. Consequently, heat fluxes, U-tube primary and outer wall temperatures, secondary temperatures, and riser void fractions calculated during the steady-state calculations were compared with measured counterparts at the test initial conditions. Calculated heat fluxes were compared with measured values as a function of normalized length (position along the tube from entrance at top of tube sheet divided by total tube length) along the U-tube. Normalized tube length was used because the Semiscale system contained two U-tubes of different lengths and the TRAC-PF1/MOD1 model contained only one U-tube that was representative of these tubes. Also, tube length was felt to be a more significant parameter than other dimensional parameters, such as elevation above the tube sheet.

Calculated and measured U-tube primary fluid temperatures and outer (secondary side) wall temperatures as a function of normalized tube length were also compared. Calculated and measured secondary temperatures were compared using a pseudo normalized flow path length where the total flow path length was equal to twice the highest temperature elevation so they could be included in the same figure with the primary and wall temperature comparisons. The highest secondary temperature elevations used for both the TRAC-PF1/MOD1 and the experimental data were nearly the same. Calculated and measured riser void fraction distributions were compared as a function of elevation above the tube sheet. Figures 6 through 8 show comparisons of calculated and measured heat fluxes and primary, secondary, and tube wall temperatures, and riser void fraction, respectively, for test S-FS-6B. These results are typical of those that were obtained for tests S-FS-7 and S-FS-11.

The comparisons for all three tests show the same general results. The calculated heat fluxes agree well with the measured heat fluxes associated with the long U-tube, as shown in Figure 6. The heat fluxes associated with the short U-tube are higher than those for the long tube because of the higher flow rates through it due to lower hydrodynamic resistance. It should be noted that the heat transfer area used for the single U-tube in the TRAC-PF1/MOD1 model accounted for the heat transfer surface areas of both Semiscale U-tubes. However, the results shown in Figure 6 indicate that it may be difficult to set up a model that accurately represents the cumulative effect of heat fluxes across different length tubes using the single tube representation that is required when using the STGEN component to model a steam generator.

The calculated primary temperatures in the U-tube were in the range of temperatures associated with the

Table 3. Measured and calculated initial conditions for tests S-FS-6B, S-FS-7, and S-FS-11

	S-FS-6B		S-FS-7		S-FS-11	
	Data	TRAC	Data	TRAC	Data	TRAC
Pressurizer pressure (MPa)	15.01	14.94	14.98	14.94	15.03	15.03
Core power (MW)	2.180[a]	2.180	2.184[a]	2.179	2.160[a]	2.160
Core differential temperature (K)	36.9	38.8	36.9	38.9	36.7	39.3
Pressurizer level (cm)	477.0	465.1	488.0	466.8	483.5	484.1
Cold leg fluid temperature (K)						
Loop to loop difference	3.9	1.7	4.2	1.3	4.5	1.5
Nominal	568.7	571.1	568.8	571.1	569.4	570.1
Mass flow rate (kg/s)						
Intact loop	7.02	7.05	6.99	7.05	6.96	6.96
Broken loop	2.30	2.35	2.26	2.35	2.32	2.32
Volumetric flow rate (L/s)						
Intact loop	9.5	9.7	9.3	9.7	9.4	9.5
Broken loop	3.2	3.2	3.2	3.2	3.3	3.2
Steam generator secondary pressure (MPa)						
Intact loop	6.28	6.30	6.23	6.30	6.27	6.28
Broken loop	6.26	6.26	6.21	6.26	6.23	6.23
Steam generator secondary mass (kg)						
Intact loop	116.0	103.0	104.9	102.9	105.0	104.7
Broken loop	37.0[b]	35.0	34.7[c]	35.5	25.0[d]	24.8
Steam generator flow rate (kg/s)						
Intact loop	0.90	0.90	0.89	0.90	0.89	0.88
Broken loop	0.26	0.27	0.27	0.27	0.25	0.27
Steam generator feedwater temperature (K)						
Intact loop	488.0	485.0	483.9	485.0	485.0	485.0
Broken loop	485.0	483.0	480.4	483.0	481.3	481.3
Broken loop steam generator						
Circulation ratio	4.6	4.7	4.3	4.8	4.0	4.0

a. Unaugmented core power.

b. Subsequent analysis indicates that the steam generator secondary mass was about 9 kg (19.8 lbm) lower than the initial value listed.

c. Subsequent analysis indicates that the steam generator secondary mass was about 6 kg (13.2 lbm) lower than the initial value listed.

d. Subsequent analysis indicates that the steam generator secondary mass was about 2 kg (4.4 lbm) higher than the initial value listed.

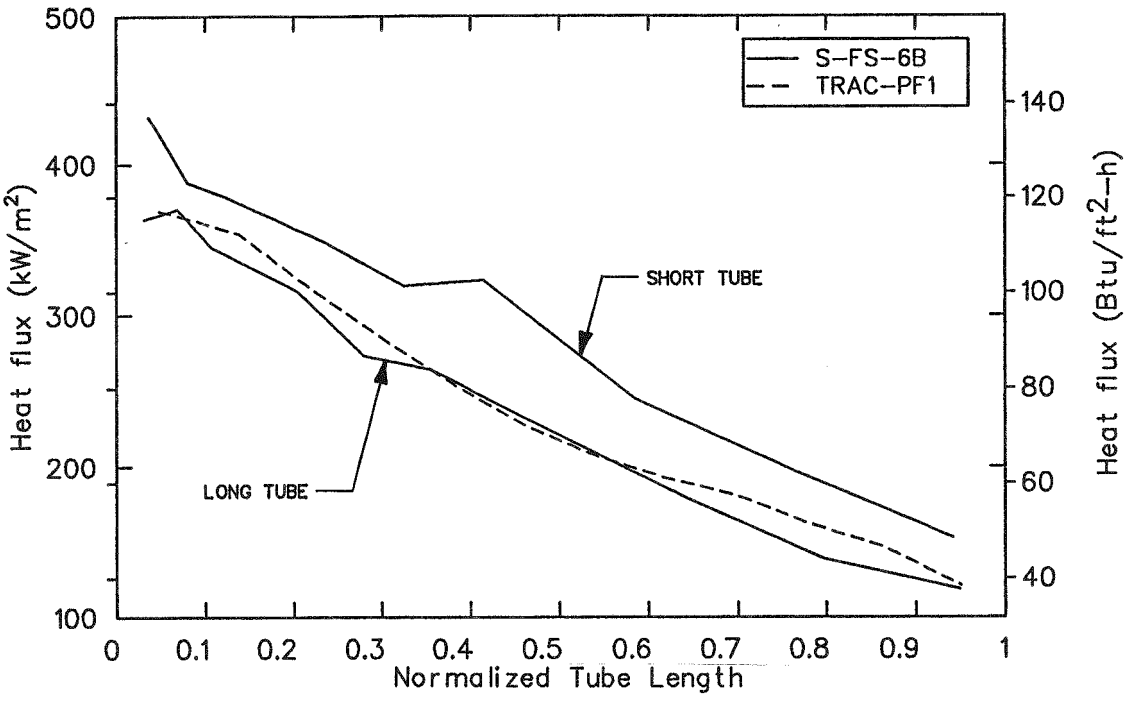

Figure 6. Comparison of measured and calculated pre-transient heat fluxes as a function of normalized tube length for test S-FS-6B.

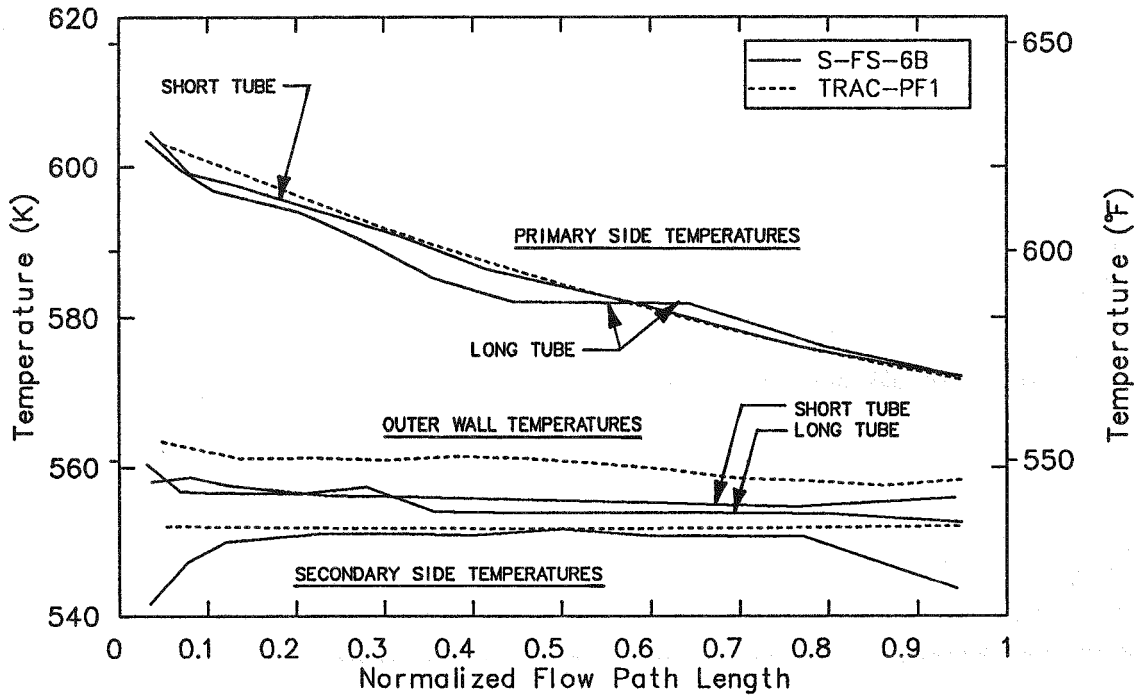

Figure 7. Comparison of measured and calculated pre-transient U-tube primary, U-tube outer wall, and secondary temperatures as a function of normalized flow path length for test S-FS-6B.

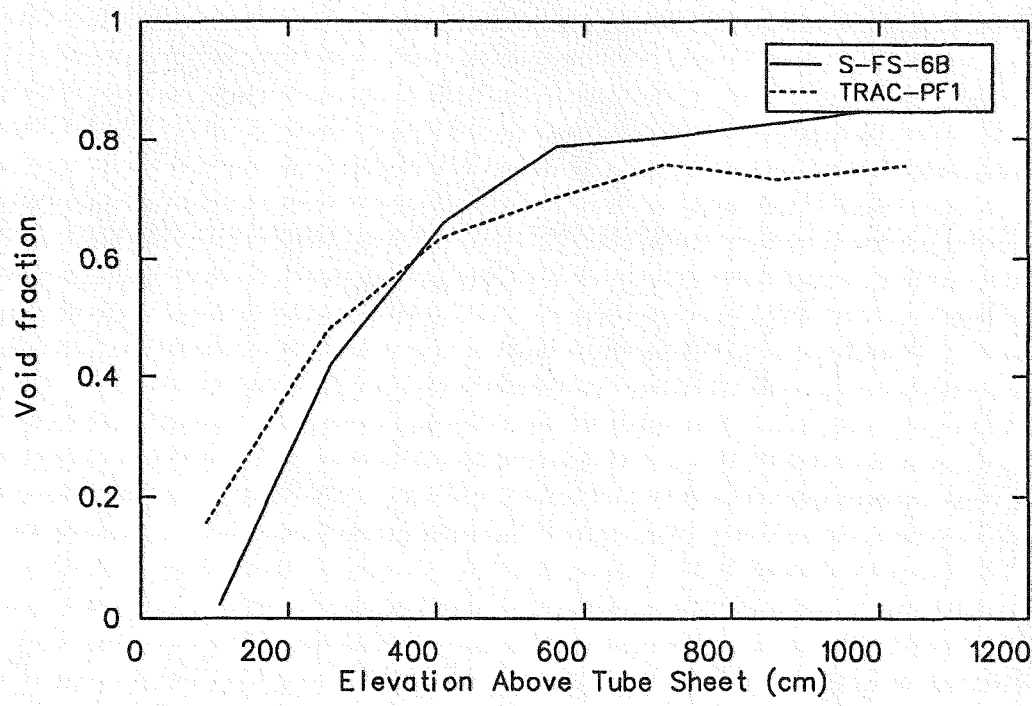

Figure 8. Comparison of measured and calculated pre-transient riser void fraction distribution as a function of elevation above the top of the tube sheet for test S-FS-6B.

Semiscale short and long tubes (as shown in Figure 7) and were, in general, in better agreement with the temperatures associated with the short tube. The calculated outer wall temperatures were higher than the measured values for both the short and the long tube, which were nearly equal. The calculated secondary temperatures were in good agreement with the measured values except at the lowest elevations that corresponded to the lowest and highest values of normalized flow path length.

Calculated and measured riser void fraction distributions are compared in Figure 8. Like the secondary temperatures, the calculated riser void fractions at the lower elevations are higher than the measured data. Because the calculated conditions at the bottom of the downcomer agreed well with the measured data, the discrepancies at the lower riser elevations indicate a difference in the amount of heat transferred to the fluid. This result is not consistent with the fact that the calculated heat fluxes at the lower elevations (minimum and maximum normalized tube length) are equal to or less than the measured data, as shown in Figure 6. The relationship between the calculated and measured heat fluxes does provide an explanation of why the calculated void fractions at the upper riser elevations are lower than the measured values. Increased calculated heat fluxes in better agreement with the mean of the measured data would result in increased riser void fractions at these locations, thus improving the agreement between the calculated and measured results at the upper elevations.

6. S-FS-6B TRANSIENT SIMULATION RESULTS

Comparisons between the results of a TRAC-PF1/MOD1 simulation and data measured during Semiscale test S-FS-6B (100% break) are discussed in this section. Subsection 6.1 presents the general response of the system from the time of the bottom feedwater line break until the end of the test at 600 s. Subsection 6.2 is devoted to the response of the broken loop steam generator until its energy removal capability was reduced to a negligible level.

6.1 General System Response

This subsection provides an evaluation of the ability of TRAC-PF1/MOD1 to calculate general system response during a bottom feedwater line break transient by comparing calculated parameters with measured counterparts, with emphasis on the primary coolant system. The discussion is organized to follow the chronology of events as simulated automated actions of the plant protection system occur and presents parameters reflecting these actions. The discussion also provides comparisons of the calculated and measured conditions at the end of the transient, when plant stabilization operations would commence.

The events influencing the system response during test S-FS-6B were the simulated break in the bottom feedwater line and simulated automated actions of the plant protection system. The first of these actions was terminating the feedwater to both of the steam generators when the feedwater line break occurred. This action resulted in pressurization of the primary coolant system due to the reduction of the energy removal capacity of the steam generators. The primary pressure eventually reached the pressurizer high pressure trip set point. With the assumption of a concurrent loss of offsite power, closures of the main steam control valves, termination of power to the primary coolant pumps, and a SCRAM of the reactor with associated delays were simulated. Comparisons of measured and calculated parameters associated with these simulated actions are given in Figure 9. Comparisons of the times of occurrence of these actions and later events in the test and the TRAC-PF1/MOD1 simulation are presented in Table 4.

Important elements of the early primary pressure response were well calculated, as shown in Figure 9a. These elements include the time when the high pressurizer pressure set point was reached, the peak system pressure, and difference between the intact loop cold leg pressure (highest pressure point in the primary system) and the pressurizer pressure. Discrepancies between the calculated and measured pressurizer pressures after the peak pressure is reached are noticeable. After 75 s, the measured and calculated pressure histories diverge, as discussed later in this section.

The calculated secondary pressure histories were set equal to the measured values until the steam valves were closed. Steam valve closure is indicated in the data by a sudden increase in the secondary pressures shortly after the SCRAM signal time at 23 or 24 s, as shown in Figure 9b. Thereafter, the trends of the calculated pressure histories are correct, but the intact loop secondary pressure is too high and the broken loop secondary pressure too low. Also, once the secondary pressures peaked and began to decrease, the rate of decrease in the calculated data is higher than that indicated by the measured data. Because the calculated and measured break flow rates were in good agreement between the time the steam valves were closed (23 s) and the time the crossover line valve closed (73 s), these differences were attributed to at least two causes. One is incorrect energy balances on the secondaries and the other is errors in modeling the secondary volumes.

The calculated energy input rates to the steam generators from the primary system during the period in question were higher than the measured values, as shown in Figure 9d. This explains why the calculated intact loop secondary pressure increased above the measured pressure, but does not explain why the calculated broken loop secondary pressure remained below its measured counterpart or why the calculated secondary pressures decreased too rapidly. The low calculated broken loop secondary pressure and the higher-than-measured rate of depressurization of the secondaries was attributed partially to the fact that the steam piping from the crossover line junction to the steam control valves was not included in the secondary system modeling for either of the steam generators. Inclusion of this piping would have increased the sum of the secondary volumes by 13% and would have reduced the depressurizing effect of losing mass from the secondaries.

The discrepancy between the calculated and measured broken loop secondary pressures was also related to the calculated crossover line flow being less than the measured data (see Figure 10) and not supplying sufficient mass to the broken loop secondary. The fact that the calculated crossover line flow was less than the measured flow suggests that the crossover line modeling needs revision. The two principal areas of revision are the loss coefficient of the crossover flow path that was lumped into the crossover line valve component and the minimum area in the valve component.

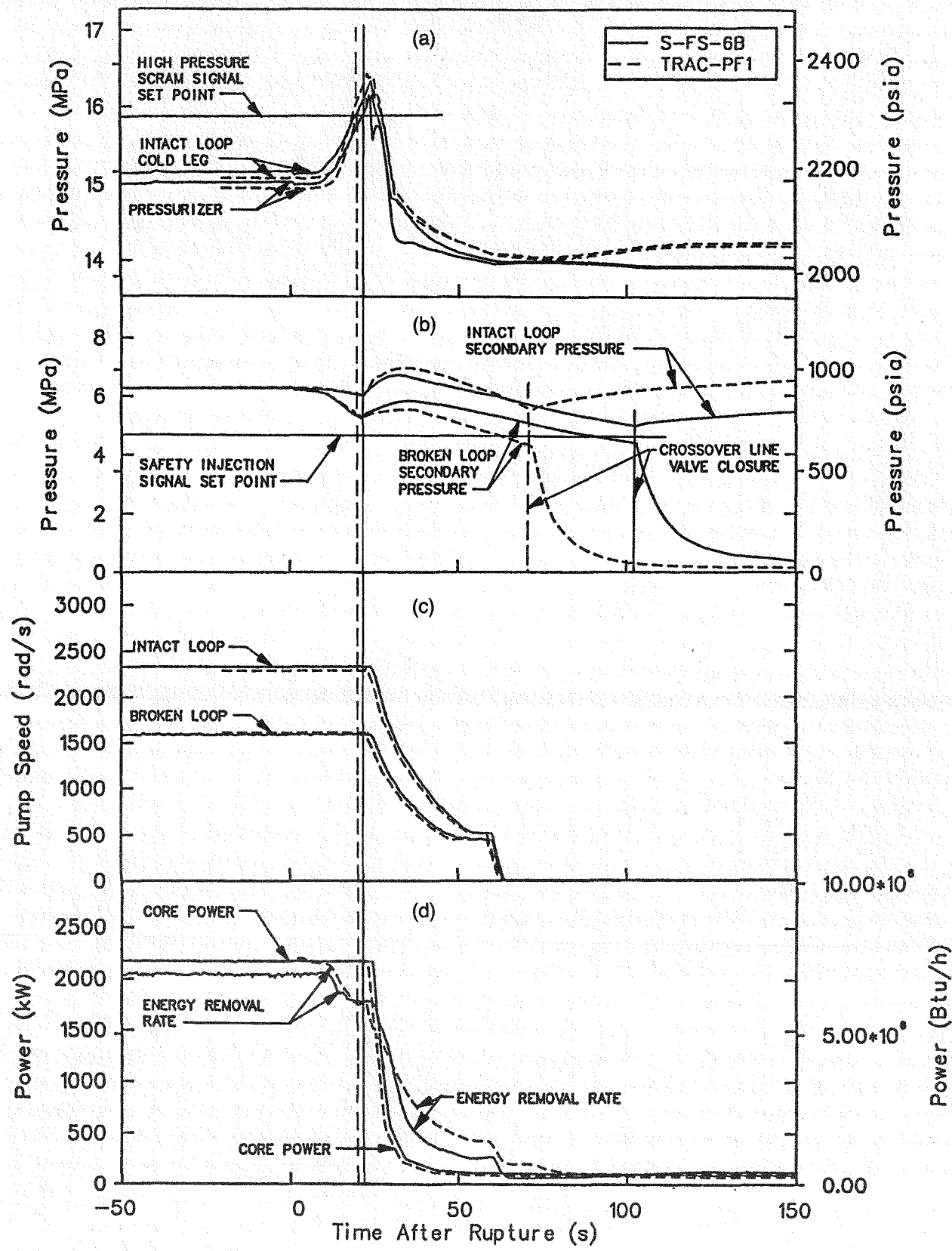

Figure 9. Composite of measured and calculated parameter histories showing the results of simulated automatic actions during the early part of test S-FS-6B.

Table 4. Sequence of events for test S-FS-6B

	Time (s)	
	Data	TRAC
Broken loop steam generator main feedwater line break		
Initiated	0.0	0.5
Fully open	1.0	2.5
Steam generator main feedwater isolated		
Intact loop	150.0[a]	150.3
Broken loop	8.5[a]	8.5
SCRAM at P_{pzr} = 15.86 MPa (2300 psia)	22.0	20.2
Main coolant pump begins coast down		
Intact loop	24.2	22.5
Broken loop	24.2	22.5
Core power decay initiated	24.6	22.9
Main steam flow control valve closed		
Intact loop	24.4	23.2
Broken loop	24.4	23.2
Power to main coolant pump tripped off		
Intact loop	60.2	58.6
Broken loop	60.2	58.6
Safety injection signal		
Broken loop secondary pressure at 4.47 MPa (648.2 psia)	99.0	67.0
High pressure injection flow available		
Intact loop	99.0	67.0
Broken loop	99.0	67.0
Auxiliary feedwater flow initiated		
Intact loop	300.0	67.0
Broken loop	99.6	67.0
Crossover line valve closed	103.0	72.7
Blowdown phase of transient completed (End of test S-FS-6B)	600.0	599.6

a. Measured feedwater flow data do not actually show flow rates going to zero until these times, although the feedwater flows were indicated to be less than 5% of their initial values by 5 s into the transient. The measured feedwater flow histories were included in the TRAC-PF1/MOD1 simulation.

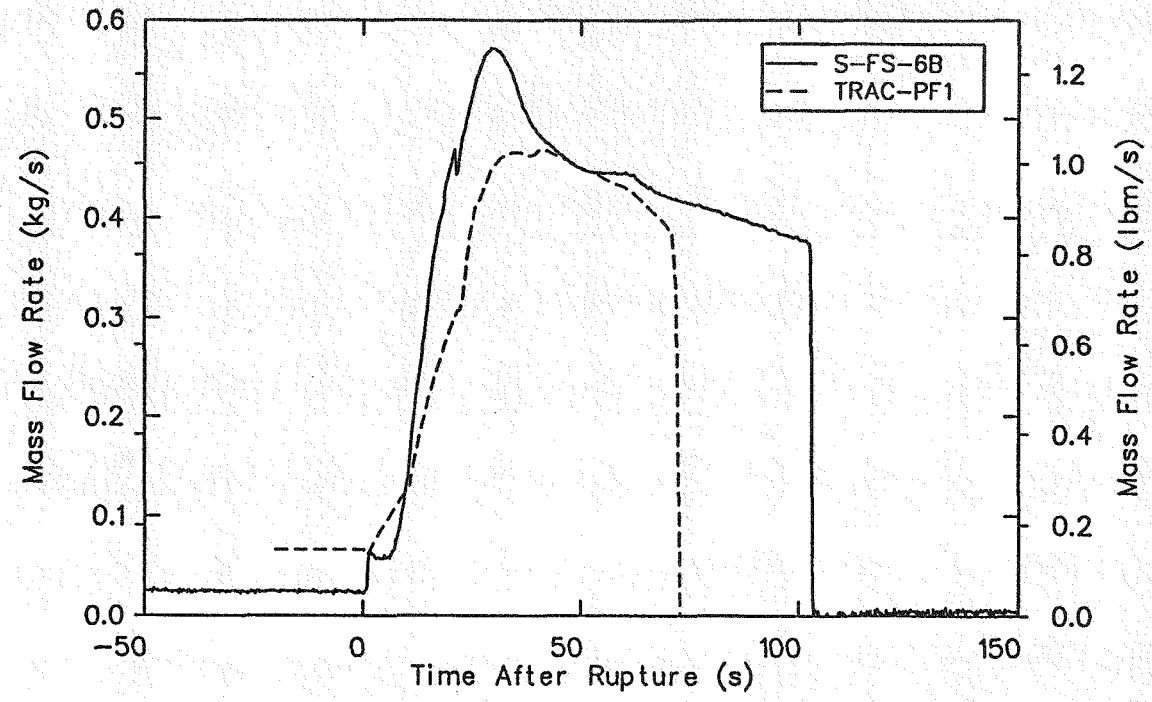

Figure 10. Comparison of measured and calculated crossover line flow rate during the early part of test S-FS-6B.

The higher resistance in the crossover line modeling caused the difference between the calculated secondary pressures to be too large. This further contributed to the lower-than-measured broken loop secondary pressure.

The pump coast down histories and core power decay were well reproduced in the TRAC-PF1/MOD1 calculation, as shown in Figures 9c and 9d, respectively. Discrepancies are evident in the history of the combined energy removal rate of the steam generators (see Figure 9d). The features of the measured and calculated histories are the same and the differences are within the tolerance on the energy removal rate calculated using measured data. The differences should not, however, necessarily be dismissed as simply due to measurement uncertainty.

The Safety Injection System (SIS) actuation signal occurred when the broken loop secondary pressure reached 4.47 MPa (648.2 psia), 67 s in the calculation compared to 99 s in the test. Auxiliary feedwater was initiated at this time and the crossover line valve was closed. Closure of the crossover line valve is reflected in the measured and calculated secondary pressure histories in Figure 9b. After closure, the broken loop secondary pressure decayed due to flow out the break and the intact loop secondary pressurized due to the loss of the energy vent via the crossover line flow. Comparison of the measured and calculated secondary pressure histories shows that crossover line valve closure occurred 30 s earlier in the TRAC-PF1/MOD1 simulation than in the test. The early occurrence of the SIS signal in the simulation resulted from the calculated broken loop secondary pressure being too low for the reasons previously discussed.

The auxiliary feedwater flow rates were well reproduced. The broken loop auxiliary feedwater was initiated in the simulation 30 s before it was initiated in the test because of the early SIS signal. The intact auxiliary feedwater was initiated the same time as that for the broken loop in the TRAC-PF1/MOD1 simulation. The test data showed that the intact loop auxiliary feedwater was not initiated until approximately 300 s, instead of at about 100 s when the SIS signal occurred. The intact loop auxiliary feedwater was initiated in the TRAC-PF1/MOD1 simulation 230 s before it was initiated in the test. This discrepancy did not have a discernible effect on the calculated system response relative to the measured data.

Closure of the crossover line valve was the last automated action to be simulated. From the time of valve closure until the end of the test at 600 s, the primary system response was governed by the energy balance on the system. The energy balance included energy input from the decaying core power, energy removal through the intact loop steam generator, heat transfer to or from the walls of the primary and intact loop secondary system components, and energy lost due to leakage from the system. The calculated primary

system pressure history during the entire blowdown is compared with the measured history in Figure 11. The measured and calculated histories are in good agreement until about 75 s. After 75 s, the measured pressures decrease monotonically. The calculated pressures rise between 75 and 115 s. The difference between the measured and calculated pressures increases slightly between 115 and 240 s and at 240 s, the calculated pressures begin an almost linear increase. At the end of the blowdown, the calculated pressures are about 1.2 MPa (174 psi) higher than the measured values.

Ideally, differences between the calculated and measured primary and secondary pressure histories would be explained solely with reference to differences in the calculated and measured energy balances on these two systems. Comparisons of calculated and measured pressurizer pressure, intact and broken loop secondary pressures, core power, and total energy removal rate (sum of the primary-to-secondary heat transfer rate in both generators) are given in Figure 12. As discussed above, both of the calculated secondary pressures decreased too rapidly resulting in an early SIS signal. Figure 12 illustrates again that the calculated total energy removal rate was larger than the corresponding measured data during the period when both of the secondary pressures were decreasing and does not provide an explanation for the observed difference between the calculated and measured data, as has been discussed. Differences in the calculated and measured relationships between the core power level and the total energy removal rate do explain differences observed between the calculated and measured primary pressure histories. After having assumed a nearly constant value at about 115 s, the calculated primary pressure began an almost linear increase at about 240 s. Figure 12 shows that this event corresponded approximately to the time the calculated total energy removal rate via the steam generators decreased below the core power resulting in a net energy input of the primary fluid. Consideration of the net energy input to the fluid from the piping walls could make the times of the energy crossover point and the change in the pressurization rate of the primary system coincide exactly. At about the same time, an abrupt change in the slope of the calculated intact loop secondary pressure history is noticeable. Further, just before the calculated total energy removal rate decreases to less than the core power, the energy removal rate exhibits an abrupt change in slope. The exact interrelationship of these events is not understood, but they may be related to a change in heat transfer mode at locations within the intact loop steam generator.

In the calculation, it appears that an event occurred on the secondary side of the intact loop steam generator that caused the energy removal capability of the

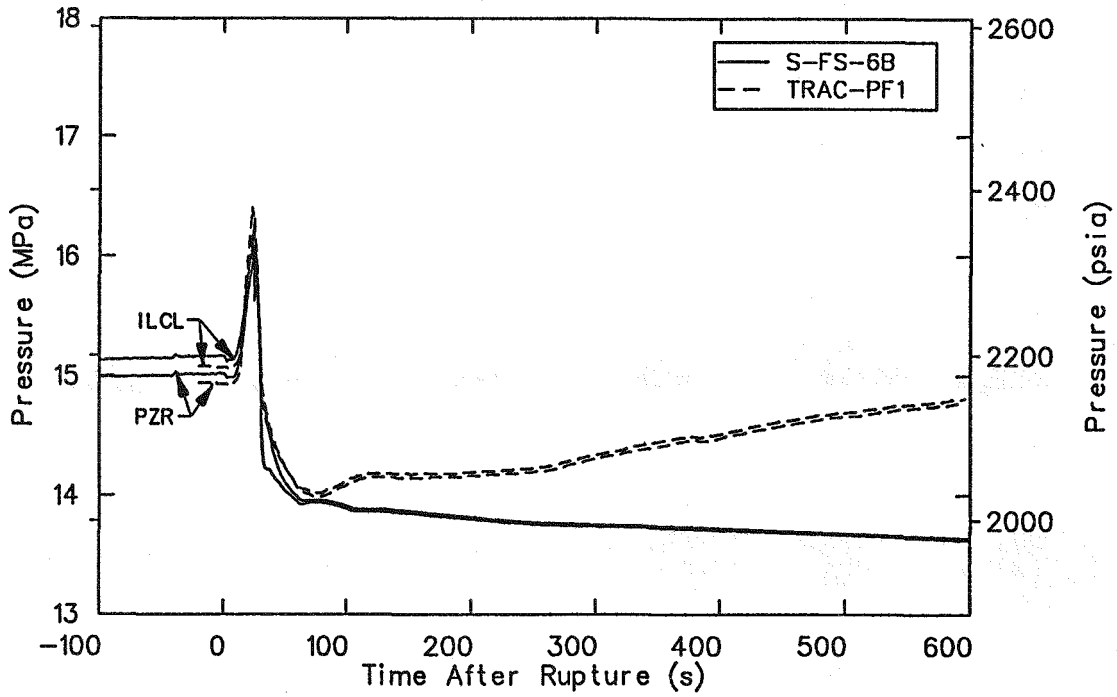

Figure 11. Comparison of measured and calculated pressurizer (PZR) and intact loop cold leg (ILCL) pressures during test S-FS-6B.

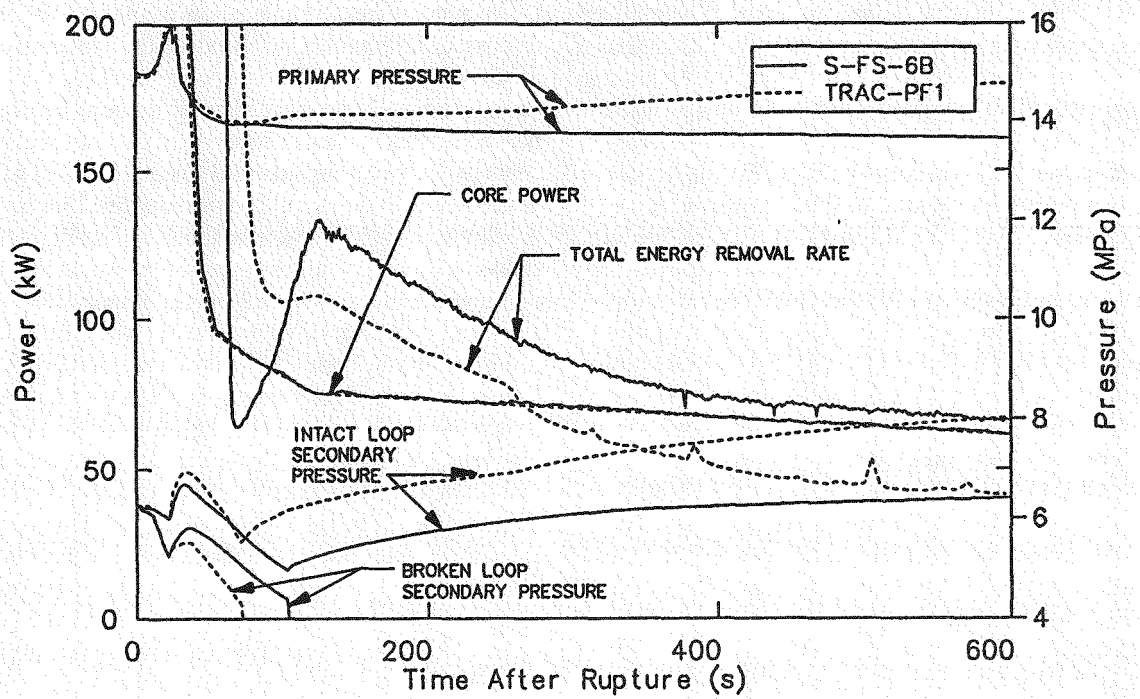

Figure 12. Comparison of measured and calculated primary and secondary pressures, core power, and total energy removal rate during test S-FS-6B.

generator to decrease abruptly. This event is reflected by a change in the slope of the secondary pressure history. The decrease in energy removal capability of the steam generator caused the energy removal rate to fall below the core power resulting in net energy addition to the primary system with subsequent pressurization. An extensive review of calculated parameters associated with the intact loop steam generator failed to show any clear reason for the abrupt decrease in energy removal capability and change in pressurization of the secondary.

Even without the abrupt decrease in the energy removal rate, the rate would have fallen below the core power, unlike the measured energy removal rate that was higher and remained greater than the core power until the end of the blowdown phase. A review of the component and heat transfer modeling associated with the intact loop steam generator is indicated. However, extensive localized heat transfer data is not available for the intact loop steam generator like that available for the broken loop steam generator. The Semiscale intact loop steam generator contains six U-tubes that were lumped into a single tube and contains riser and downcomer filler pieces that were lumped into the riser shell and the downcomer in the TRAC-PF1/MOD1 model. These simplifications may have caused distortions in heat transfer areas and flow resistances that adversely affected the accuracy of simulating the heat removal rate in the steam generator.

Loop temperature histories calculated in the TRAC-PF1/MOD1 simulation are compared with corresponding measured histories in Figures 13 and 14. Most of the trends of the calculated histories are in good agreement with the measured data. The calculated broken loop transport temperature histories in Figure 13 exhibit the phenomena of the cold leg temperature being hotter than the hot leg temperature for a period of about 60 s, as observed in the measured data. This phenomena is the result of the hot leg temperature decreasing due to the SCRAM and the cold leg temperature increasing due to the degradation of the energy removal capacity of the generator and the loop transit time.

The major discrepancy between the calculated and measured broken loop temperature histories is the difference between the hot and cold leg temperatures after the hot leg temperature again becomes higher than the cold leg. The measured data show a sustained temperature difference, while the calculated data show little or no temperature difference. This difference in results is indicative of lower heat removal rates in the broken loop in the calculation than in the test. The calculated hot leg temperatures are high due to the reduced energy removal from the primary system via the intact loop steam generator relative to the test data. The higher

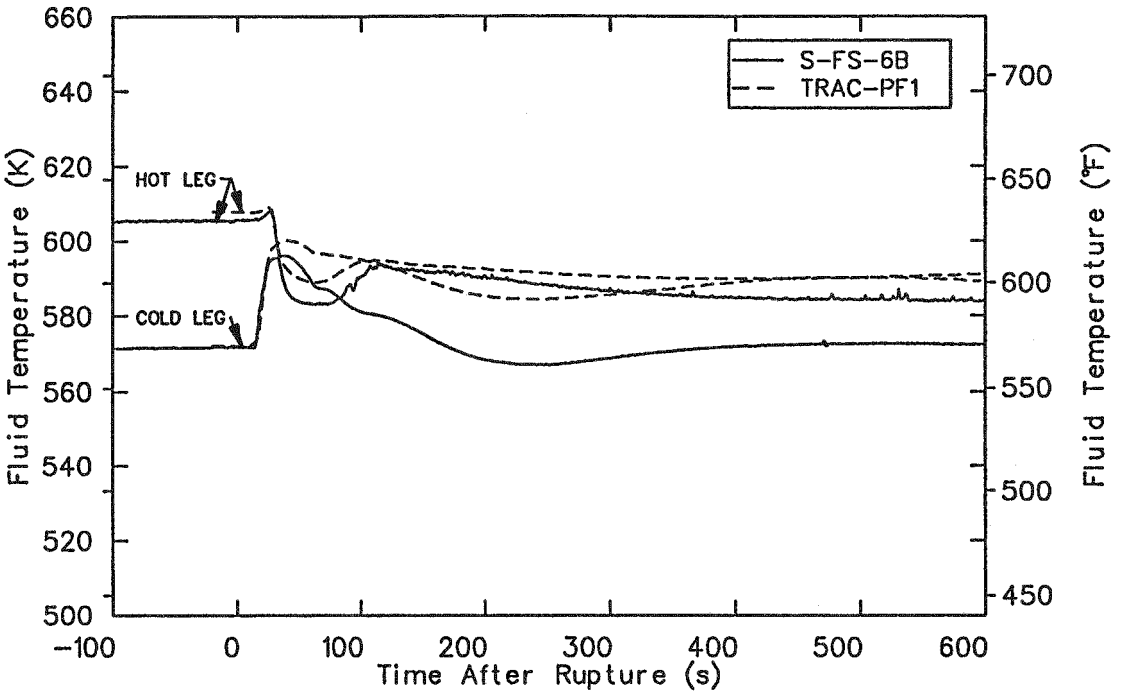

Figure 13. Comparison of measured and calculated broken loop hot and cold leg fluid temperatures during test S-FS-6B.

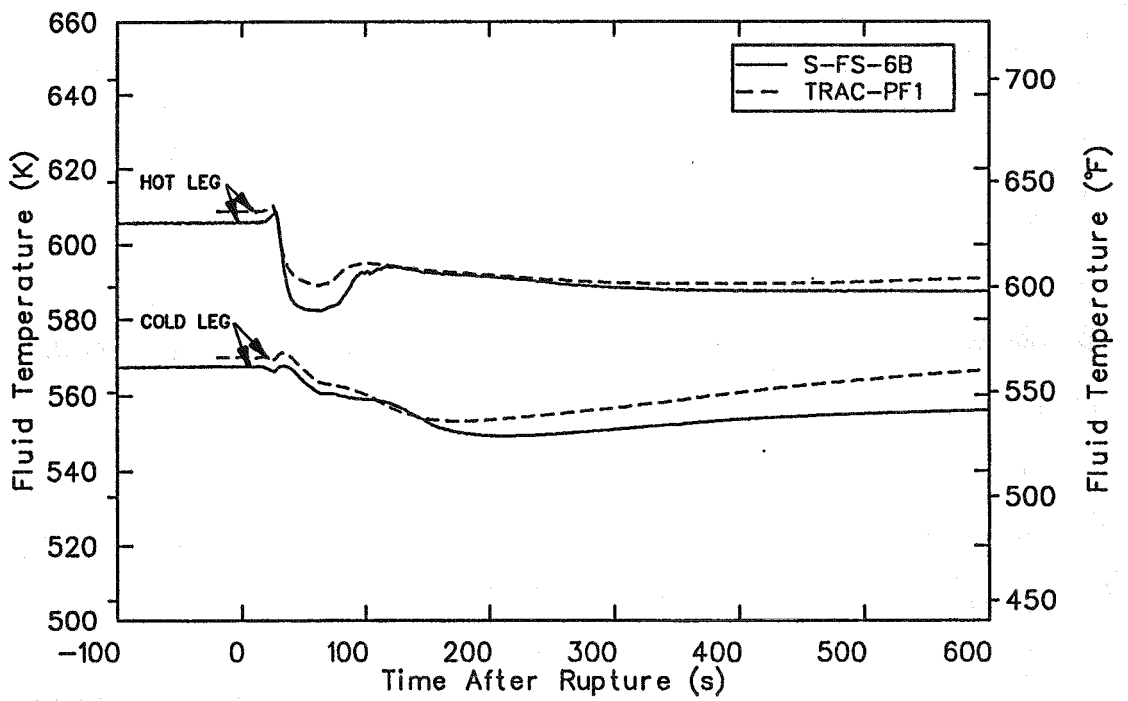

Figure 14. Comparison of measured and calculated intact loop hot and cold leg fluid temperatures during test S-FS-6B.

calculated cold leg temperature indicates that energy removal occurred in the test that was not simulated. This may be due to energy removal in the steam generator and also to heat loss to the environment from the broken loop piping that was not modeled in the TRAC-PF1/MOD1 simulation. The calculated broken loop hot and cold leg temperatures are 3 K (5°F) and 8 K (14°F) too high, respectively, at the end of the blowdown phase of the transient.

The intact loop temperature histories, shown in Figure 14, were well simulated with the difference between the measured and calculated hot and cold leg temperatures being 2 K (4°F) and 5 K (9°F), respectively, at the end of the blowdown phase. The difference between the calculated and measured hot-to-cold leg temperature difference is consistent with the lower heat removal rates in the intact loop in the calculation than in the test.

In summary, TRAC-PF1/MOD1 has demonstrated the ability to calculate most of the trends exhibited in selected data recorded during Semiscale feedwater line break test S-FS-6B. The results of the calculation were in good agreement with the data until the steam control valves were closed at 23 s in the calculation. The calculated results were in fair agreement with the data thereafter until the SIS signal occurred and the crossover line valve was closed at 73 s in the calculation. After 73 s, the calculated results show significant divergences from the measured data that would have jeopardized the ability to continue the calculation into the recovery phase.

Several areas were identified that could improve the TRAC-PF1/MOD1 simulation. Primary-to-secondary heat transfer in the steam generators, particularly in the intact loop steam generator, needs to be modified. Before approximately 100 s, the calculated energy removal rate through the steam generators was too high, which contributed to discrepancies in the the secondary pressure responses relative to the measured data. After 100 s, it was too low, which resulted in the calculated primary pressure differing significantly from its measured counterpart and rising to an unacceptable level by the end of the transient. Simplifications in modeling the steam generators may have been a major cause of the discrepancies in the energy removal rates. In addition to energy removal rate, at least two other reasons were identified for the differences between the calculated and measured secondary pressure response between the time the steam control valves were closed and the SIS signal occurred. Events during this period were important because they determined the time of the SIS signal, which affected the timing of all events thereafter. One reason for the differences in secondary pressure response was lower-than-measured crossover line flow. This result is related to modeling of the crossover line resistance and the minimum area in the crossover line valve. The other reason is that parts of the steam lines connected to each of the steam generators were not modeled, which means that the volumes of the secondary systems were too small. Energy transfer between the metal and the fluid in the steam generators may also have been a contributing cause. Primary system temperature responses indicate that the model may also have to be modified to include modeling of localized heat losses to the environment.

6.2 Broken Loop Steam Generator Response

This subsection provides an evaluation of the ability of TRAC-PF1/MOD1 to calculate the responses of a steam generator during a transient where a break occurs in the bottom feedwater line to the generator. The results of the evaluation are provided by comparing measured and calculated parameters within the affected steam generator. The presentation begins with parameters associated with the feedwater line break flow, includes secondary side flows and inventory and primary and secondary temperatures, and concludes with local and total primary-to-secondary heat transfer.

The principal boundary condition affecting the broken loop steam generator was a simulated 100% break in the bottom feedwater line to the steam generator. A composite of measured and calculated parameter histories associated with the feedwater line break flow are presented in Figure 15. The general features of the calculated break flow history (see Figure 15a) are in fair agreement with the measured data. Notable similarities include the magnitude of the break flow once the supply conditions become single-phase steam and the decay in break flow as the secondary pressure decreases due to closure of the crossover line valve. Notable discrepancies between the calculated and measured break flow histories include the magnitude of the break flow during the first 32 s of the transient and the magnitude of the break flow after the crossover line valve was closed in the TRAC-PF1/MOD1 simulation at 73 s. These discrepancies do not clearly indicate a problem in the break flow modeling in the code, as discussed below.

The comparison of the measured and calculated void fraction histories in Figure 15c indicates that the discrepancies in break flow rate that occurred during the first 32 s of the transient are primarily the result of the calculated void fraction history differing from the measured data. This difference may be the result of the suspected differences between the initial secondary masses used in the calculation [35 kg (77 lbm)] and deduced from a reevaluation of the test data [27 kg

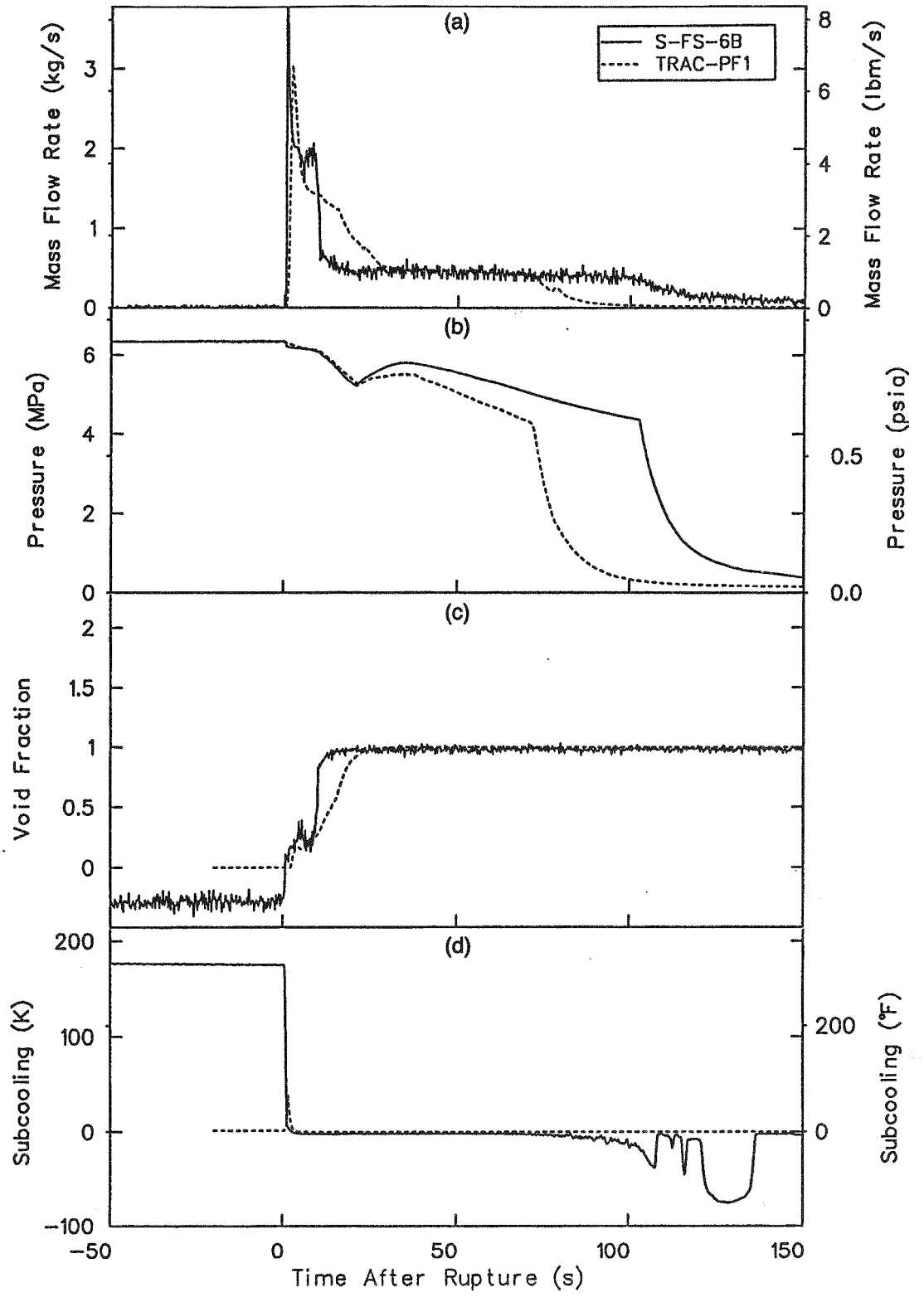

Figure 15. Composite of measured and calculated parameter histories associated with feedwater line break flow during the early part of test S-FS-6B.

(59 lbm)]. (The reevaluation of the initial secondary mass was performed too late to be used in the TRAC-PF1/MOD1 simulation.) The discrepancies in the break flow after 73 s, when the crossover line valve was closed in the TRAC-PF1/MOD1 simulation, is due to the resulting differences in the secondary pressure histories shown in Figure 15b. If the timing of the crossover line valve closure had been predicted properly, the calculated break flow history would have been in good agreement with the data at all times after 32 s.

Comparison of the calculated and measured peak break flow rates shows that the measured value was much higher than the calculated value. This result is understandable because of a large difference between the calculated and measured subcooling immediately upstream of the break valve at the start of the transient, as shown in Figure 15d. The data indicate a high degree of subcooling in the dead leg above the valve before the break was opened. The TRAC-PF1/MOD1 data indicates a saturated liquid condition at the same time and location, which was traced to an error in the input initial conditions where the conditions at this location were set equal to the nominal secondary conditions instead of the conditions that existed before the test.

Calculated and measured flow rates at the steam outlet and internal to the broken loop steam generator are given in Figures 16 and 17, respectively. The calculated histories in Figure 16 are discussed first because they provide a more consistent picture of the flow histories than the measured data. Before the initiation of the transient, the riser flow is equal to the sum of the downcomer flow and the steam flow exiting the steam generator. The riser and steam flows decrease after the break is opened and eventually reverse direction. After closure of the broken loop steam valve, the crossover line supplies flow into the generator and the reversed direction steam flow is equal to, but opposite in sign from, the crossover line flow. The steam flow splits into the reverse riser flow and the downcomer flow. These relationships exist until the crossover line valve is closed, then all the flows go quickly to zero.

Measured broken loop steam generator flow rate histories are presented in Figure 17. These histories indicate the proper relationship between the riser, downcomer, and steam flows before transient initiation. The initial calculated riser and downcomer flows are slightly higher than the measured values. After the break was opened, the riser and steam flows decreased. The steam flow reversed although the measurement became unreliable shortly thereafter, but the riser flow did not. After closing the steam valve, the relationships that are indicated by the calculated results do not exist in the test data. The steam flow may have been equal to the crossover line flow, but opposite in sign, as in the calculation. The riser and downcomer flows were equal and of the same sign, seeming to indicate

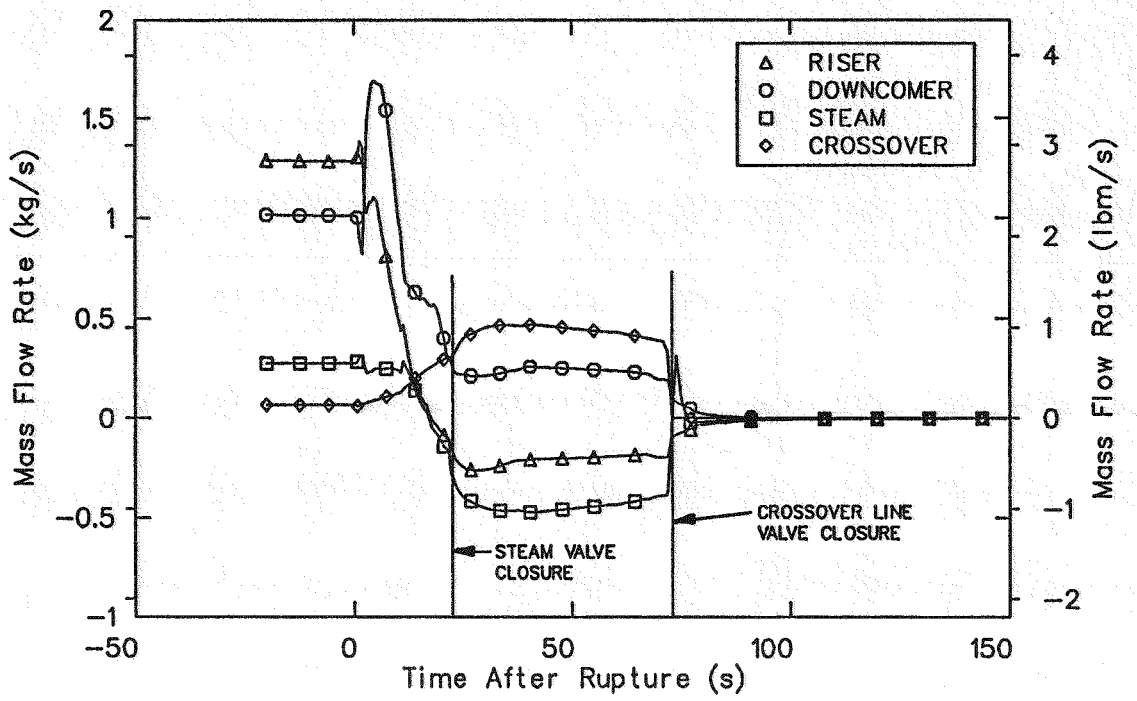

Figure 16. Calculated broken loop steam generator external and internal flow rates during the early part of test S-FS-6B.

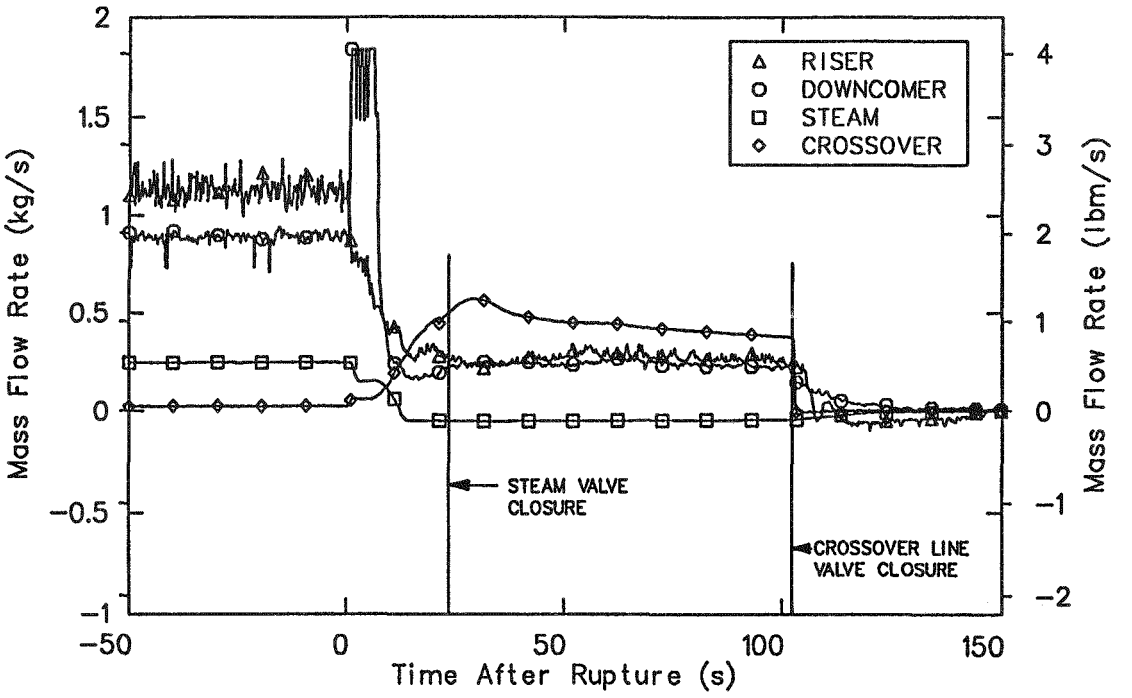

Figure 17. Measured broken loop steam generator external and internal flow rates during the early part of test S-FS-6B.

that flow continued to come up the riser instead of reversing direction, and all of the flow coming up the riser passed into the downcomer. The path of the incoming steam flow from the crossover line remains in question. Significant differences exist between the calculated and measured flows in the steam generator, which are believed to be due to measurement errors.

In order to verify whether the relationships between the flow rates associated with the broken loop steam generator (presented in Figure 17) were correct, similar flow data measured in test S-FS-6 (the first 100% break test) were reviewed and are presented in Figure 18. These data verify the relationships exhibited in the TRAC-PF1/MOD1 data both before transient initiation and after the steam valves were closed. Following closure of the steam valve, a reversed riser flow is indicated and the absolute sum of the riser and downcomer flows equals the crossover line flow. The data do not show that the steam flow was equal to, but opposite in sign from, the crossover line flow, as indicated by the calculated results because the steam flow measurement was unreliable for reversed flows.

Heat transfer in the generator is partially dependent upon secondary side liquid level and void fraction distribution. Comparisons between calculated and measured collapsed liquid levels in the riser and downcomer are given in Figures 19 and 20, respectively. Both the measured and the calculated collapsed liquid level histories indicate that the riser and the downcomer drained nearly uniformly. In general, the calculated histories are in good agreement with the measured data. The principal differences between the calculated and measured data are the initial values and a brief holdup in the decrease of the liquid level in the calculated histories, which is reflected in the void fraction histories in the riser and at the break. These results may be due to the suspected differences between the simulated and measured initial secondary masses.

The calculated and measured riser void fraction histories, shown in Figures 21 and 22, indicate that the void fraction begins to rise immediately after the break was opened because of vaporization due to the decreasing secondary pressure. The measured data indicate a rapid rise in void fraction to a steam condition at all elevations. The calculated histories at elevations corresponding approximately to the lower half of the U-tube (see Figure 21) differ from the measured data part of the time during the first 17 s of the transient by indicating a holdup in the void fraction rise at some point before reaching a void fraction of 1.0. The calculated void fraction histories at the upper elevations corresponding approximately to the upper half of the U-tube (see Figure 22) indicate a nearly monotonic rise from the initial void fraction to a steam condition, which is in good agreement with the measured data although slightly delayed. The holdup in the rises of the calculated void fraction histories may be due to a greater initial secondary mass than indicated

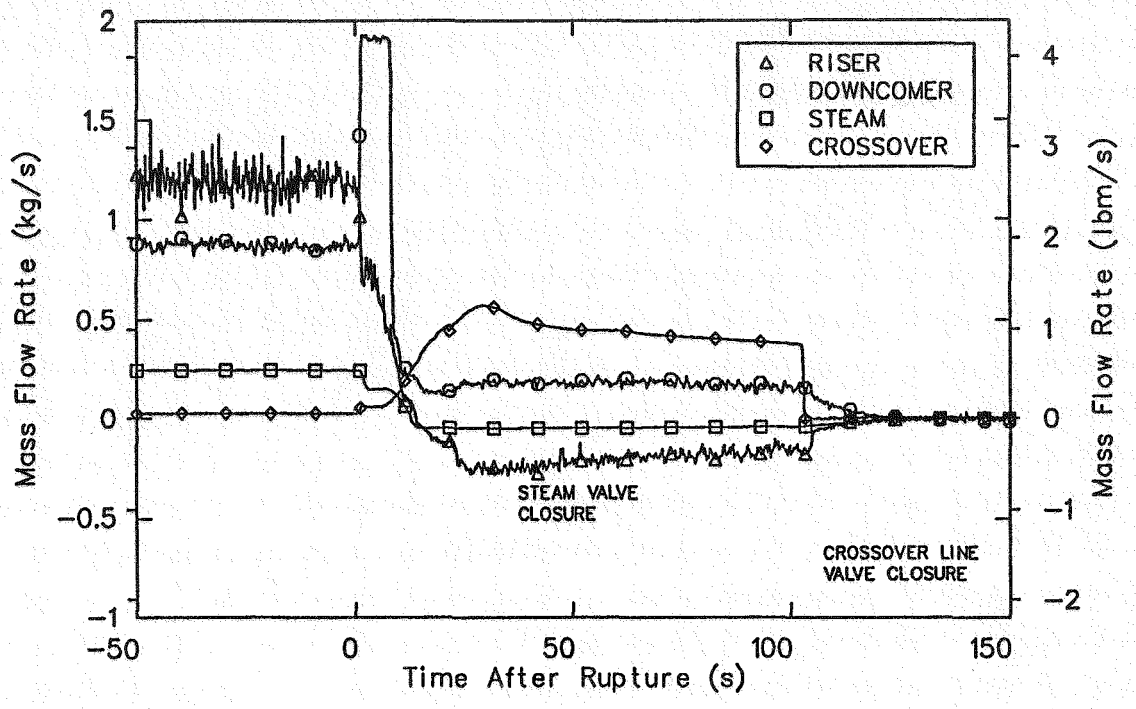

Figure 18. Measured broken loop steam generator external and internal flow rates during the early part of test S-FS-6.

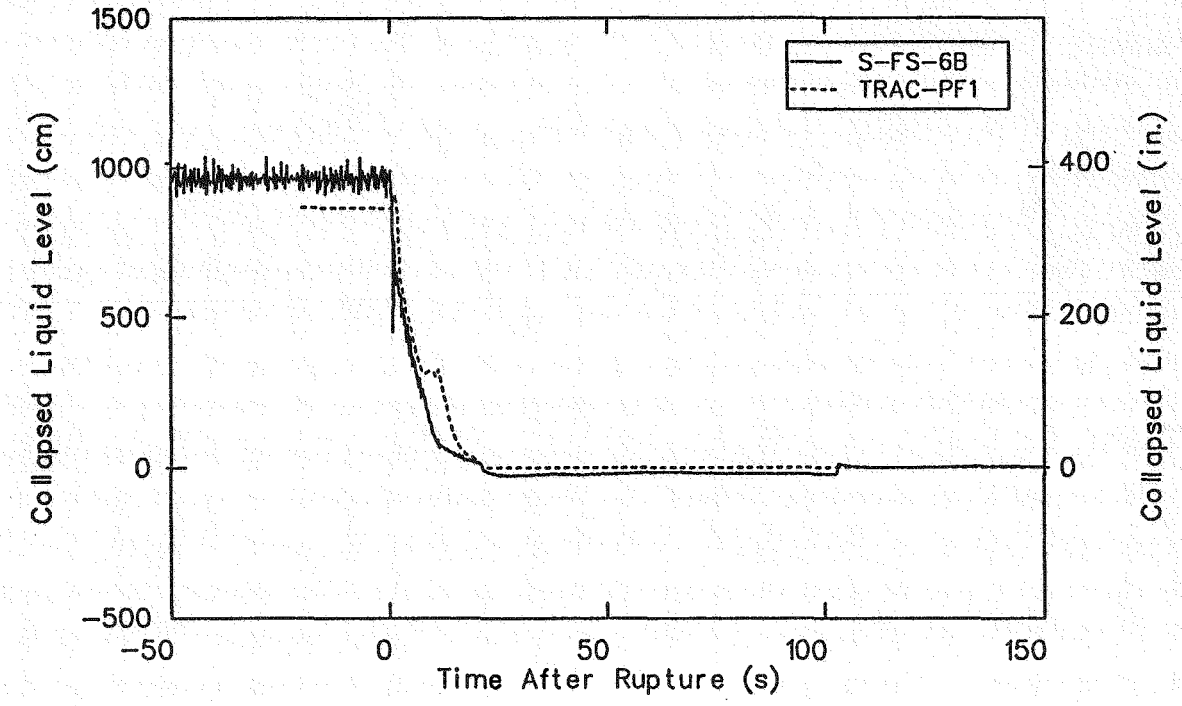

Figure 19. Comparison of measured and calculated broken loop steam generator riser collapsed liquid level during the early part of test S-FS-6B.

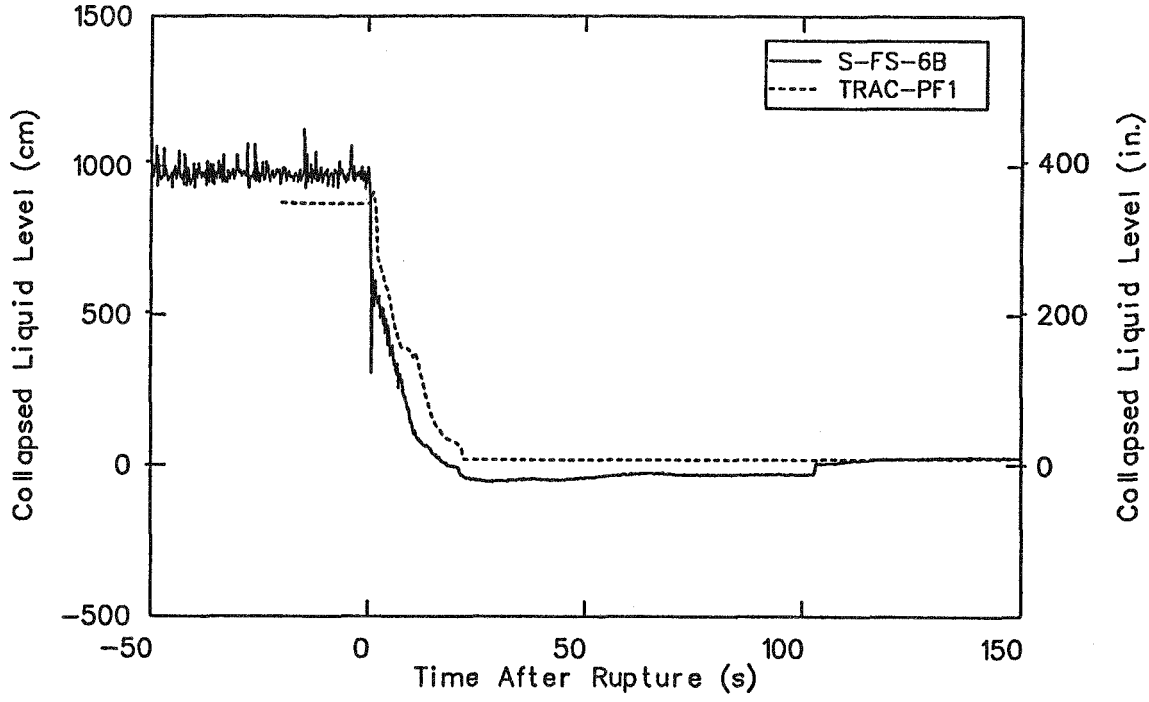

Figure 20. Comparison of measured and calculated broken loop steam generator downcomer collapsed liquid level during the early part of test S-FS-6B.

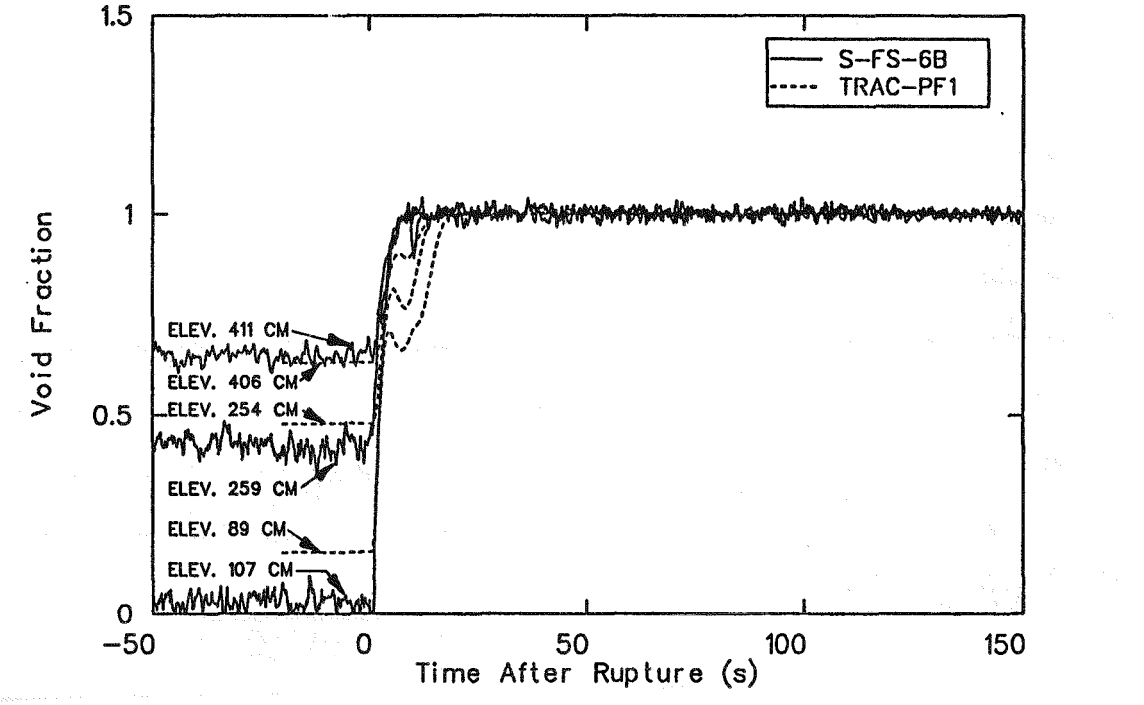

Figure 21. Comparison of measured and calculated lower riser void distribution during the early part of test S-FS-6B.

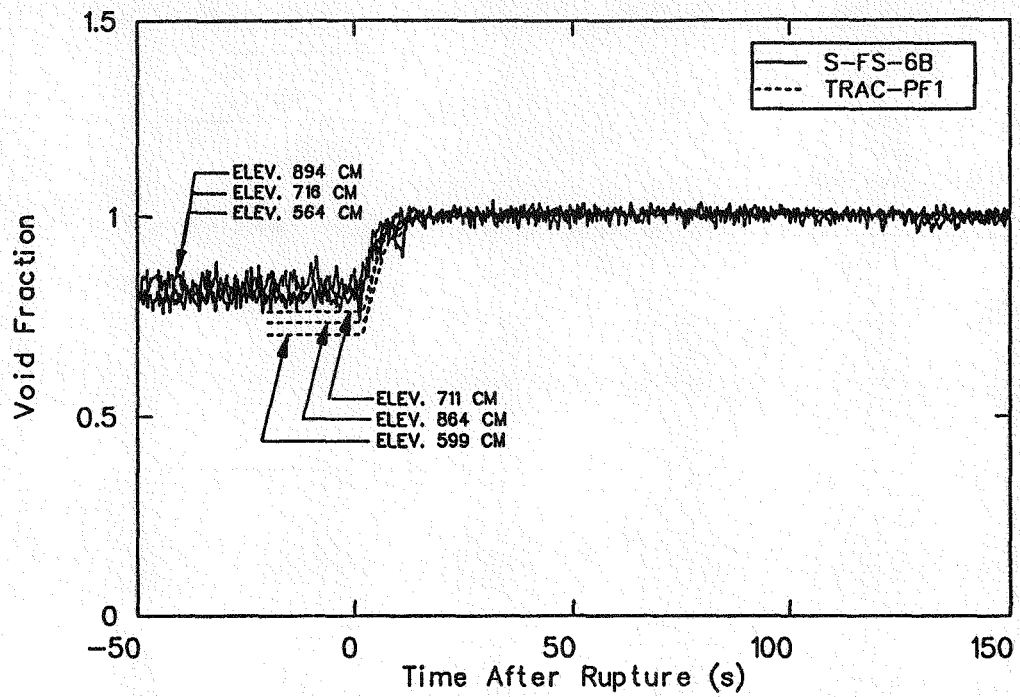

Figure 22. Comparison of measured and calculated upper riser void distribution during the early part of test S-FS-6B.

by the experimental data, as previously discussed. Another possible source of the differences could be the riser resistance used in the model. Increasing the riser resistances would increase the rate of voiding and the calculated collapsed liquid levels, making them equal to or greater than the measured data and more consistent with the initial secondary mass used in the calculation being greater than the measured mass.

Measured and calculated primary and secondary temperatures at lower and upper elevations occupied by the U-tubes are compared in Figures 23 and 24 for the upside and downside of the U-tube, respectively. The measured primary temperatures in these figures are for the long tube and are typical of the primary temperature histories. The calculated primary temperatures are liquid temperatures. The calculated secondary temperatures are vapor temperatures. These temperatures are the most representative of the conditions that existed in the U-tubes and the riser, respectively, during the transient. Calculated secondary liquid temperature is included in Figures 23 and 24 for comparison. The figures show that the calculated histories are either in good agreement with the measured data or at least exhibit the correct trends where the two sets of data do not agree well numerically. Proper timing of the SIS signal in the calculated data would have resulted in much improved agreement between the calculated and measured riser fluid temperatures.

The ability of TRAC-PF1/MOD1 to calculate local heat transfer under transient conditions was evaluated by comparing calculated heat transfer coefficients and heat fluxes with heat transfer data evaluated using primary and secondary fluid temperature and wall temperature measurements made at the same elevation. Comparisons of calculated and measured primary side heat transfer coefficients are presented in Figures 25 through 27 for lower elevations on the upside of the tube, upper elevations on the upside of the tube, and the full range of elevations on the downside of the tube, respectively. Measured data for both the long and short tubes in the Semiscale broken loop steam generator are given. The comparisons at all locations indicate the same results. The calculated heat transfer coefficients are bounded by the measured values, with the calculated values being in better agreement with the data corresponding to the short tube than that corresponding to the long tube. This result is not reflective of the fact that the comparison of steady-state heat fluxes in Section 5 indicated that the calculated heat fluxes were in better agreement with the data associated with the long tube than that associated with the short tube. This is the result of differences between the measured and calculated wall and primary fluid temperatures.

Comparisons of calculated and measured secondary side heat transfer coefficients on the upside and downside of the U-tubes are provided in Figures 28 and 29, respectively. The data in both figures show significant

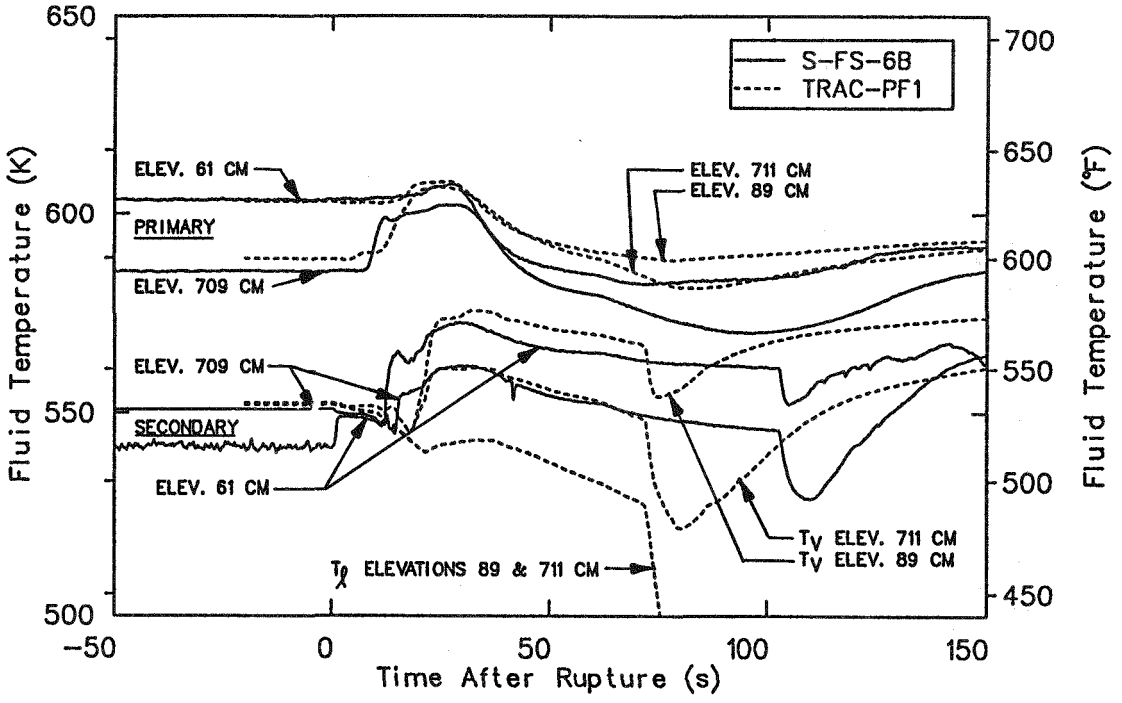

Figure 23. Comparison of measured and calculated primary upside and secondary temperatures at U-tube upper and lower elevations during the early part of test S-FS-6B.

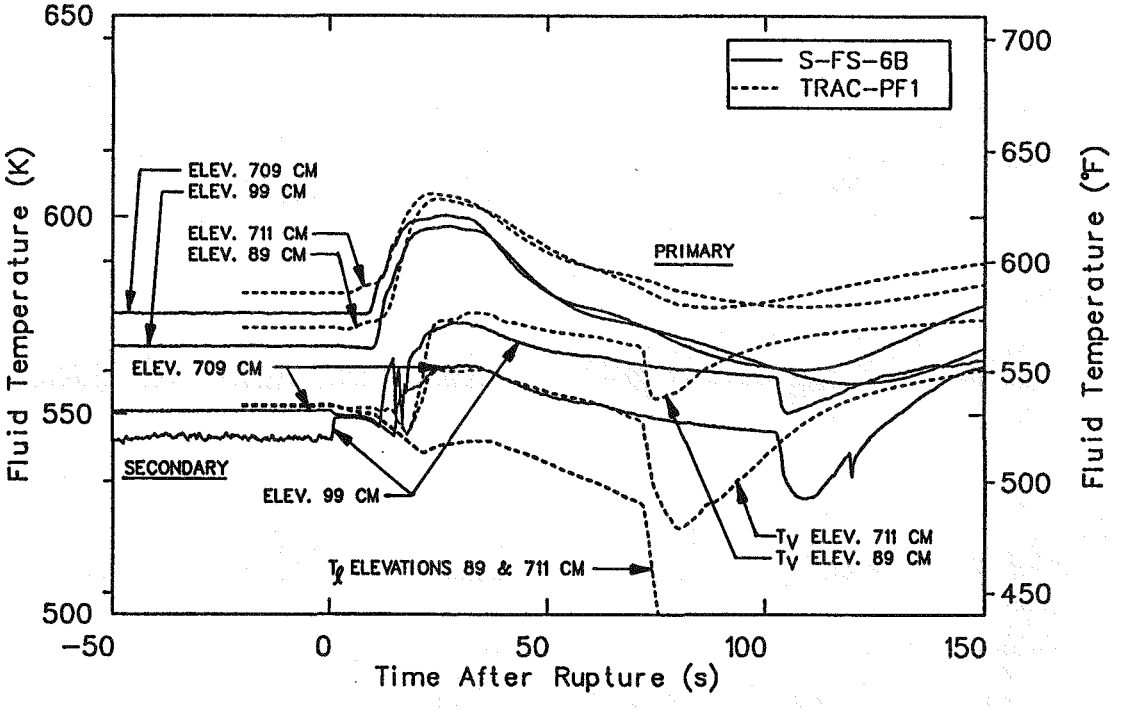

Figure 24. Comparison of measured and calculated primary downside and secondary temperatures at U-tube upper and lower elevations during the early part of test S-FS-6B.

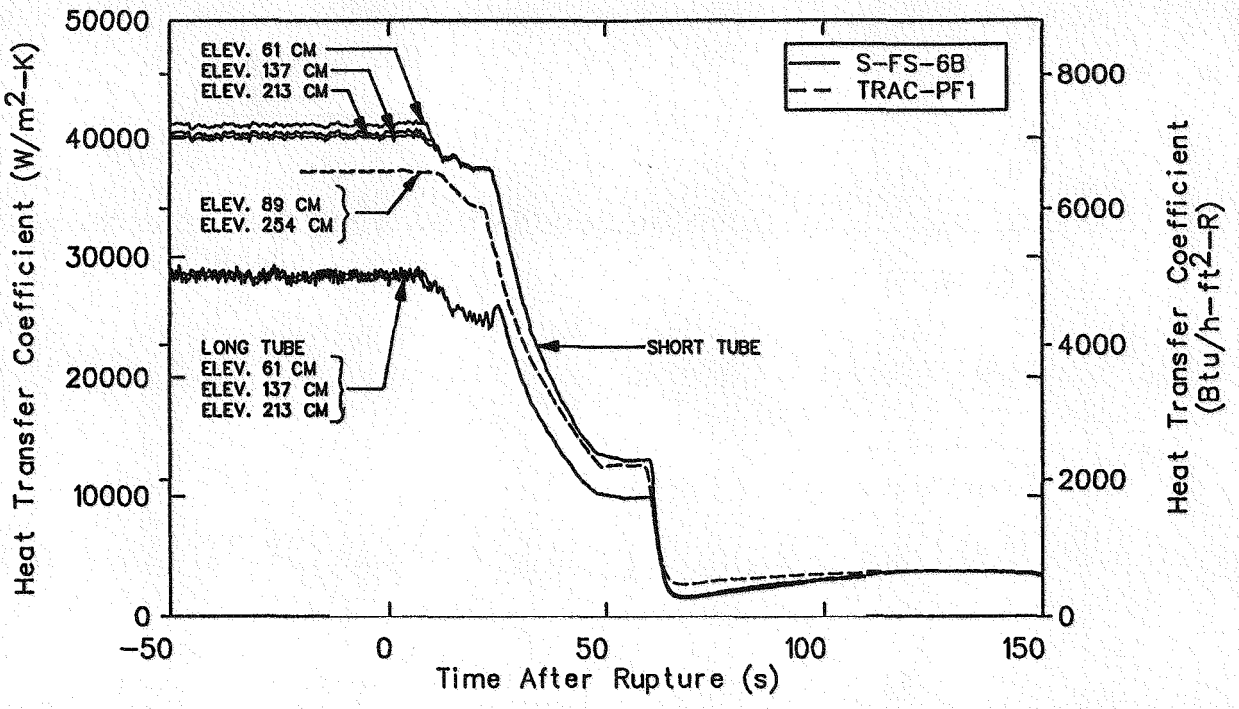

Figure 25. Comparison of measured and calculated primary upside heat transfer coefficients at the lower elevations during the early part of test S-FS-6B.

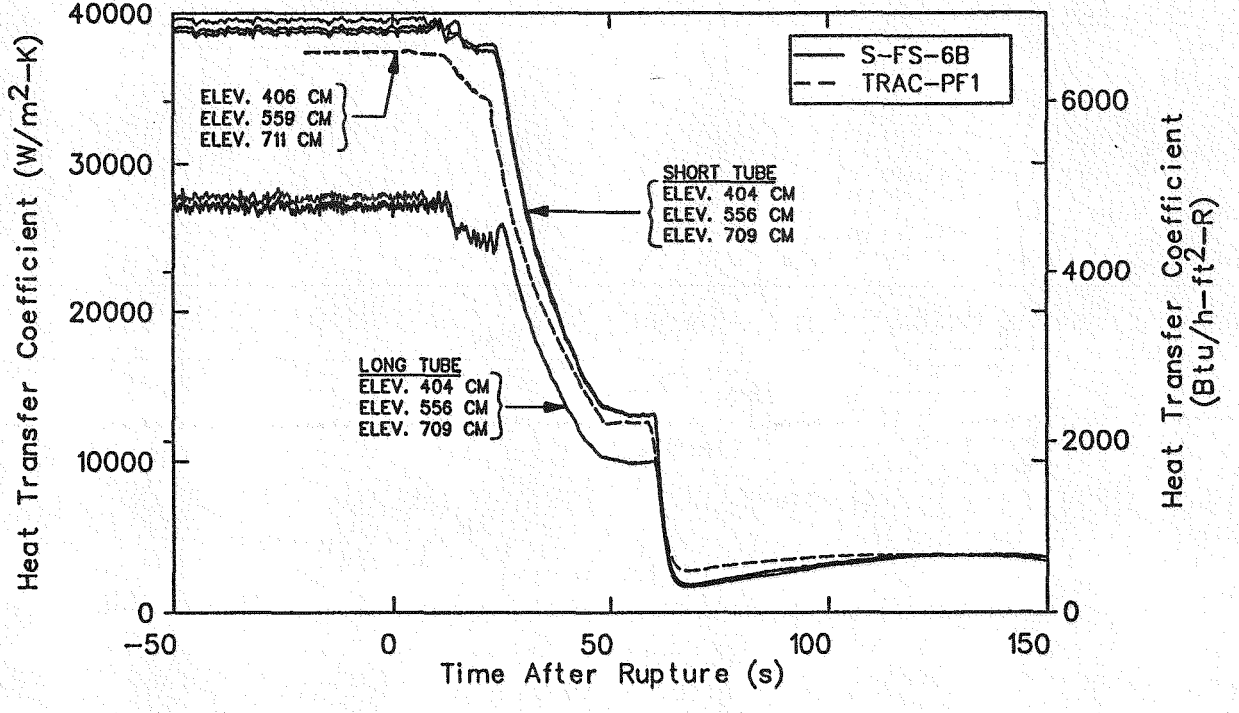

Figure 26. Comparison of measured and calculated primary upside heat transfer coefficients at the upper elevations during the early part of test S-FS-6B.

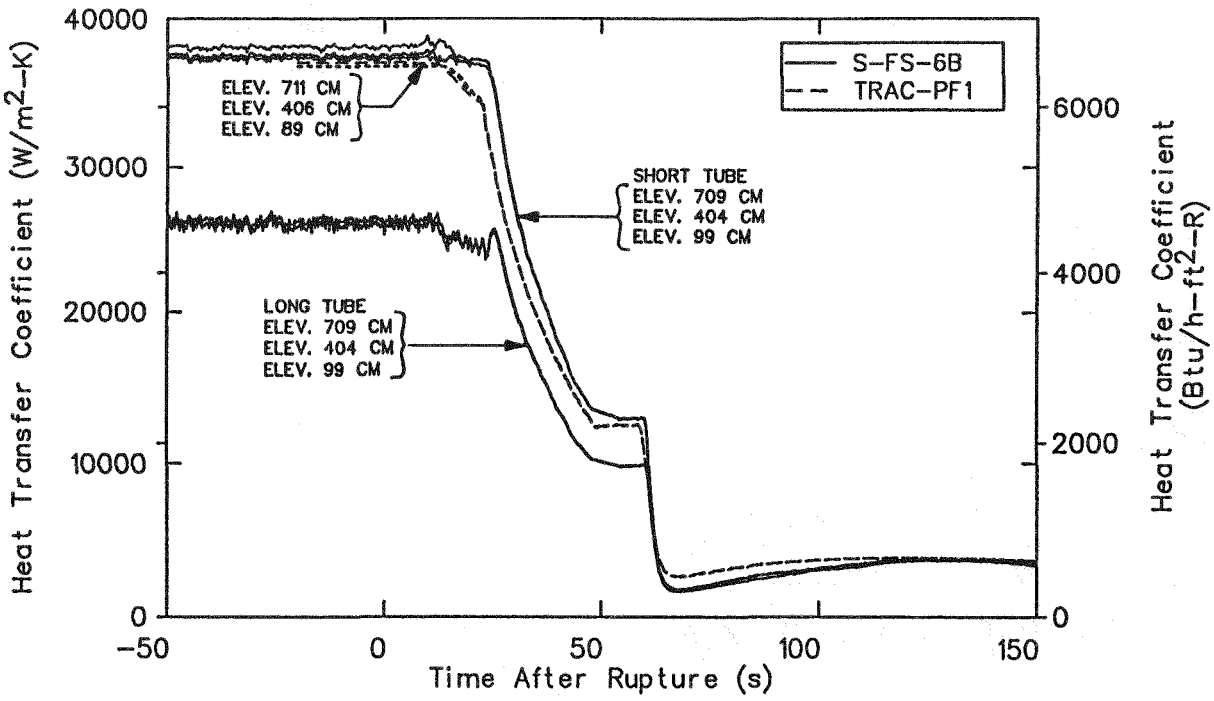

Figure 27. Comparison of measured and calculated primary downside heat transfer coefficients during the early part of test S-FS-6B.

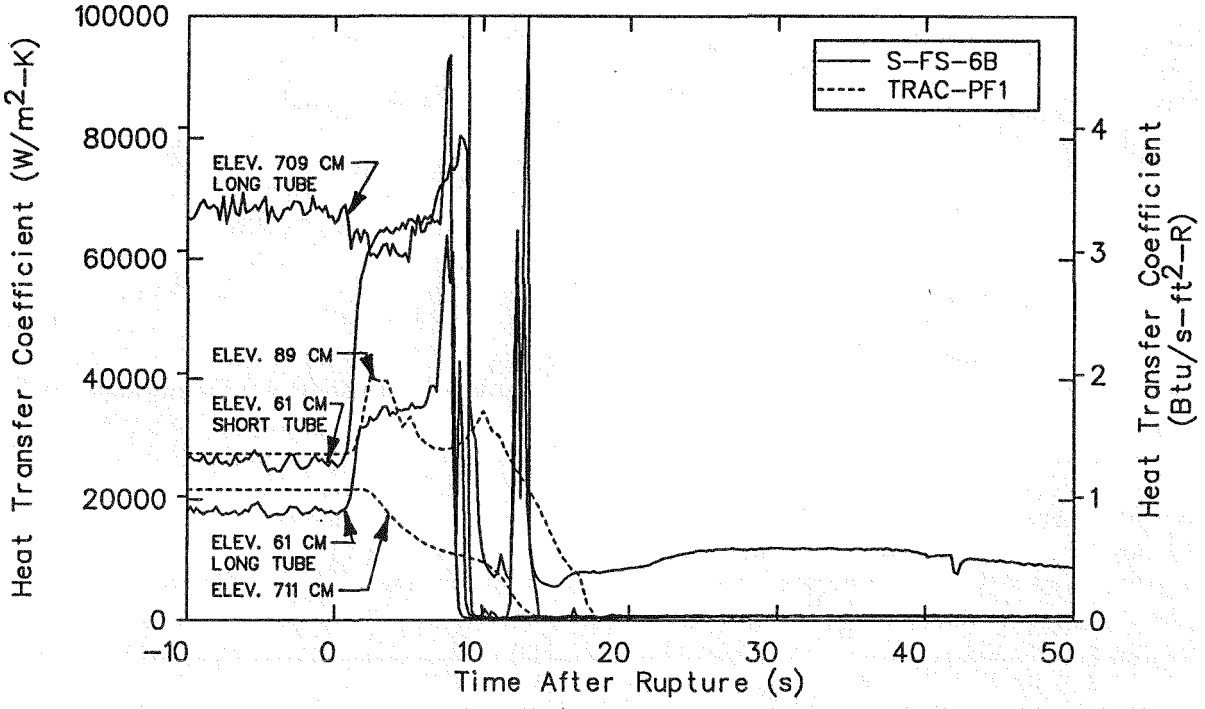

Figure 28. Comparison of measured and calculated secondary upside heat transfer coefficients during the early part of test S-FS-6B.

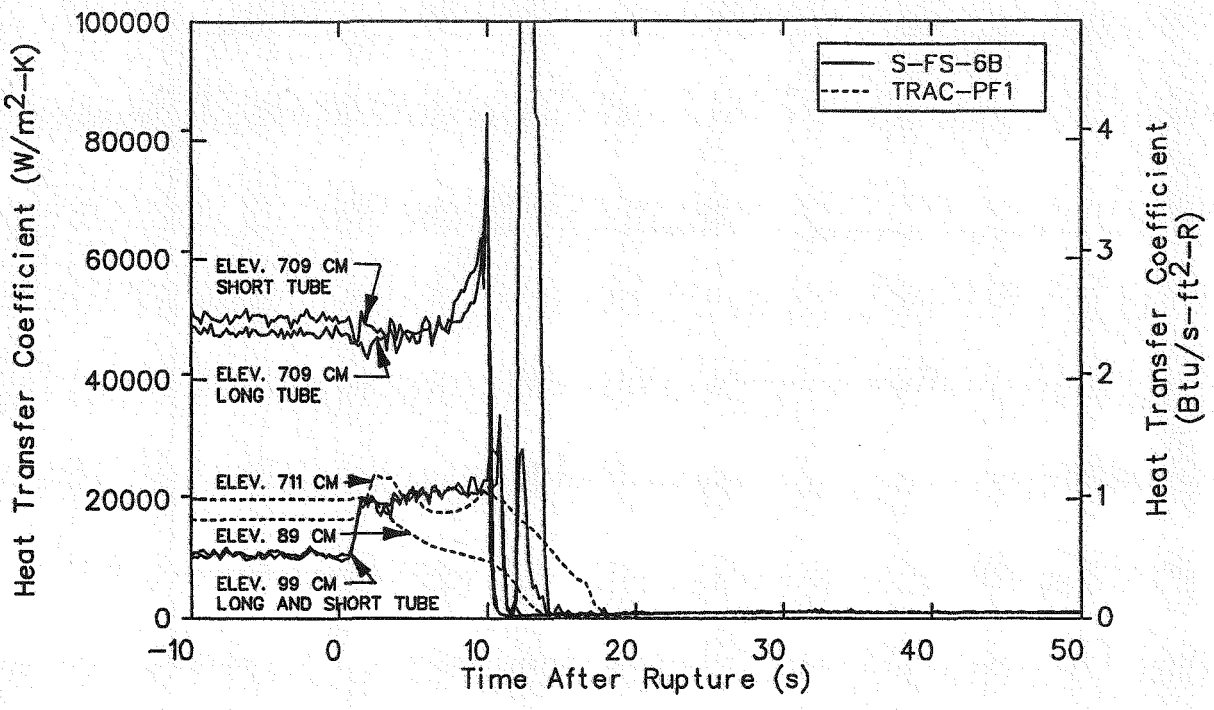

Figure 29. Comparison of measured and calculated secondary downside heat transfer coefficients during the early part of test S-FS-6B.

differences between the calculated and measured results. The measured data in Figure 28 indicate that before the start of the transient, the value of the heat transfer coefficient increased with increasing elevation. The measured data also show that the heat transfer coefficient associated with the short tube was higher than that associated with the long tube at the same elevation. In contrast to the measured data, the calculated heat transfer coefficients decrease with increasing elevation and indicate a much smaller variation in value from the bottom to the top of the tube. The calculated heat transfer coefficient at the lowest elevation was in reasonable agreement with the values for the lowest measurement station. It is interesting to note that in spite of the large differences between the measured and calculated data, the calculated heat transfer coefficients in Figure 28 do exhibit some of the same behavior as seen in the measured data during the transient. Shortly after transient initiation, the calculated coefficient at the lowest elevation rises immediately while the calculated coefficient at the upper elevation begins to decrease similar to their measured counterparts. The measured coefficients decrease to zero abruptly between 8 and 9 s, while the calculated coefficients begin their decrease to zero at 11 s. The differences in the starting time and the rate of the decrease are probably related to the larger initial secondary mass used in the calculation.

The comparison of downside heat transfer coefficients (shown in Figure 29) shows better agreement between the calculated and measured results. The variation of heat transfer coefficient with elevation, indicated by the measured data, was reproduced in the calculation although the variation in the calculated heat transfer coefficients is much smaller than that indicated by the data. As with the upside, the calculated heat transfer coefficient at the lowest elevation is in reasonable agreement with its measured counterparts. The calculated coefficients also exhibit some of the correct trends during the transient. The calculated coefficient at the lowest elevation increased shortly after transient initiation while the calculated coefficient at the highest elevation did not, which is consistent with the measured results. The calculated results also began their decrease to zero at 10 s, which coincided with the time indicated by the measured data. As with the upside, the calculated coefficients decreased gradually compared to a rapid decrease indicated by the measured data, which is probably associated with the difference between the secondary mass used in the calculation and what existed in the test.

Calculated and measured primary side heat fluxes for the upside and downside are compared in Figures 30 and 31, respectively, and show the same results. The initial calculated heat fluxes were in fair agreement with, but lower than, the data measured at

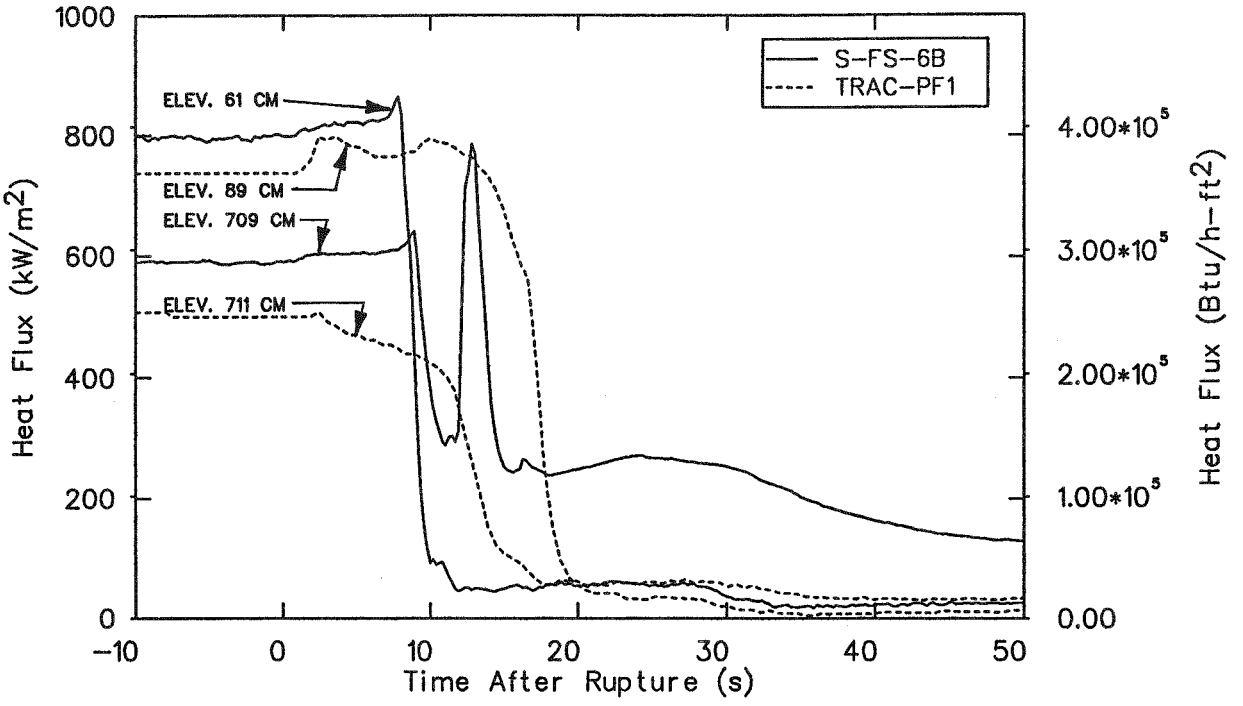

Figure 30. Comparison of measured and calculated primary upside heat fluxes during the early part of test S-FS-6B.

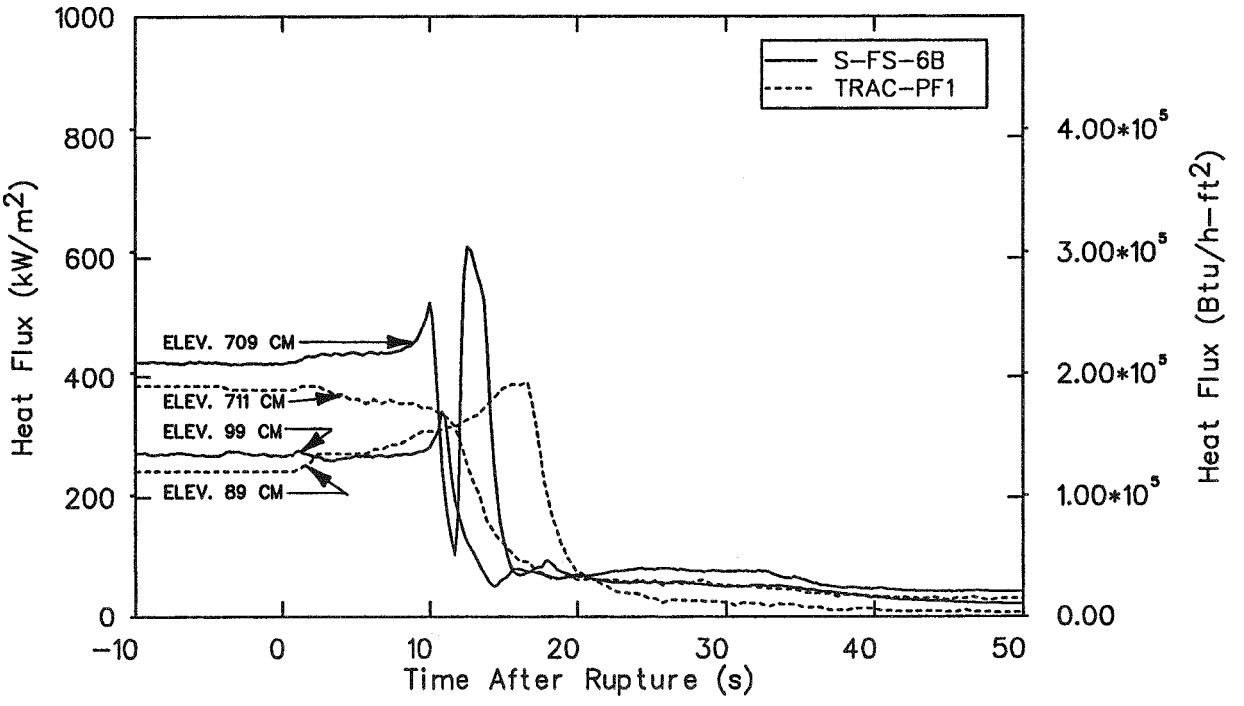

Figure 31. Comparison of measured and calculated primary downside heat fluxes during the early part of test S-FS-6B.

approximately the same elevation. The calculated heat fluxes generally do not agree well with the measured data during the transient. The calculated data also do not show a resurgence in the heat flux at the upper elevations as indicated by the measured data after 10 s. Correcting the initial secondary mass used in the calculation would probably increase the agreement with the measured data after about 8 s.

The integrated effect of the local heat fluxes are shown in Figure 32, where the calculated history of primary-to-secondary energy removal rate through the broken loop steam generator is compared with corresponding experimental data. This comparison shows that the decay in the calculated energy removal started at the same time as that indicated by the test data. However, discrepancies between the calculated and measured histories are evident in the decay history between 17 and 100 s. The difference in initial values and differences during the transient are in varying degrees, the result of the combined measurement uncertainties of the experimental data used to determine the energy removal rate.

Another approach to looking at the net energy removal rate is to view it as a function of secondary mass rather than as a function of time. Calculated and measured data are presented in this form for comparison in Figure 33. This figure shows that although the calculated energy removal rate history agreed well with the experimental data in a temporal reference, significant differences are evident when viewed as a function of secondary mass. Figure 34 shows that the difference in behavior shown in Figure 33 is the result of the difference in the secondary mass histories. The initial calculated and measured secondary masses are indicated to differ by 9 kg (19.8 lbm). If the measured mass history shown in Figure 34 is correct, it is clear from Figure 33 that the calculated correspondence between secondary mass and energy removal rate is not the same as exhibited by the experimental data.

Viewed in total, the ability of TRAC-PF1/MOD1 to calculate the response of the broken loop steam generator during a simulated 100% bottom feedwater line break must be considered to be fair. The code calculated the correct general trends in the histories of nearly all of the hydraulic parameters that were compared. The evaluation was clouded by an uncertainty in measurement of the initial mass in the broken loop steam generator secondary and by shortcomings in simulating the response of other system components that influenced the broken loop steam generator response. Correction of these deficiencies would significantly improve the accuracy of modeling the broken loop steam generator response.

An evaluation of the ability of TRAC-PF1/MOD1 to calculate localized heat transfer parameters under the transient conditions caused by the simulated 100%

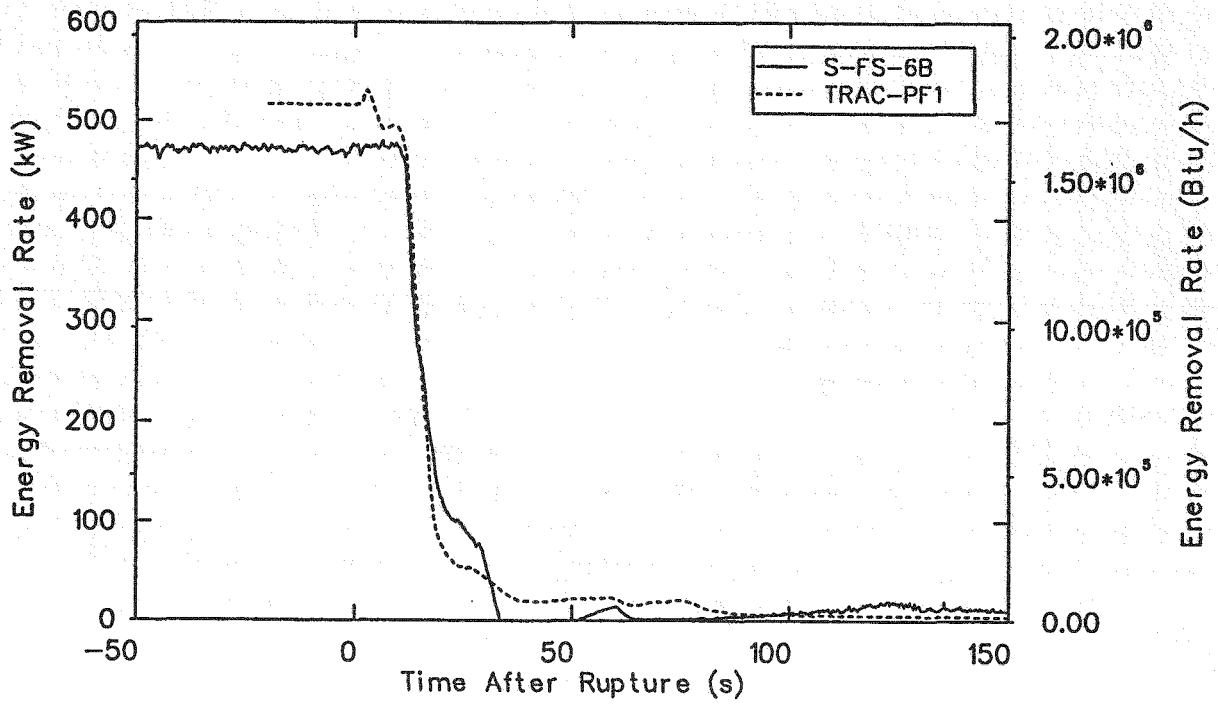

Figure 32. Comparison of measured and calculated broken loop primary-to-secondary heat transfer rate during the early part of test S-FS-6B.

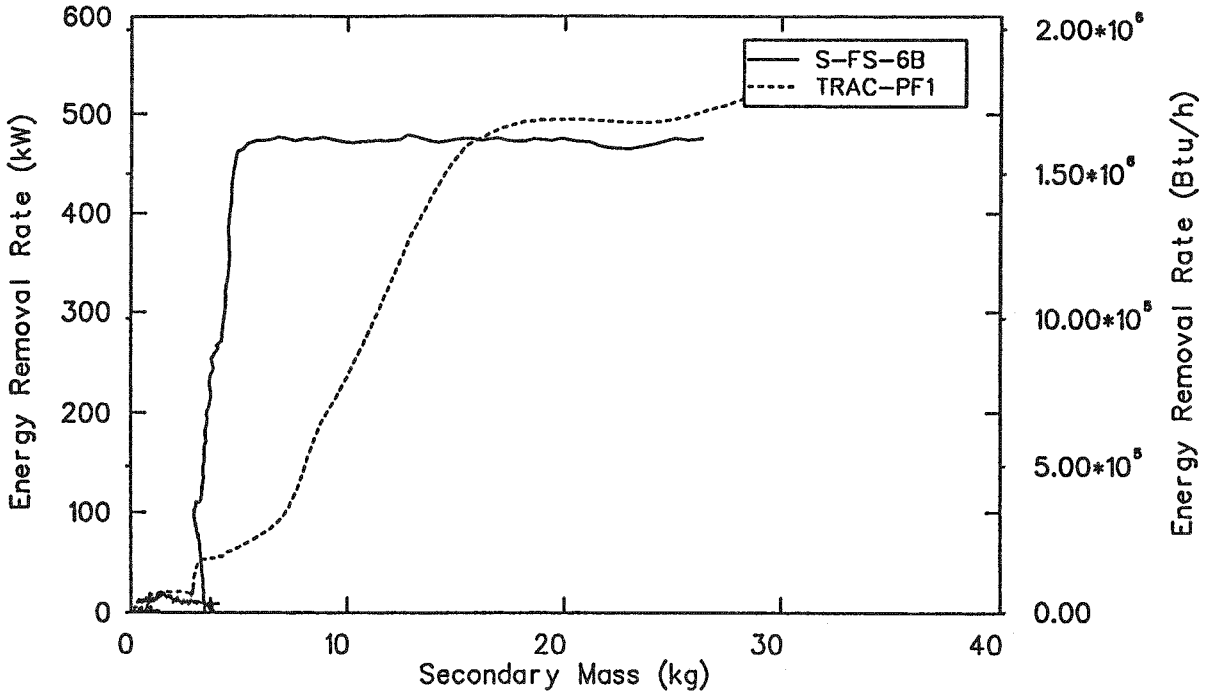

Figure 33. Comparison of measured and calculated broken loop steam generator energy removal rate as a function of total secondary mass during the early part of test S-FS-6B.

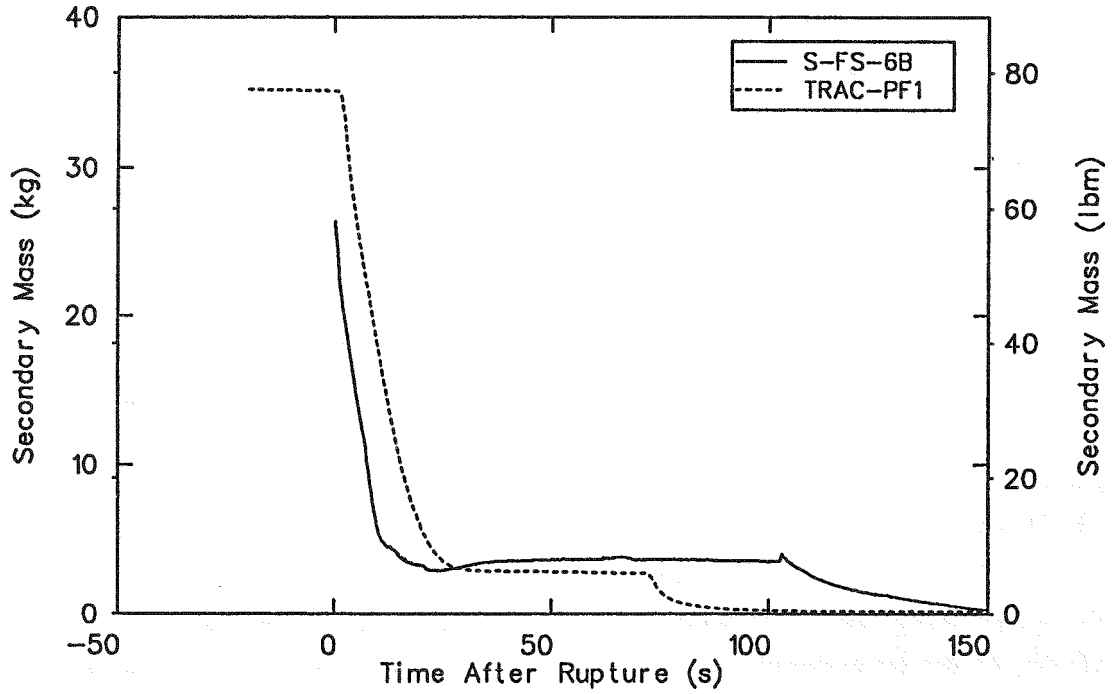

Figure 34. Comparison of measured and calculated broken loop steam generator secondary mass during the early part of test S-FS-6B.

bottom feedwater line break has shown mixed results. The calculated primary side heat transfer coefficients were bounded by, and had the same characteristics as, the measured coefficients at all times during the period when the coefficients decreased from their initial to negligible values. The calculated secondary side heat transfer coefficients exhibited some of the proper trends during the transient and probably would have agreed better with the data if the initial secondary mass agreed better with the test value. The initial values of the calculated coefficients at the lower elevations agreed reasonably well with the measured values. However, the calculated and measured values at the upper elevations were very different and the variations of the upside coefficients with elevation, indicated by the two sets of data, were opposite to each other. The calculated primary heat fluxes agreed reasonably well with the measured data before transient initiation, but exhibited significant differences during the transient. Again, correction of the initial secondary mass would have improved the results. The total energy removal rate through the steam generator was in reasonable agreement with the measured data during the loss in heat removal capability, although the calculated reduction in heat transfer versus mass inventory did not agree with the data.

7. S-FS-7 TRANSIENT SIMULATION RESULTS

Comparisons between the results of a TRAC-PF1/MOD1 simulation and data measured during Semiscale test S-FS-7 (14.3% break) are provided in this section. Subsection 7.1 presents the general response of the system from the time of the bottom feedwater line break until the end of the blowdown phase of the test at 926 s. Subsection 7.2 is devoted to the response of the broken loop steam generator until its energy removal capability was reduced to a negligible level.

7.1 General System Response

This subsection presents an evaluation of the ability of TRAC-PF1/MOD1 to calculate general system response during a bottom feedwater line break transient by comparing calculated parameters with measured counterparts, with emphasis on the primary system. The discussion is organized to follow the chronology of events as simulated automated actions of the plant protection system occur and provides parameters reflecting these actions. The discussion also provides comparisons of the calculated and measured conditions at the end of the blowdown phase of the transient, when plant stabilization operations would commence. Comparisons of measured and calculated parameters associated with the simulated actions of the plant protection system are given in Figure 35. Comparisons of the times of occurrence of these actions and later events in the test[8] and the TRAC-PF1/MOD1 simulation are presented in Table 5.

Important elements of the early primary pressure response were well calculated, as shown in Figure 35a. These elements include the time when the high pressurizer pressure set point was reached, the peak system pressure, and the difference between the intact loop cold leg pressure (highest pressure point in the primary system) and the pressurizer pressure. The calculated primary pressure history differed from the measured history as soon as the peak pressure was reached and remained so until the end of the calculation, as shown in Figure 36. The higher-than-measured primary pressures are not consistent with the calculated total energy removal rate (sum of primary-to-secondary heat transfer rate in both steam generators) being higher than measured, as shown in Figure 35d. Figure 36 shows that if the calculated primary pressure had decreased to the measured value after the pressure peak, as in the S-FS-6B calculation, the calculated primary pressure history would have been in good agreement with the measured data. At the end of the calculation, the calculated primary pressure was 0.9 MPa (130.5 psia) higher than the measured value.

The secondary pressures histories, shown in Figure 35b, were well set equal to the measured values until the steam valves were closed. Steam valve closure is indicated by a sudden increase in the secondary pressures shortly after the SCRAM signal time, between 47 and 49 s. Thereafter, the trends of the calculated pressure histories are correct but the calculated pressures are initially too high, decrease too rapidly, and fall below the measured data, as shown in Figure 37. The fact the calculated secondary pressures are initially too high is consistent with the calculated energy removal rate being higher than measured. The relationship between the measured and calculated energy removal rates does not explain why the calculated secondary pressures decreased too rapidly. The larger-than-measured secondary depressurization rates resulted in the broken loop secondary pressure decaying to the set point [4.47 MPa (648.2 psia)] for the safety injection system (SIS) actuation signal at 746 s in the calculation compared to 903 s in the test.

The pump coast down histories and core power decay were well reproduced in the TRAC-PF1/MOD1 calculation, as shown in Figures 35c and 35d, respectively. Differences between the measured and calculated histories of the combined energy removal rate of the steam generators are evident in Figure 35d. The features of the measured and calculated histories are the same. These results are the same as those for test S-FS-6B.

An explanation for the discrepancies between the calculated and measured primary and secondary pressure histories was sought with reference to the energy balances on the two systems. Comparisons of calculated pressurizer pressure, intact and broken loop secondary pressures, core power, and total energy removal rate through the steam generators are provided in Figure 38. A major source of discrepancy between the results of the TRAC-PF1/MOD1 simulation and the test data was the timing of the SIS signal, which was a function of the broken loop steam generator secondary pressure. Both of the calculated secondary pressures decreased too rapidly resulting in an early SIS signal, as has been previously discussed, and is shown again in Figure 38a. This result is not consistent with the fact that at the same time the calculated secondary pressures were decreasing too rapidly, the total energy removal rate through the steam generators was higher than measured, as shown in Figure 38. Higher-than-measured secondary depressurization rates were also noted in the S-FS-6B simulation. In that case, these results are thought to be caused by the calculated

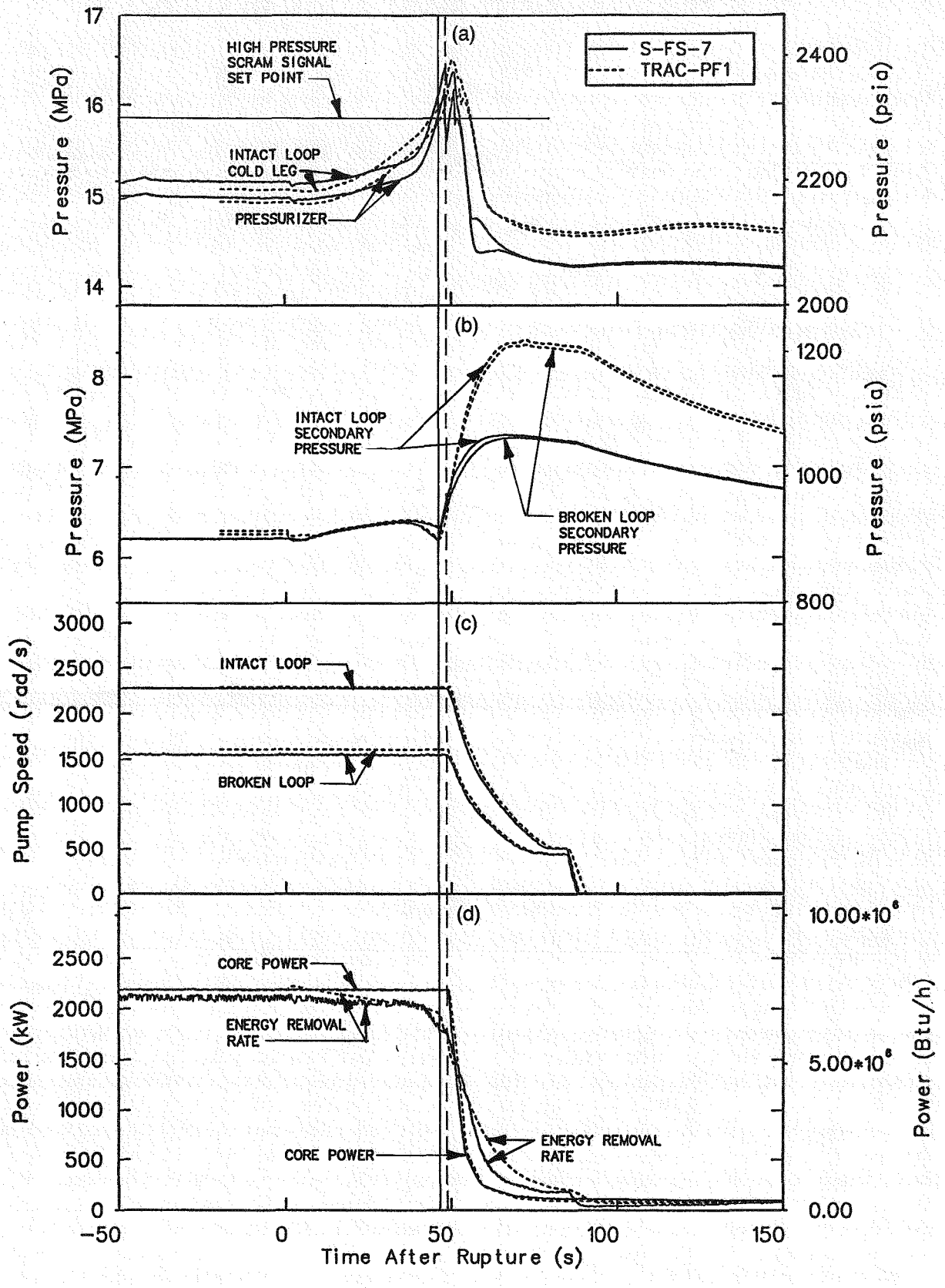

Figure 35. Composite of measured and calculated parameter histories showing the results of simulated automatic actions during the early part of the blowdown phase of test S-FS-7.

Table 5. Sequence of events for test S-FS-7

	Time (s)	
	Data	TRAC
Broken loop steam generator main feedwater line break		
Initiated	0.0	0.5
Fully open	1.0	2.5
Steam generator main feedwater isolated		
Intact loop	4.6	4.6
Broken loop	3.3	3.3
SCRAM at P_{pzr} = 15.86 MPa (2300 psia)	46.0	47.0
Main coolant pump begins coast down		
Intact loop	49.0	49.2
Broken loop	49.0	49.2
Core power decay initiated	49.0	49.7
Main steam flow control valve closed		
Intact loop	47.0	49.0
Broken loop	47.0	49.0
Power to main coolant pump tripped off		
Intact loop	85.0	85.3
Broken loop	85.0	85.3
Safety injection signal		
Broken loop secondary pressure at 4.47 MPa (648.2 psia)	903.0	746.3
High pressure injection flow available		
Intact loop	903.0	746.3
Broken loop	903.0	746.3
Auxiliary feedwater flow initiated		
Intact loop	923.0	746.3
Broken loop	921.0	746.3
Crossover line valve closed	925.0	[a]
Blowdown phase of transient completed	926.0	750.1

a. The crossover line valve was not closed before the end of the transient calculation due to the long closure time indicated by the measured crossover line flow data.

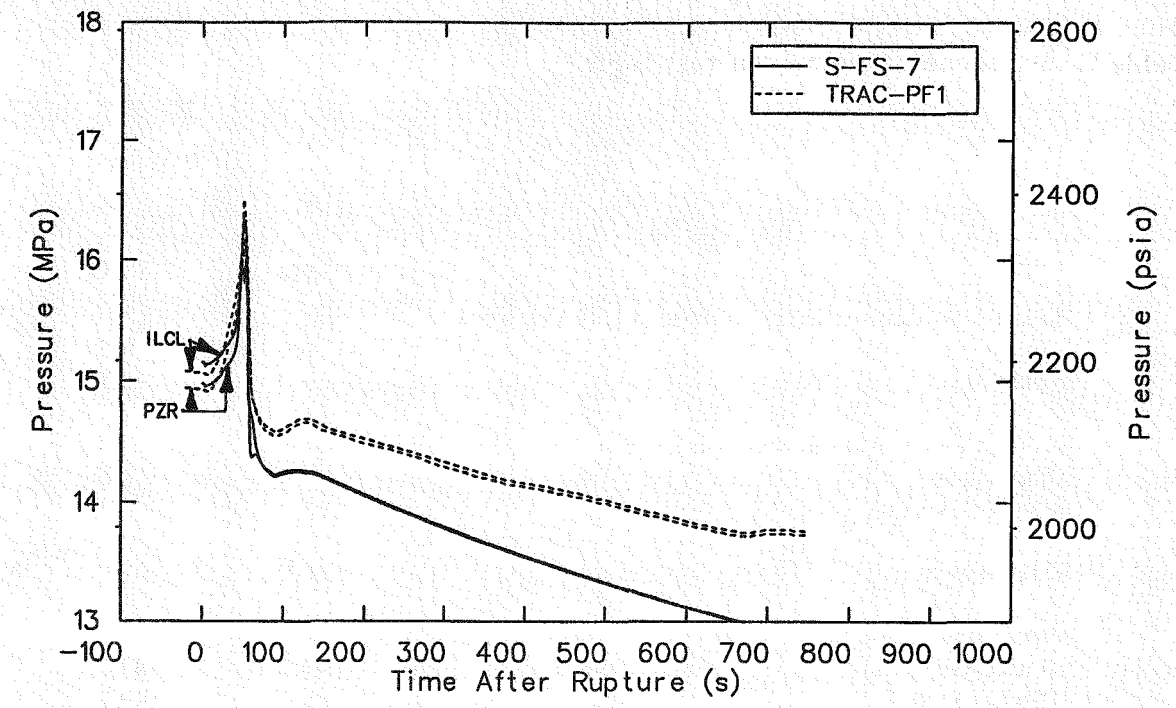

Figure 36. Comparison of measured and calculated pressurizer (PZR) and intact loop cold leg (ILCL) pressures during the blowdown phase of test S-FS-7.

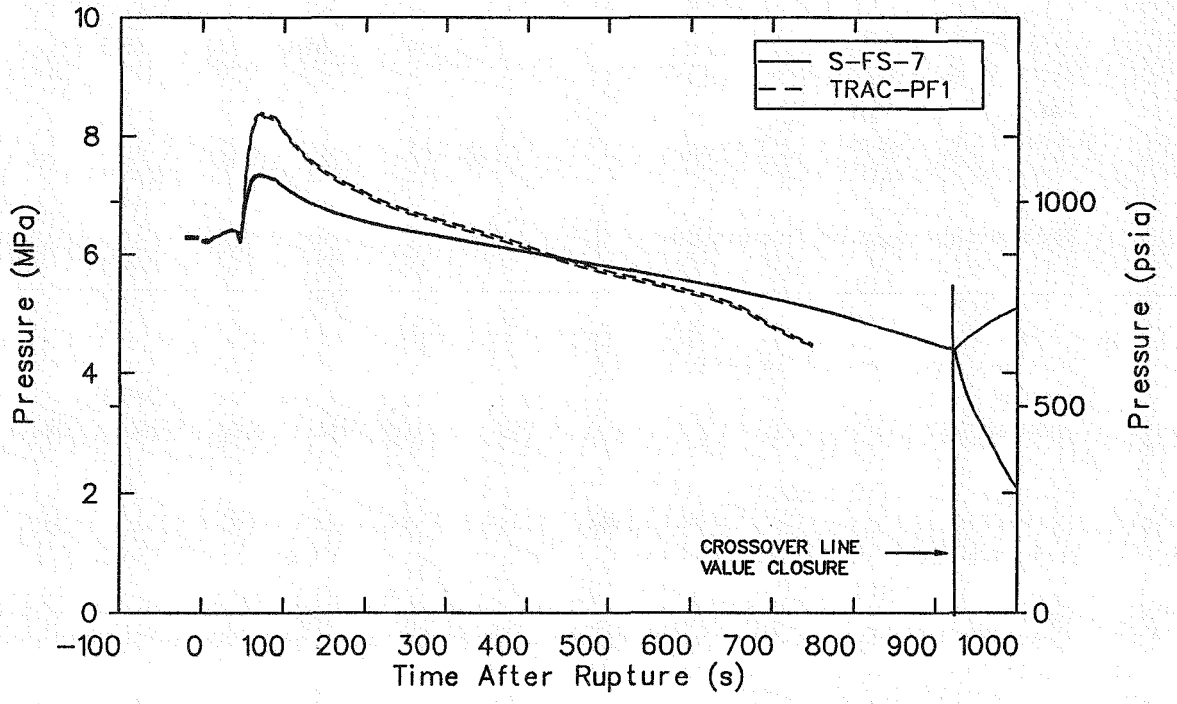

Figure 37. Comparison of measured and calculated broken and intact loop secondary pressure during the blowdown phase of test S-FS-7.

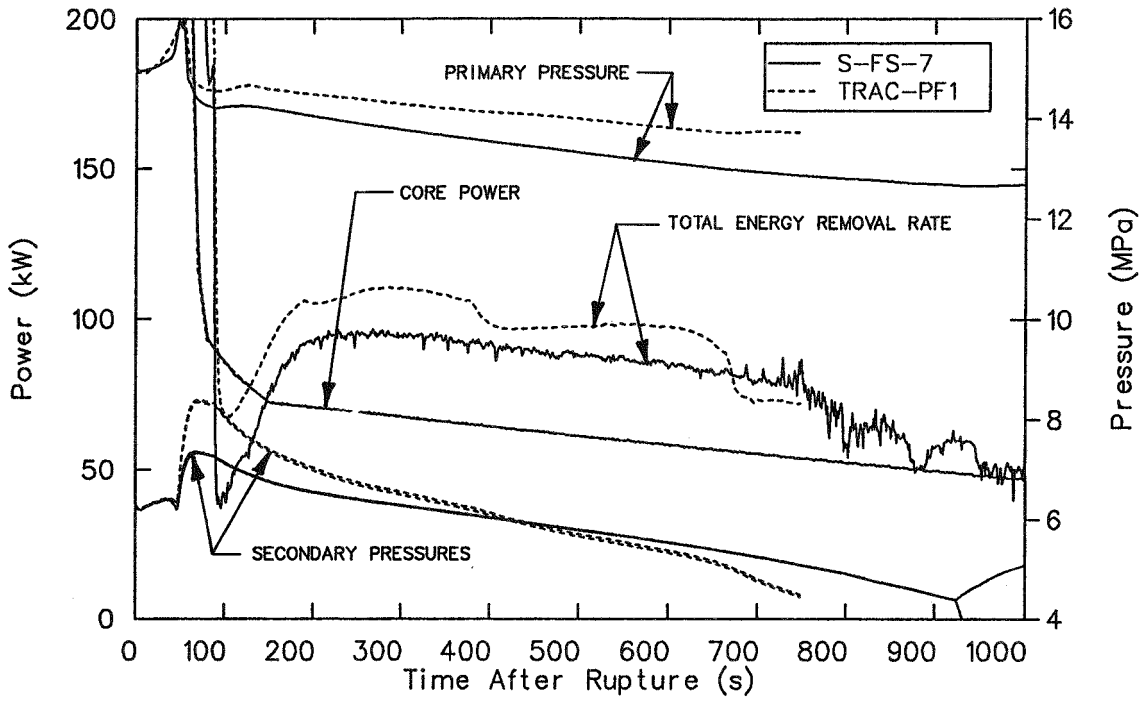

Figure 38. Comparison of measured and calculated primary and secondary pressures, core power, and total energy removal rate during the blowdown phase of test S-FS-7.

crossover line flow rates being too low and by the secondary volumes of both generators in the TRAC-PF1/MOD1 model being too small because portions of the steam lines were not modeled. In the S-FS-7 simulation, the calculated crossover line flow was higher than the measured data during the first 43 s of the transient, and was in excellent agreement with the measured flow rates thereafter, as shown in Figure 39. Thus, the crossover line flow does not help to explain why the secondaries depressurized too rapidly. This leaves the error in modeling the secondary volumes as the principal reason for the observed differences. Another possible cause may be associated with modeling the energy transfer from the structure of the steam generators to the fluid in them.

Differences between the calculated and measured primary pressure histories is also not explained by the energy balances indicated in Figure 38. Both the measured and the calculated energy removal rates are higher than the core decay power, indicating that the primary system should undergo a depressurization. The measured and calculated pressure histories do show depressurization. However, the calculated energy removal rate is higher than measured and, therefore, a higher-than-measured depressurization rate would seem to result. This is not the case. The calculated primary pressure decreased more slowly than the measured pressure. Explanations for this result may lie in the modeling of energy transfer between the structures of the primary system and the primary fluid and in heat losses to the environment that were not modeled in the simulation.

Loop temperature histories calculated in the TRAC-PF1/MOD1 simulation are compared with corresponding measured histories in Figures 40 and 41. For the most part, the trends of the calculated histories are in good agreement with the measured data. The calculated broken loop histories in Figure 40 exhibit the phenomena of the cold leg temperature being hotter than the hot leg temperature for a period of time. This phenomena is the result of the hot leg temperature decreasing due to the SCRAM, and the cold leg temperature increasing due to the degradation of the energy removal capacity of the generator and the loop transit time. The hot leg temperature history agrees well with the measured data, but the cold leg history differs significantly from the measured data. The cold leg temperature does not decrease and assume a nearly constant difference from the hot leg temperature like the measured data, which indicates that energy was not being removed in the broken loop in the calculation at the same rate as it was in the test. This result may be due to modeling of the steam generator and to the fact that heat loss from the broken loop piping to the environment was not modeled. The hotter-than-measured cold leg temperatures are consistent with the

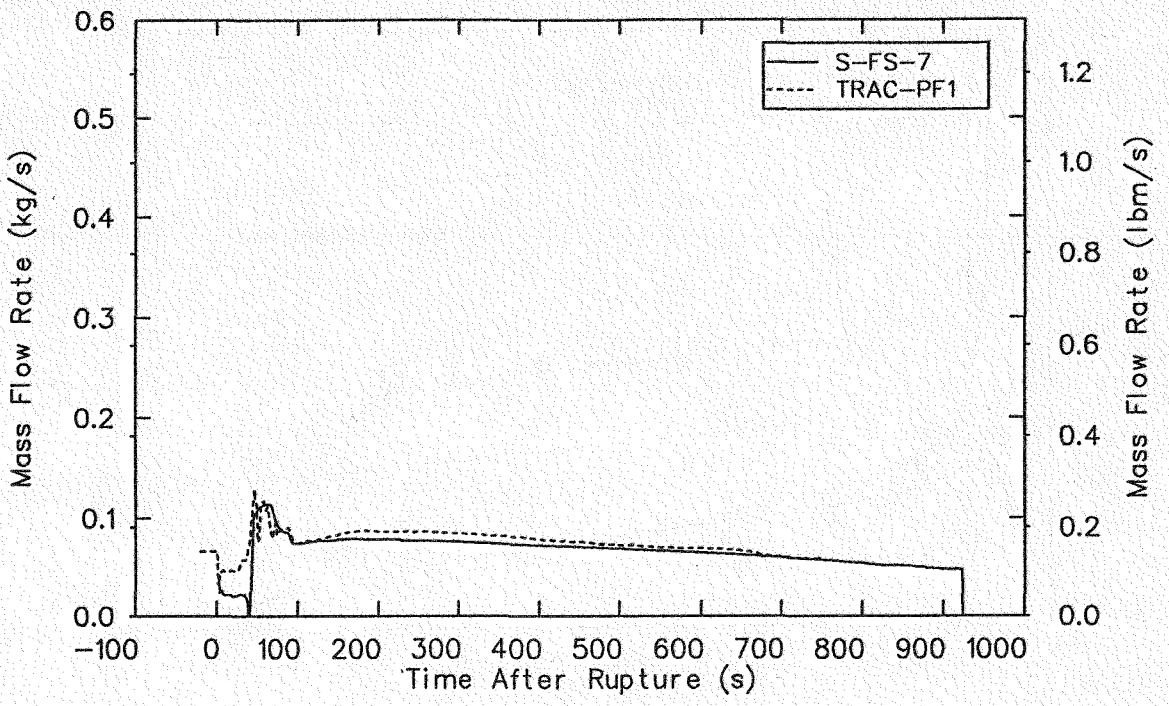

Figure 39. Comparison of measured and calculated crossover line flow rate during the blowdown phase of test S-FS-7.

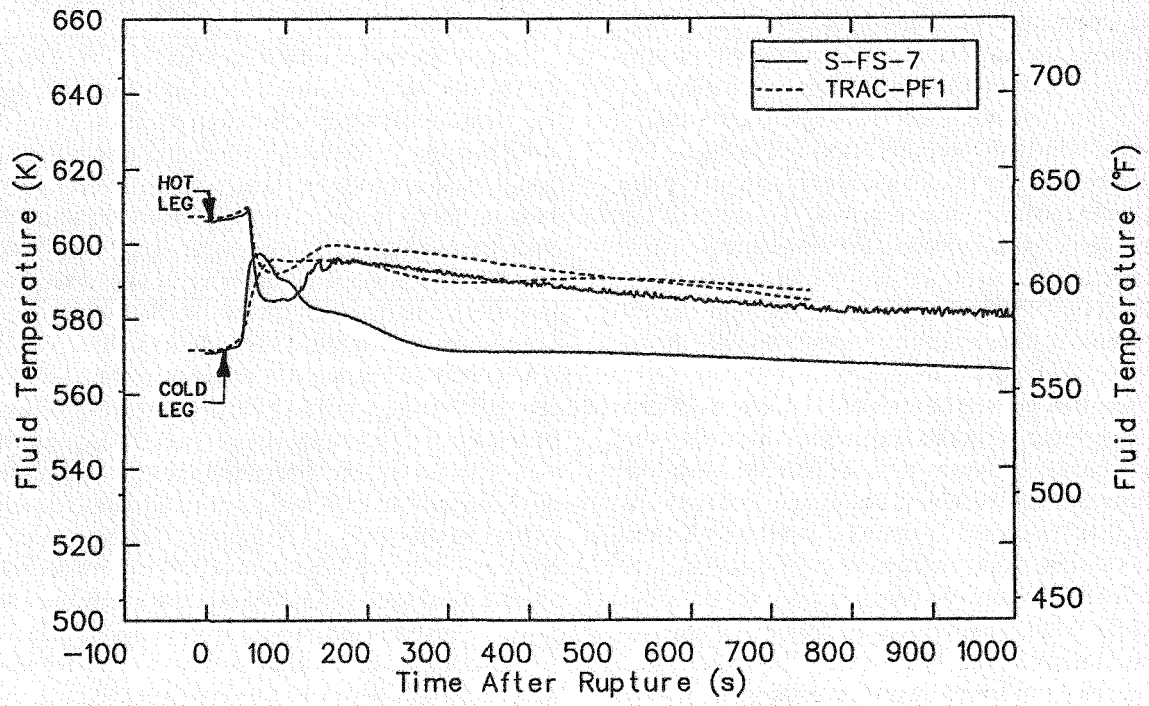

Figure 40. Comparison of measured and calculated broken loop hot and cold leg fluid temperatures during the blowdown phase of test S-FS-7.

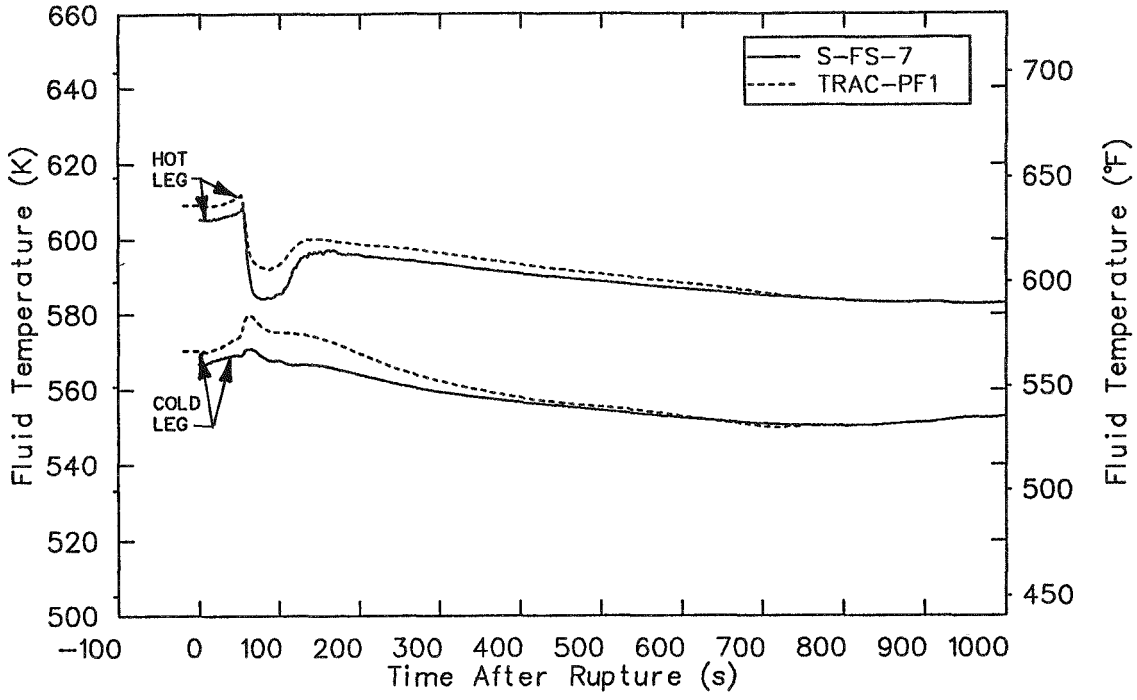

Figure 41. Comparison of measured and calculated intact loop hot and cold leg fluid temperatures during the blowdown phase of test S-FS-7.

higher-than-measured primary pressures and indicate energy removal that occurred in the test was not simulated. The calculated broken loop hot and cold leg temperatures are 1 K (2°F) and 10 K (18°F) too high, respectively, at the end of the blowdown phase of the transient.

The intact loop temperature histories (shown in Figure 41) were well simulated. The calculated hot and cold leg temperatures agreed with the measured data at the end of the calculation, in spite of differences earlier in the transient that were no larger than 4 K (7°F).

In summary, TRAC-PF1/MOD1 has demonstrated the ability to calculate most of the trends exhibited in selected data recorded during Semiscale bottom feedwater line break test S-FS-7. The results of the calculation were in good agreement with the data until the steam control valves were closed around 47 s. Thereafter, the calculated results exhibit the correct trends, but differ in magnitude from the measured data. Several reasons for the observed discrepancies have been identified. The energy removal rates through the steam generators, particularly through the intact loop steam generator, were too high almost throughout the simulation. Simplifications such as combining U-tubes into a single tube and lumping intact loop steam generator riser and downcomer filler pieces with other parts in the steam generator model may have had an adverse effect on the simulation. The high energy removal rates resulted in the secondary pressures rising too high after the steam valves were closed, but did not provide an explanation of why the secondary pressures decreased too rapidly or why the primary pressure did not decrease as rapidly as indicated by the data. The discrepancies in the secondary pressure response is related to the fact that part of the steam lines on each of the steam generators was not modeled, and perhaps to energy transfer between the structure and the fluid, including the effect of environmental heat losses that were not modeled. Consideration of improved modeling of energy transfer between the structure of the primary system and the primary fluid and modeling of primary system heat losses to the environment, particularly in the broken loop, may be necessary to improve the primary system response.

7.2 Broken Loop Steam Generator Response

This subsection provides an evaluation of the ability of TRAC-PF1/MOD1 to calculate the responses of a steam generator during a transient in which the feedwater to the generator is lost. The results of the evaluation are presented by comparing measured and calculated parameters within the affected steam generator. The presentation begins with parameters

associated with the feedwater line break flow, includes secondary side flows and inventory and primary and secondary temperatures, and concludes with local and total heat transfer.

The principal boundary condition affecting the broken loop steam generator was a simulated 14.3% break in the feedwater line to the steam generator. A composite of measured and calculated parameter histories associated with the feedwater line break flow are given in Figure 42. In general, the calculated break flow history is in good agreement with the measured data, particularly over the long term, as shown in Figure 43. The most notable discrepancies that occur early in the transient are the initial peak flow rate and a second peak that occurred in the calculated values between 47 and 67 s. The lack of an initial peak in the measured data is highly questionable in light of the high degree of subcooling of the fluid upstream of the break when the transient was initiated, as shown in Figure 42d. The calculated peak break flow is probably more representative of what actually happened during the test. The second peak is not justifiable and is the result of differences in the pressure and void fraction upstream of the break, as shown in Figures 42b and 42c, respectively. The differences in calculated and measured void fraction histories are related to differences between the initial secondary mass used in the calculation [35.5 kg (78.1 lbm)] and that deduced from a reevaluation of the test data [30 kg (66.0 lbm)]. (The reevaluation of the initial secondary mass was performed too late to be used in the TRAC-PF1/MOD1 simulation.)

Calculated and measured flow rates at the steam outlet and internal to the broken loop steam generator are presented in Figures 44 and 45, respectively. The calculated histories in Figure 44 are discussed first because they provide a more consistent picture of the flow histories than the measured data. Before the initiation of the transient, the riser flow is equal to the sum of the downcomer flow and the steam flow exiting the steam generator. The riser and steam flows decrease after the break is opened and eventually reverse direction. After closure of the broken loop steam valve, the crossover line supplies flow into the generator and the reversed direction steam flow is equal to, but opposite in sign from, the crossover line flow. The steam flow splits into the reverse riser flow and the downcomer flow. These relationships exist until the crossover line valve is closed, then all the flows go quickly to zero.

Measured broken loop steam generator flow rate histories are provided in Figure 45. These histories indicate the proper relationship between the riser, downcomer, and steam flows before transient initiation, as they did in the S-FS-6B results. However, the S-FS-6B results do not assume a consistent relationship after steam valve closure occurs. The initial calculated riser and downcomer flows are slightly higher than the measured values. After the break was opened, the riser and steam flows decreased. The steam flow reversed, although the measurement became unreliable shortly thereafter, but the riser flow did not reverse. After closure of the steam valve, the relationships that are indicated by the calculated results do not exist. The steam flow may have been equal to the crossover line flow, but opposite in sign as in the calculation, but the riser flow remained positive and the downcomer flow has slightly negative values. The data imply that the crossover line, riser, and downcomer flows are all converging in the steam dome with no outlet for the flow, which is highly unlikely. In the previous section, flow data from test S-FS-6 were presented to show that the calculated flows in the steam generator exhibit the proper relationships. This applies to the S-FS-7 data as well.

Heat transfer in the generator is partially dependent upon secondary side liquid level and void fraction distribution. Comparisons between calculated and measured collapsed liquid levels in the riser and downcomer are presented in Figures 46 and 47, respectively. Both the measured and the calculated collapsed liquid level histories indicate that the riser and the downcomer drain nearly uniformly. The calculated histories are in fair-to-poor agreement with the measured data because they indicate the steam generator secondary drains too rapidly. The differences may be partially due to the difference between the initial measured secondary mass and the value used in performing the simulation. The differences may indicate the need for modifications to the riser and downcomer hydraulic resistances in the TRAC-PF1/MOD1 model.

The calculated and measured riser void fraction histories, shown in Figures 48 and 49, have the same general features. The measured data at the lower elevations (see Figure 48) show a stepped increase from the initial value to a void fraction of 1.0 that was not duplicated in the calculated data. The calculated data show a void fraction of 1.0 was reached earlier the higher the elevation, while the measured data indicate this condition was reached at all elevations at the same time and earlier than shown by the calculated data. The calculated data for the upper elevations (see Figure 49) show good agreement with the characteristics of the measured data, but is lower than the measured data during the rise to a void fraction of 1.0 at all elevations. Again, the differences observed at the lower elevations may be related to the difference between the initial secondary mass in the simulation and the test.

Measured and calculated primary and secondary temperatures at lower and upper elevations occupied

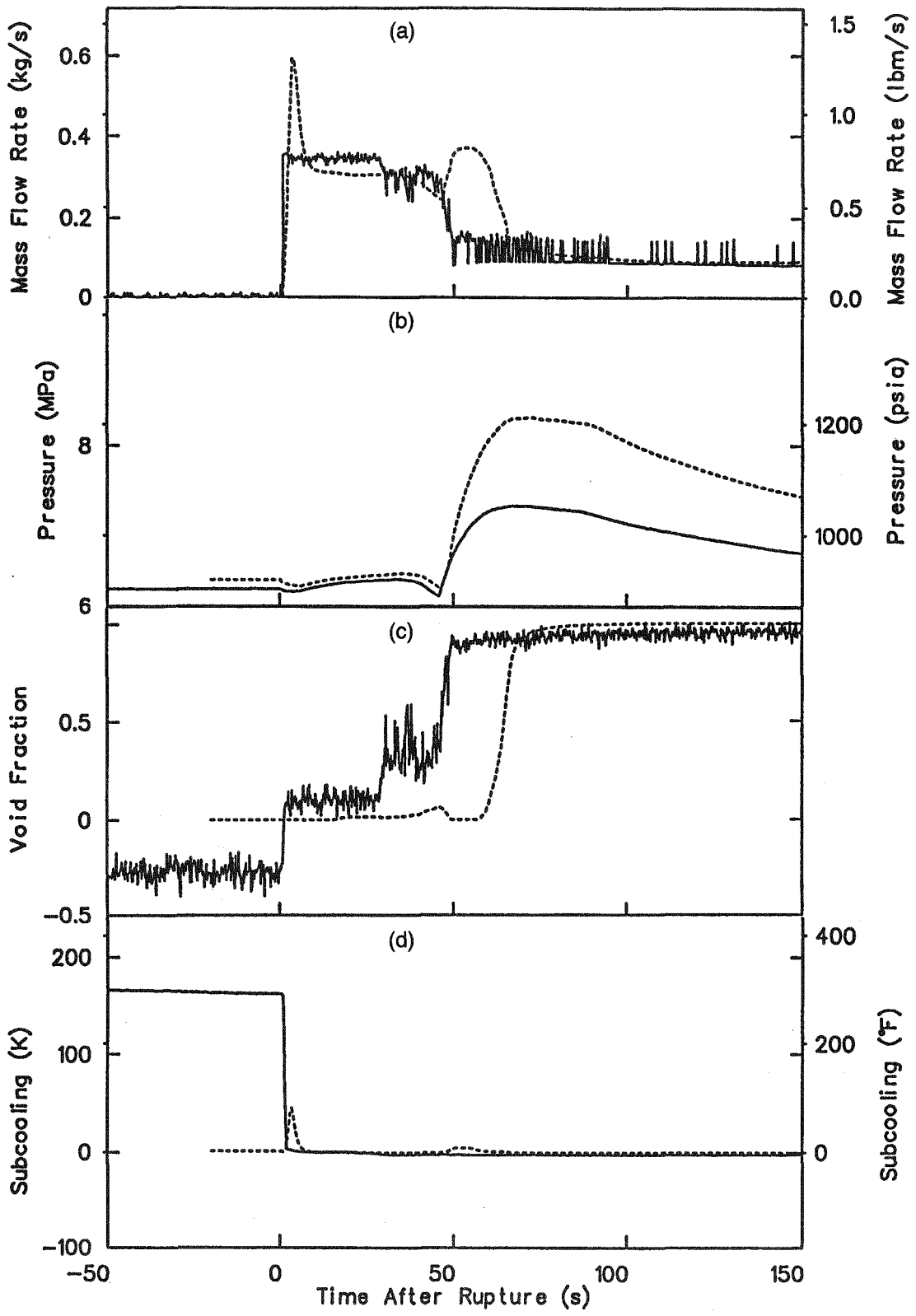

Figure 42. Composite of measured and calculated parameter histories associated with feedwater line break flow during the early part of the blowdown phase of test S-FS-7.

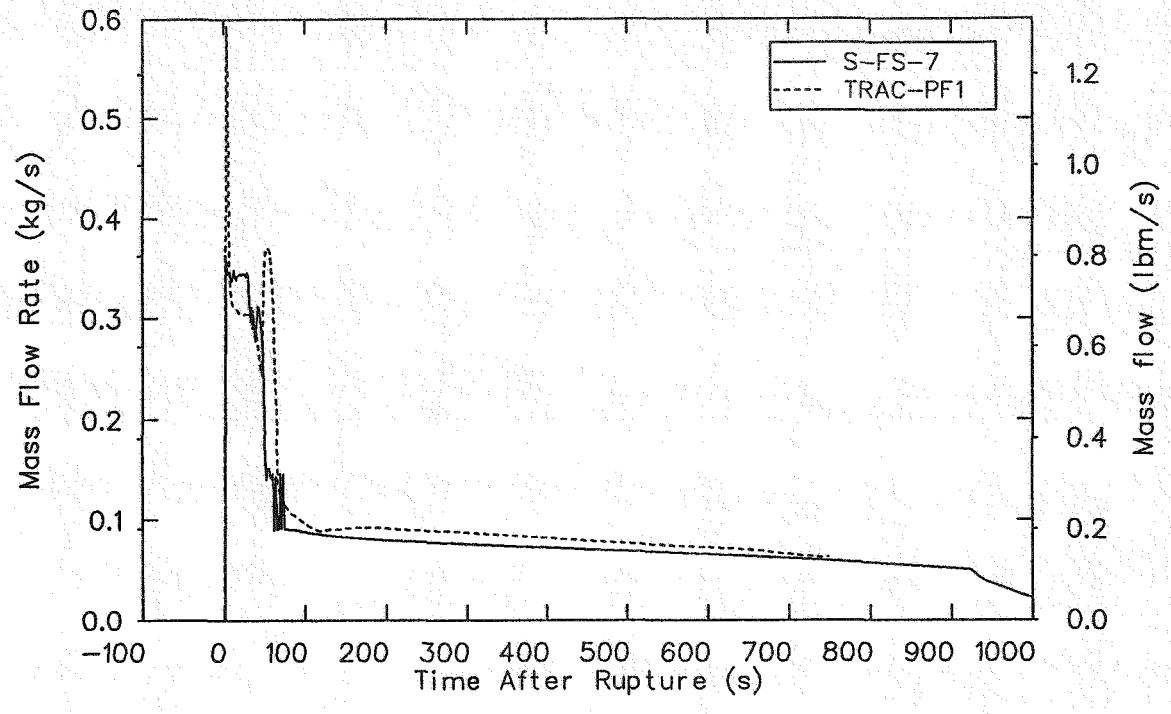

Figure 43. Comparison of measured and calculated break flow rate during the the blowdown phase of test S-FS-7.

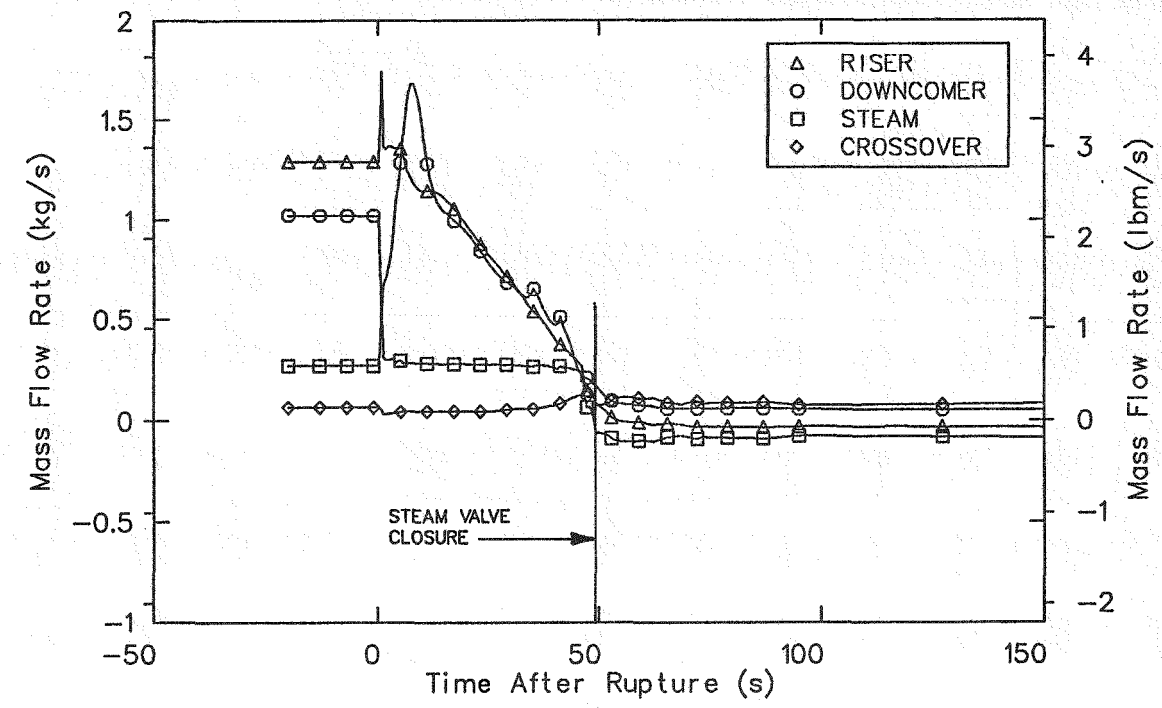

Figure 44. Calculated broken loop steam generator external and internal flow rates during the early part of the blowdown phase of test S-FS-7.

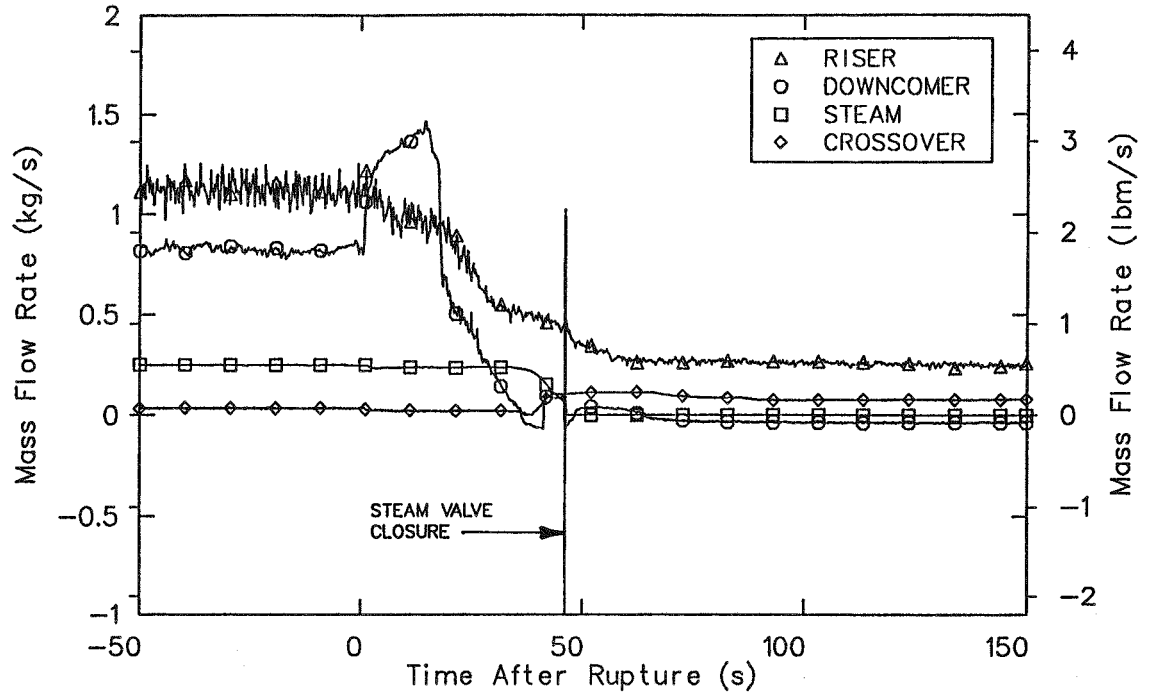

Figure 45. Measured broken loop steam generator external and internal flow rates during the early part of the blowdown phase of test S-FS-7.

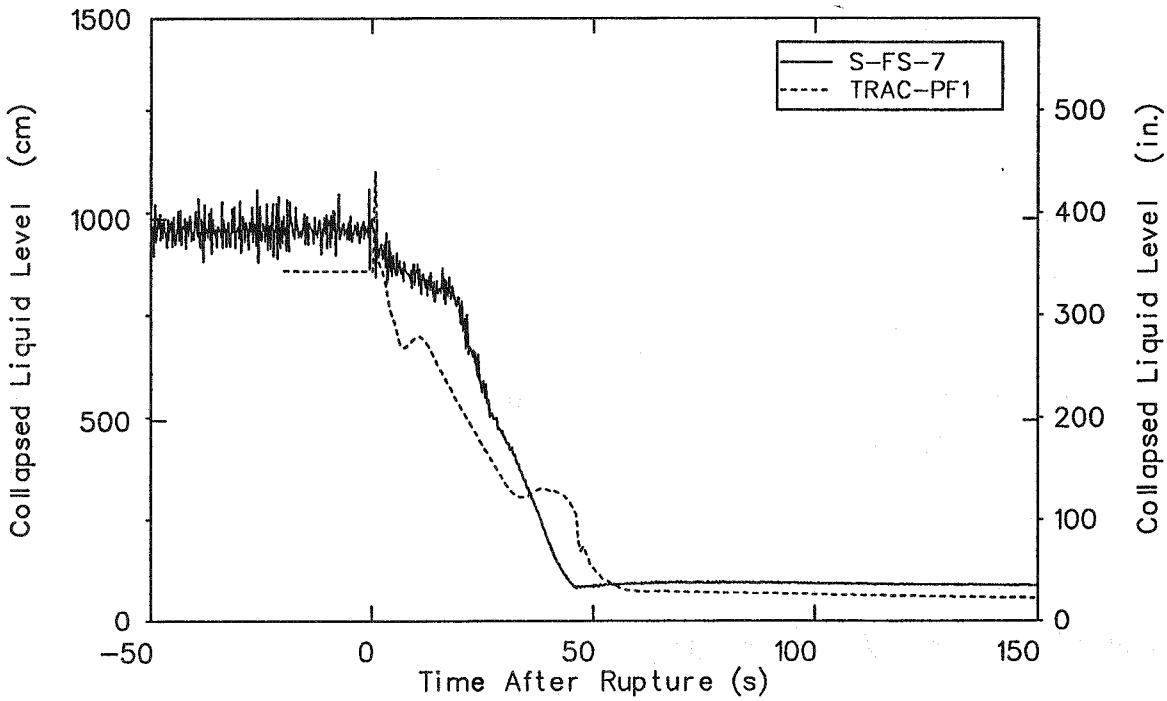

Figure 46. Comparison of measured and calculated broken loop steam generator riser collapsed liquid level during the early part of the blowdown phase of test S-FS-7.

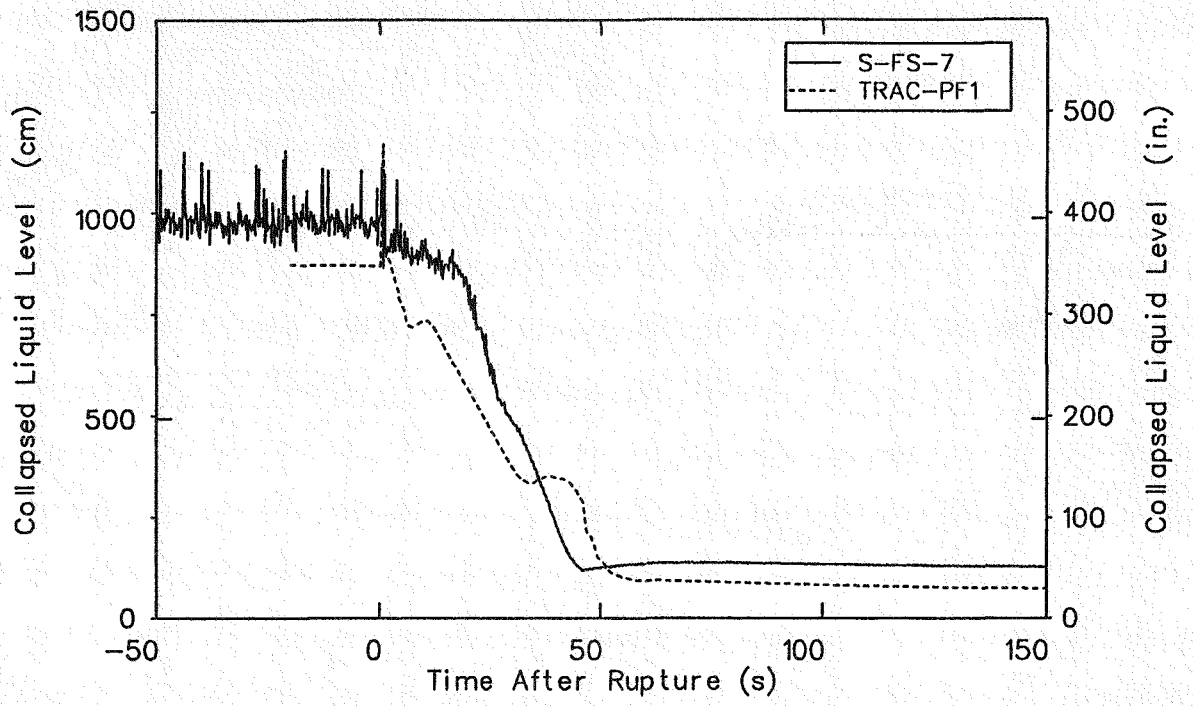

Figure 47. Comparison of measured and calculated broken loop steam generator downcomer collapsed liquid level during the early part of the blowdown phase of test S-FS-7.

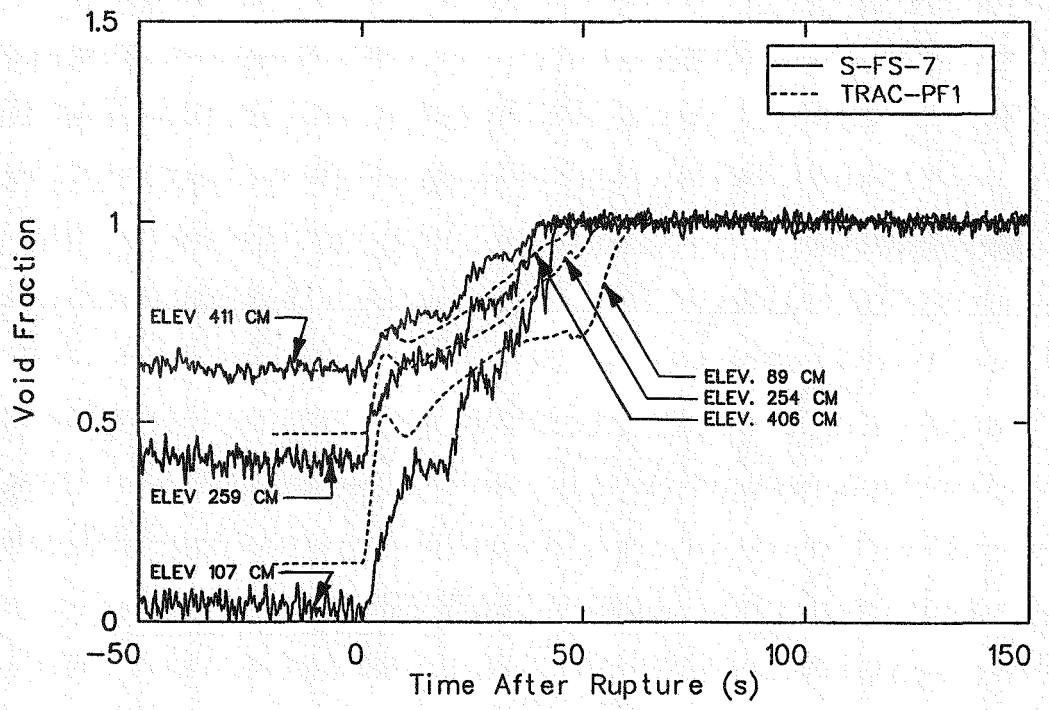

Figure 48. Comparison of measured and calculated lower riser void distribution during the early part of the blowdown phase of test S-FS-7.

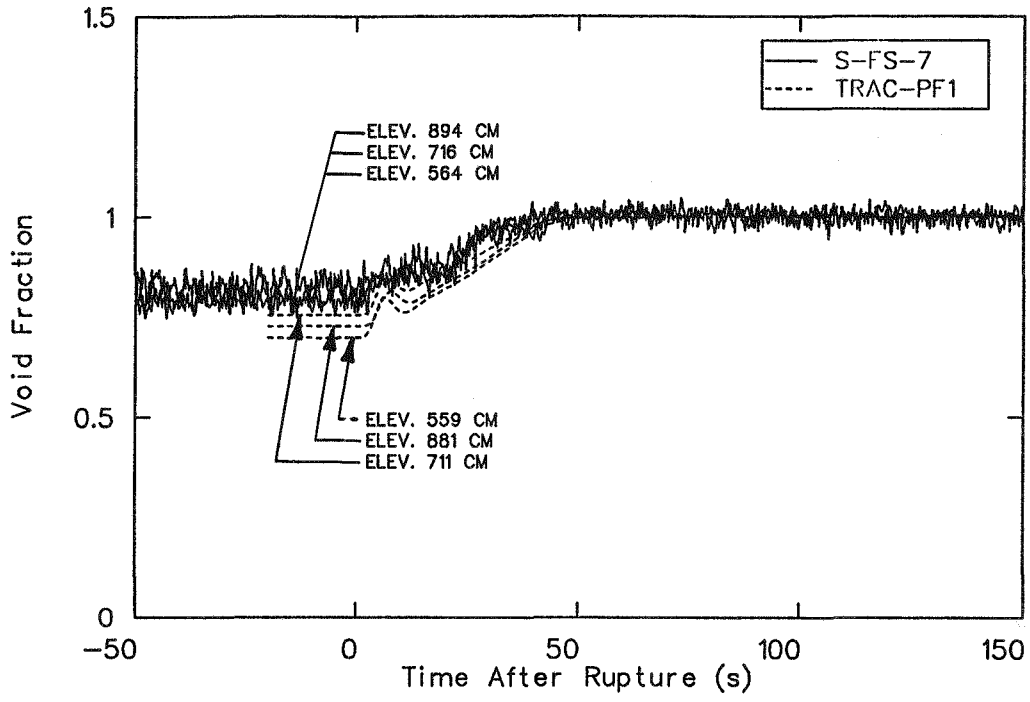

Figure 49. Comparison of measured and calculated upper riser void distribution during the early part of the blowdown phase of test S-FS-7.

by the U-tubes are compared in Figures 50 and 51 for the upside and downside of the U-tube, respectively. The measured primary temperatures in these figures are for the long tube and are typical of the primary temperature histories. The calculated primary temperatures are liquid temperatures. The calculated secondary temperatures are vapor temperatures. These temperatures are the most representative of the conditions that existed in the U-tubes and the riser, respectively, during the transient. The figures show that the calculated temperature histories exhibit the same trends as the measured data, but the calculated temperatures are significantly higher than the measured data during most of the transient. Calculated secondary liquid temperature is included in Figures 50 and 51 for comparison. The primary temperature agreement is better for the upside primary temperatures than for the downside primary temperatures, which is consistent with the results for S-FS-6B.

Comparisons of calculated and measured heat transfer coefficients are given in Figures 52 through 54 for lower elevations on the upside of the tube, upper elevations on the upside of the tube, and the full range of elevations on the downside of the tube, respectively. Measured data for both the long and short tubes in the broken loop steam generator are given. The comparisons at all locations indicate the same results. The calculated heat transfer coefficients are bounded by the measured values, with the calculated values being in better agreement with the data corresponding to the short tube than that corresponding to the long tube. The results of the comparisons in Figures 52 through 54 are virtually identical to the results of similar comparisons for test S-FS-6B. As noted previously for test S-FS-6B, the calculated steady-state heat fluxes were in better agreement with measured heat fluxes associated with the long tube, while the calculated heat transfer coefficients were in better agreement with values associated with the short tube during the transient.

Comparisons of calculated and measured secondary side heat transfer coefficients on the upside and downside of the U-tubes are presented in Figures 55 and 56, respectively. The data in both figures show significant differences between the calculated and measured results. These differences are similar to those noted in the same type of comparisons for S-FS-6B. The measured data in Figure 55 indicate that before the start of the transient, the value of the heat transfer coefficient increased with increasing elevation. The measured data also show that the heat transfer coefficient associated with the short tube was higher than that associated with the long tube at the same elevation. In contrast to the measured data, the calculated heat transfer coefficients decrease with increasing elevation and indicate a much smaller variation in value

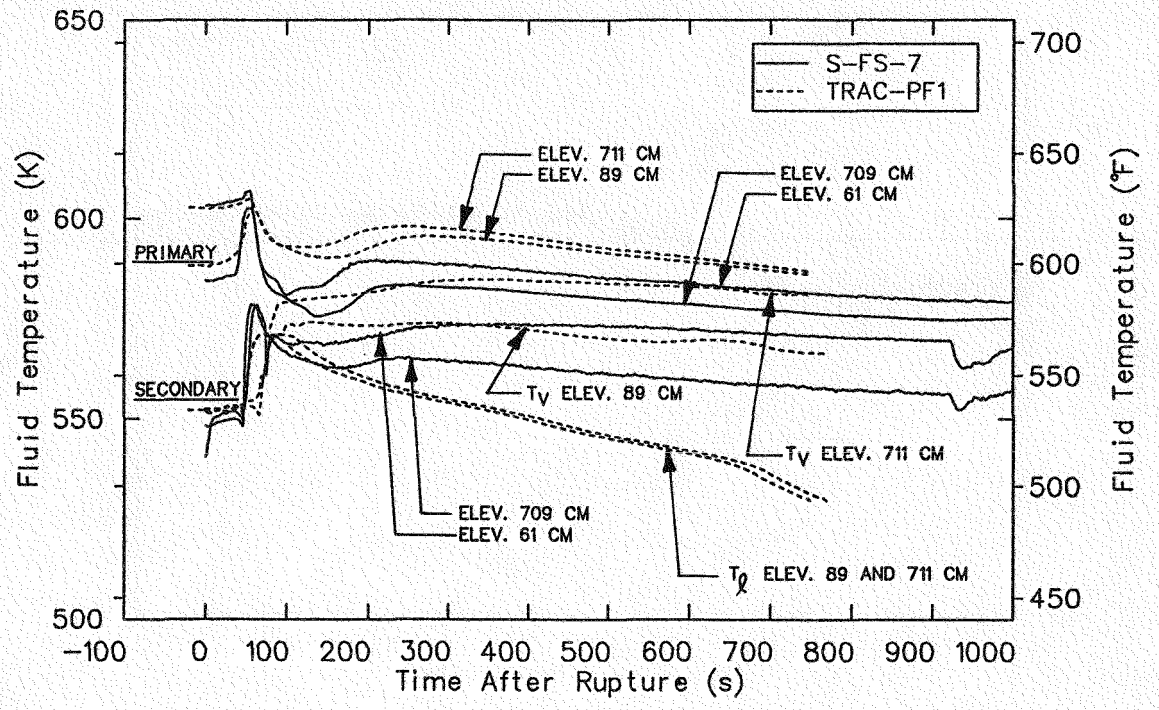

Figure 50. Comparison of measured and calculated primary upside and secondary temperatures at U-tube upper and lower elevations during the blowdown phase of test S-FS-7.

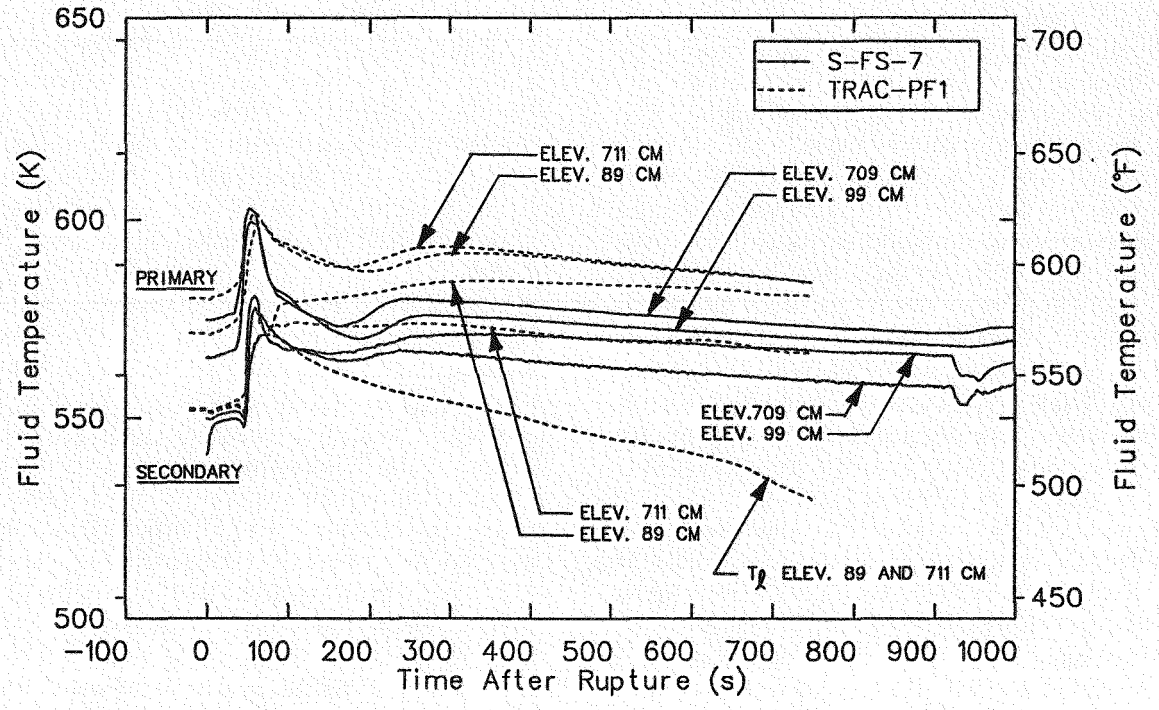

Figure 51. Comparison of measured and calculated primary downside and secondary temperatures at U-tube upper and lower elevations during the blowdown phase of test S-FS-7.

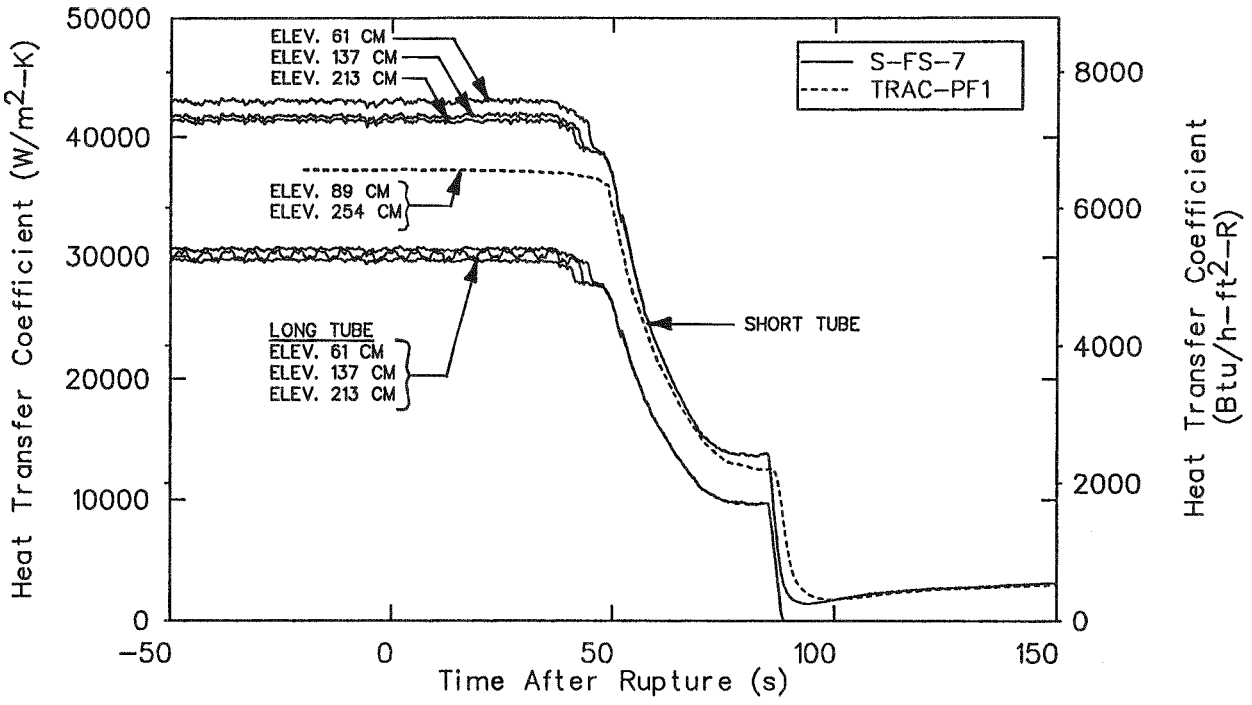

Figure 52. Comparison of measured and calculated primary upside heat transfer coefficients at the lower elevations during the early part of the blowdown phase of test S-FS-7.

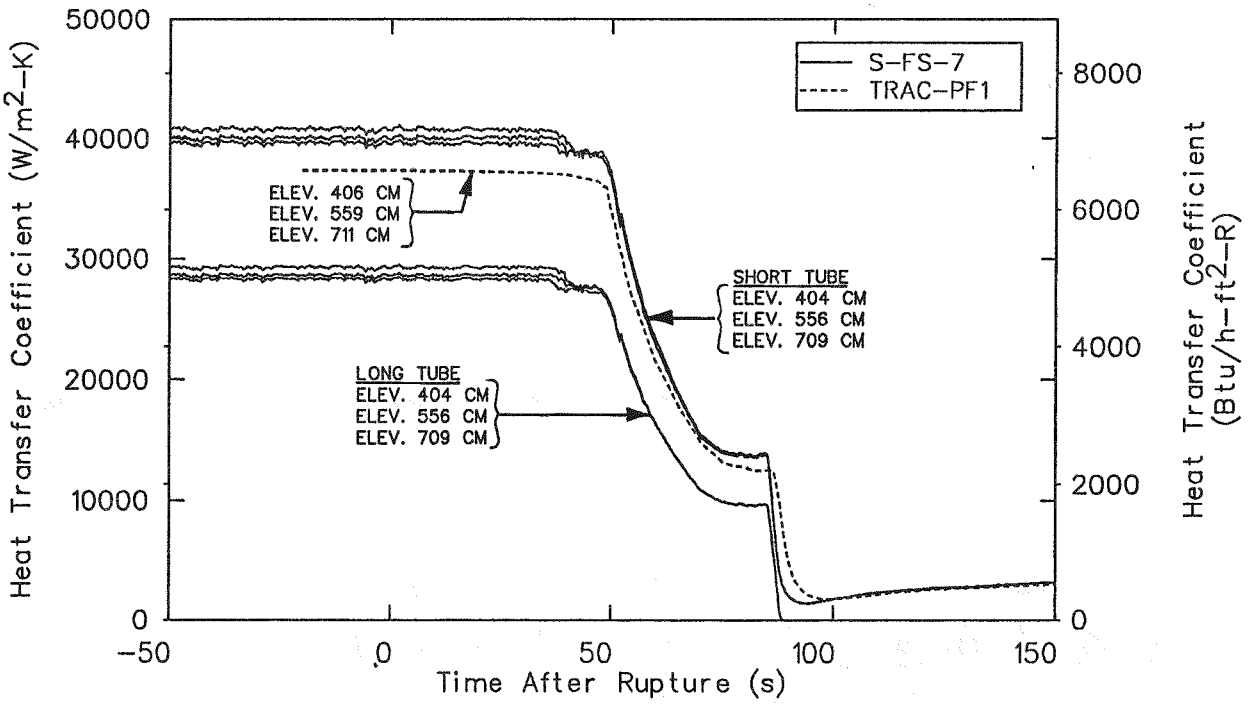

Figure 53. Comparison of measured and calculated primary upside heat transfer coefficients at the upper elevations during the early part of the blowdown phase of test S-FS-7.

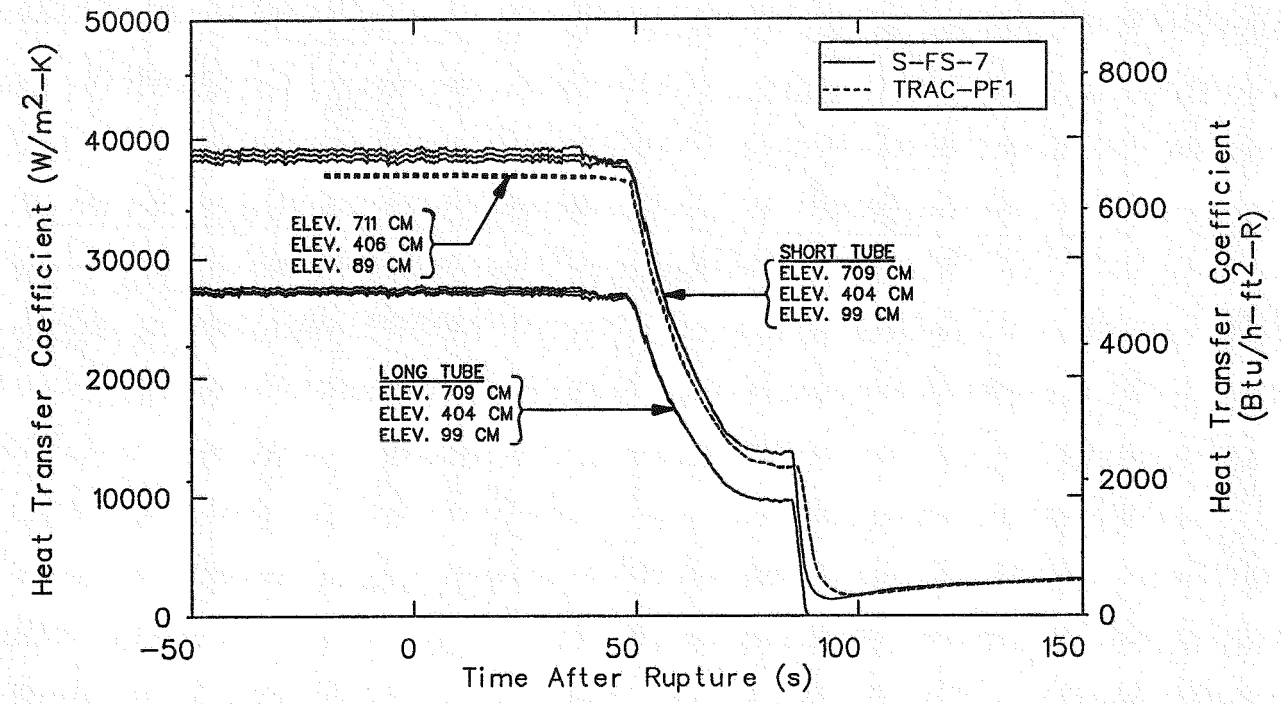

Figure 54. Comparison of measured and calculated primary downside heat transfer coefficients during the early part of the blowdown phase of test S-FS-7.

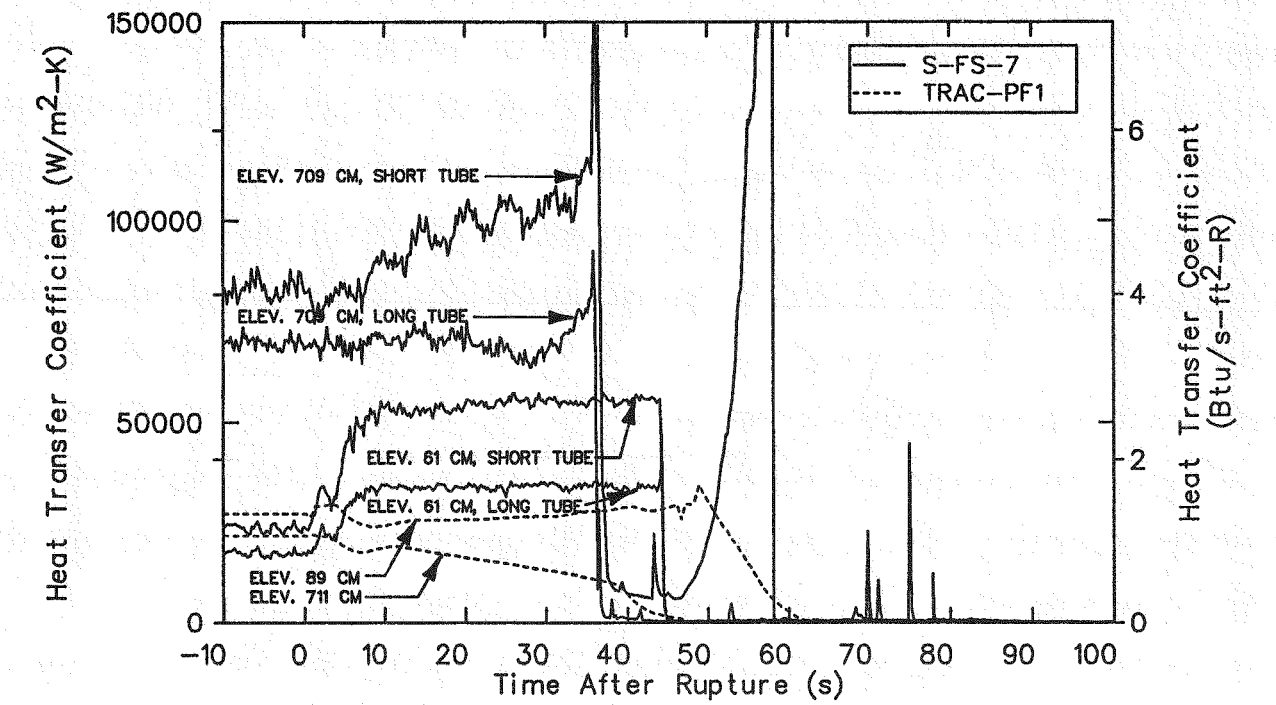

Figure 55. Comparison of measured and calculated secondary upside heat transfer coefficients during the early part of the blowdown phase of test S-FS-6B.

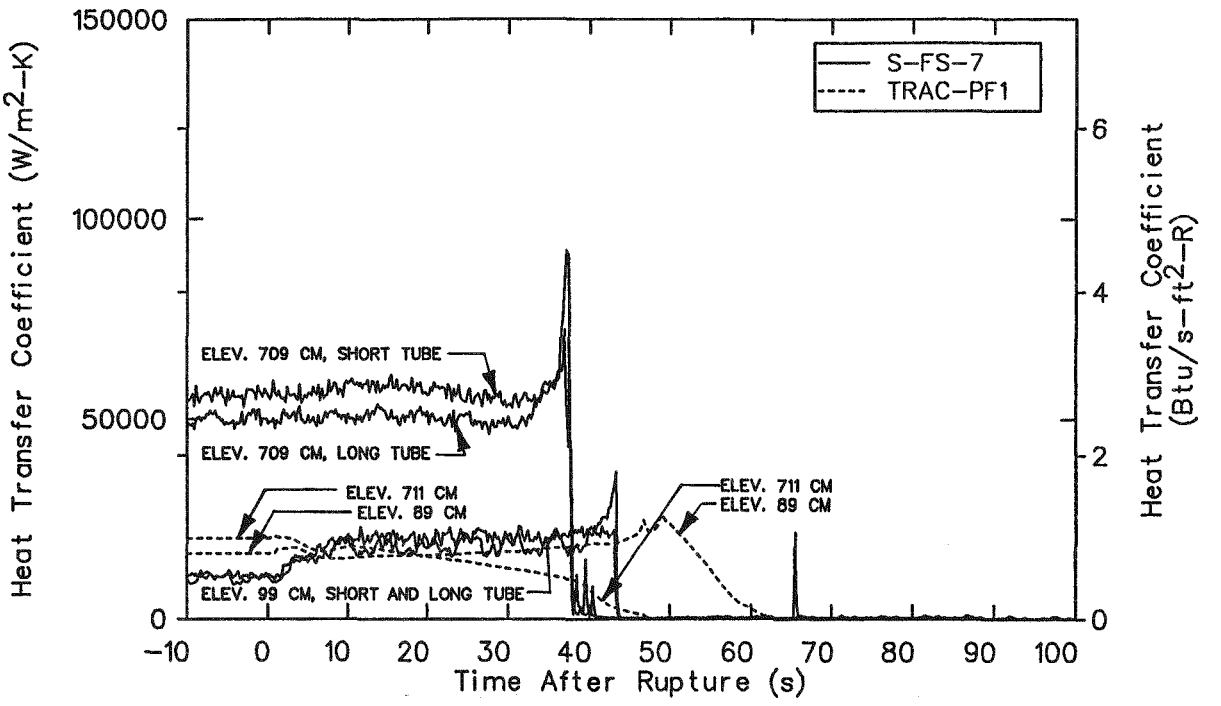

Figure 56. Comparison of measured and calculated secondary downside heat transfer coefficients during the early part of the blowdown phase of test S-FS-6B.

from the bottom to the top of the tube. The calculated heat transfer coefficient at the lowest elevation was in fair agreement with the values for the lowest measurement station. It is interesting to note that in spite of the large differences between the measured and calculated data, the calculated heat transfer coefficients (given in Figure 55) do exhibit some of the same behavior as that seen in the measured data associated with the long tube. Like the measured data, the calculated coefficient at the lower elevation remained nearly constant until the secondary mass was depleted. The calculated coefficient at the upper elevation decreased slowly, like its measured counterpart, until it began a more rapid decrease to zero, even though the values of the calculated and measured coefficients were greatly different. Perhaps the calculated coefficients would have begun to decrease to zero and matched the rate of decrease exhibited by the test data if the initial secondary masses had agreed more closely. The calculated coefficient at the upper elevation on the upside does not include the spike after 50 s that is exhibited by the measured coefficient associated with the short tube, but is not exhibited by the measured coefficient associated with the long tube.

The comparison of downside heat transfer coefficients, shown in Figure 56, shows better agreement between the calculated and measured results in some respects. The variation of heat transfer coefficient with elevation, indicated by the measured data, was reproduced in the calculation although the variation in the calculated heat transfer coefficients was much smaller than that indicated by the data. As with the upside, the calculated heat transfer coefficient at the lowest elevation is in reasonable agreement with its measured counterparts. The calculated coefficients also exhibit approximately the correct trends during the transient. As with the upside coefficients, the effect of too large an initial secondary mass is evident.

Calculated and measured primary side heat fluxes for the upside and downside are compared in Figures 57 and 58, respectively, and show the same results. The initial calculated heat fluxes were in fair agreement with, but lower than, the data measured at approximately the same elevation. The calculated heat flux histories have the same characteristics as their measured counterparts. An exception is the data for the upper elevation on the upside. The calculated heat flux shows a relatively rapid decrease beginning at 40 s. The measured data shows the end of a rapid decrease that began shortly before 40 s, and then the data decreases to zero at varying rates between 40 and 90 s. Again, revision of the initial secondary mass used in the calculation to more closely match the data would improve the agreement in the heat flux histories. It is noteworthy than the measured heat fluxes do not exhibit the resurgence indicated by the secondary heat

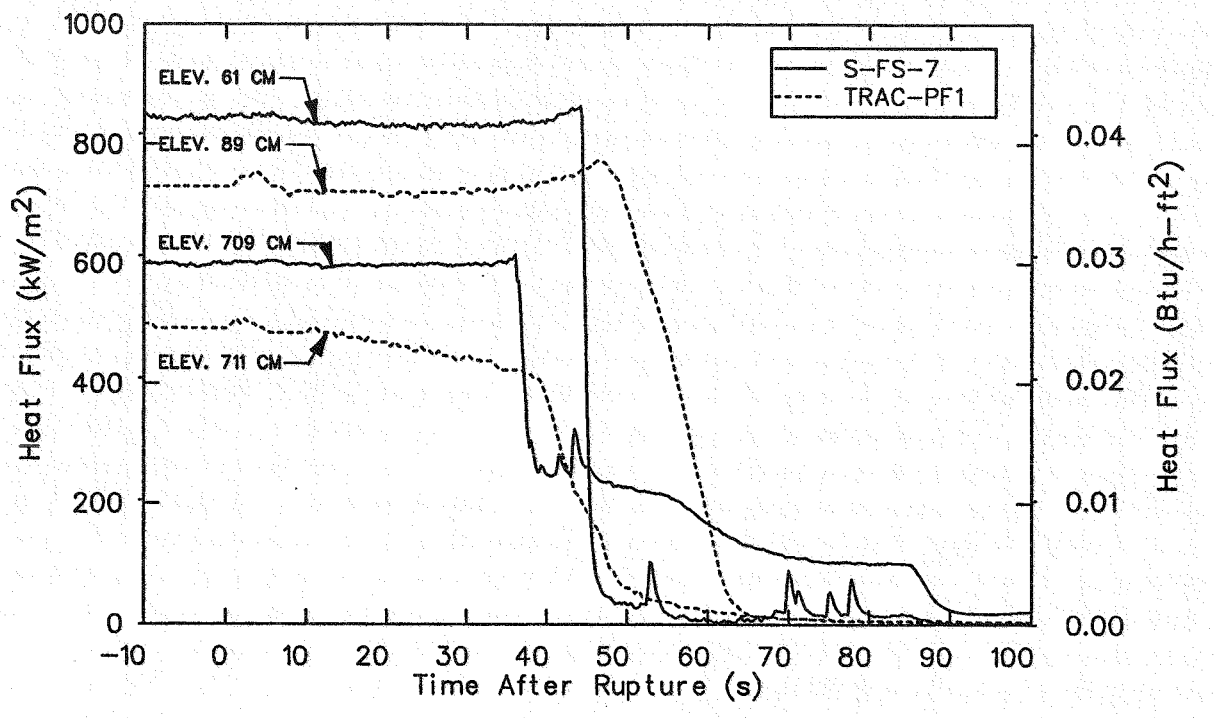

Figure 57. Comparison of measured and calculated primary upside heat fluxes during the early part of the blowdown phase of test S-FS-6B.

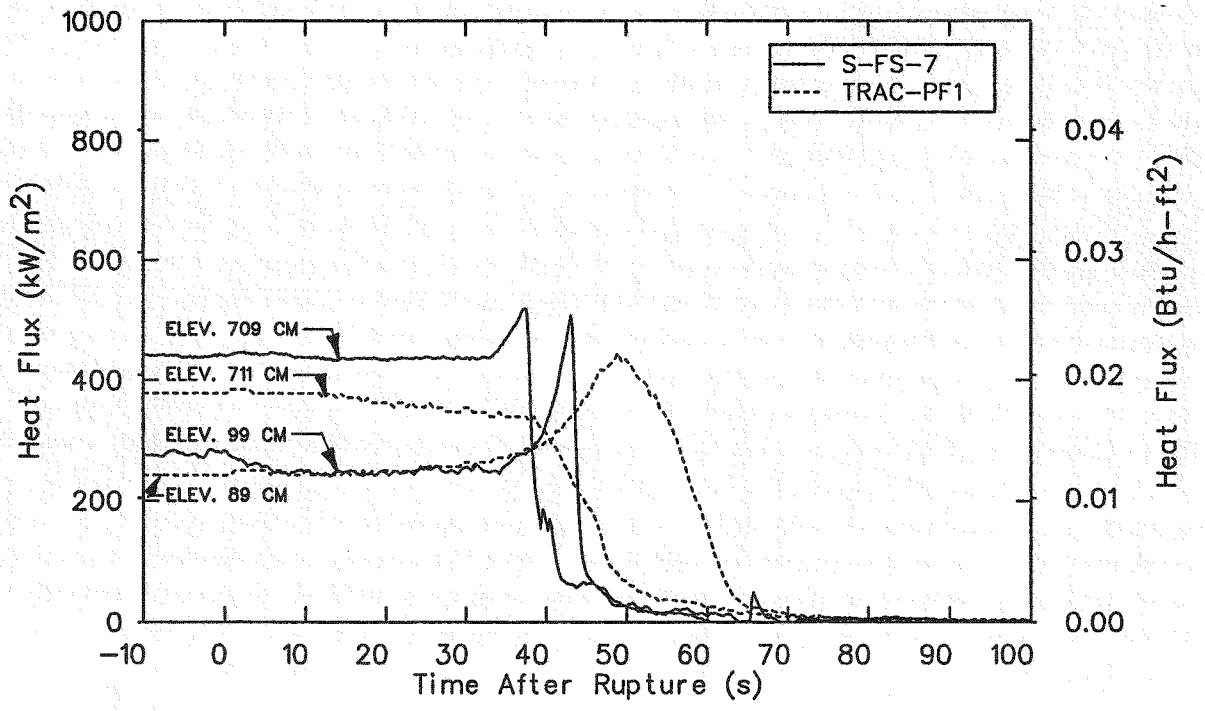

Figure 58. Comparison of measured and calculated primary downside heat fluxes during the early part of the blowdown phase of test S-FS-6B.

transfer coefficients, and by the both the secondary heat transfer coefficients and the heat fluxes measured in S-FS-6B.

The integrated effect of the local heat fluxes are shown in Figure 59, where the calculated history of primary-to-secondary energy removal rate through the broken loop steam generator is compared with corresponding experimental data. This comparison shows that the large decay in the calculated energy removal started at the same time as indicated by the test data, but the calculated decay was not as rapid.

Another approach to looking at the net energy removal rate is to view it as a function of secondary mass rather than a function of time. Calculated and measured data are presented in this form for comparison in Figure 60. This figure shows better agreement between the calculated and measured data than was shown in Figure 33 for S-FS-6B. The calculated and measured energy removal rates both roll off at nearly the same secondary mass [13 kg (28.6 lbm) compared to 11 kg (18.9 lbm)], although the calculated data exhibit a more gradual rate of decrease. The agreement shown in Figure 60 is particularly noteworthy because differences were noted in the calculated and measured energy removal rate histories in Figure 59 and in the calculated and measured secondary mass histories shown in Figure 61. Evidently the calculated correspondence between secondary mass and energy removal rate is the same as exhibited by the experimental data, in spite of differences in the initial secondary mass and the energy removal rate and secondary mass histories, although this agreement could be fortuitous.

The ability of TRAC-PF1/MOD1 to calculate the response of the broken loop steam generator during a simulated 14.3% bottom feedwater line break must be rated fair. The results of the calculation did not agree as well with the measured data as did the results of the calculation of the 100% break transient (S-FS-6B). While the S-FS-7 calculation generally produced results that were at least in agreement with the trends in the measured data, many of the comparisons showed discrepancies between the characteristics of the measured and calculated data histories for some period of time. As was the case with the S-FS-6B simulation, the evaluation of the ability of TRAC-PF1/MOD1 to simulate the broken loop steam generator response was clouded by an uncertainty in the measurement of the initial mass in the broken loop steam generator secondary and shortcomings in simulating the response of other system components that influenced the broken loop steam generator response. Correction of these deficiencies would significantly improve the accuracy of modeling the broken loop steam generator response.

An evaluation of the ability of TRAC-PF1/MOD1 to calculate localized heat transfer parameters under

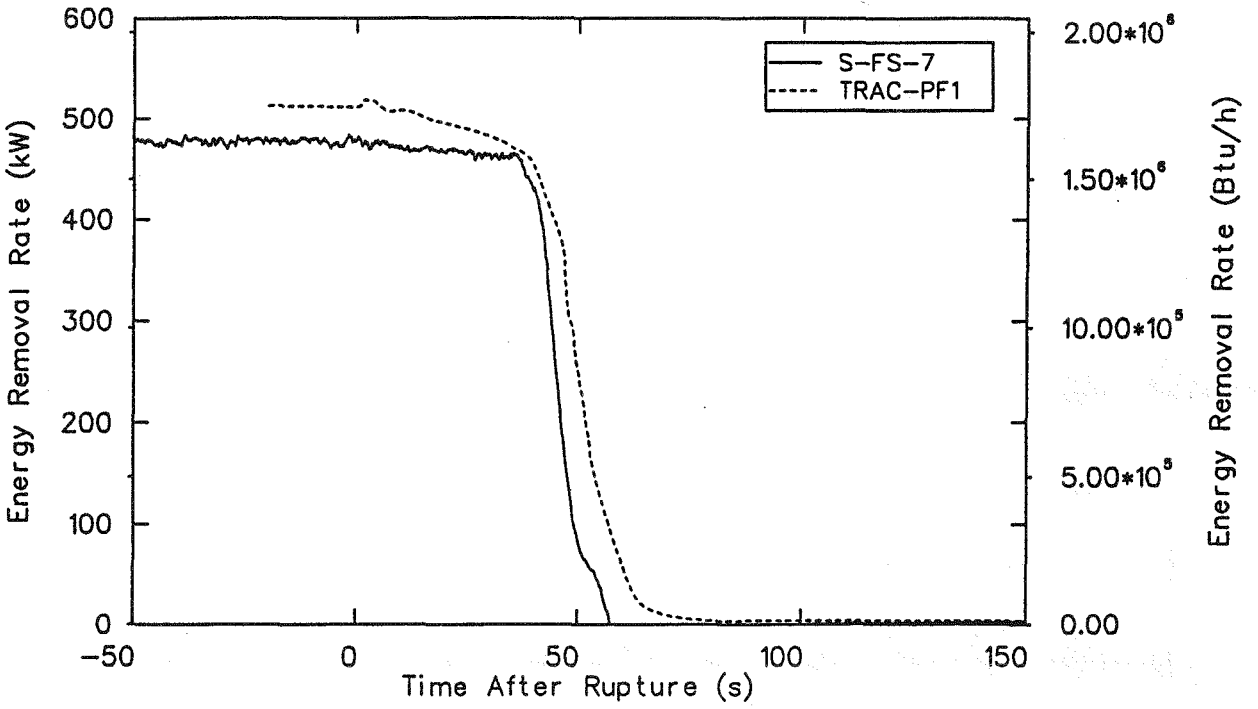

Figure 59. Comparison of measured and calculated broken loop primary-to-secondary heat transfer rate during the early part of the blowdown phase of test S-FS-7.

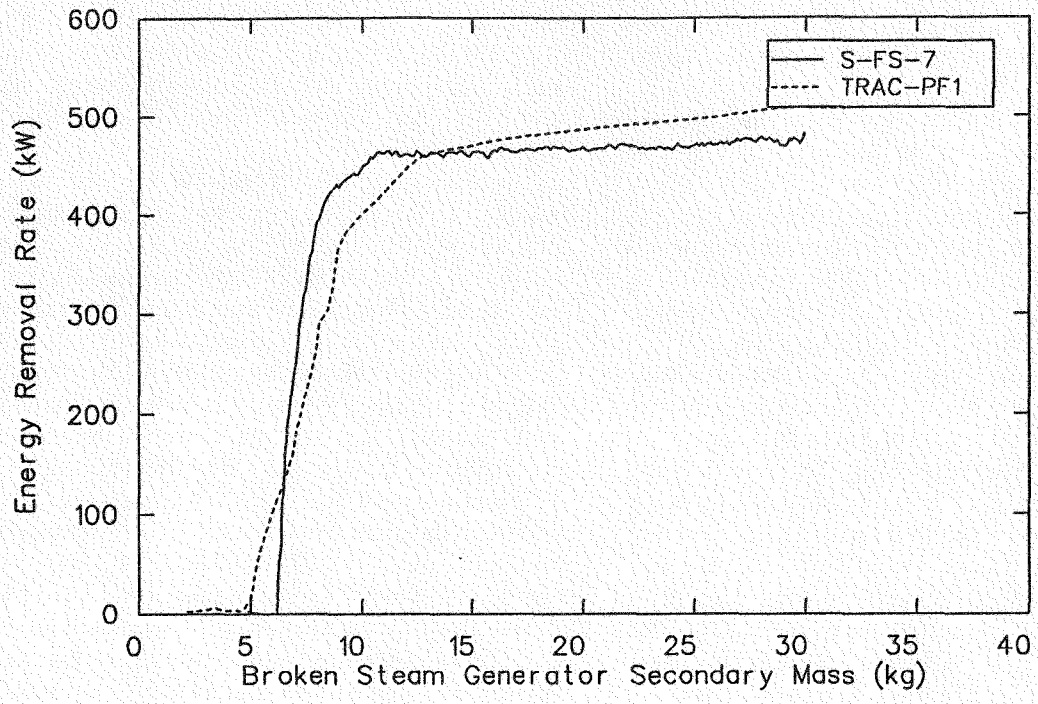

Figure 60. Comparison of measured and calculated broken loop steam generator energy removal rate as a function of total secondary mass during the early part of the blowdown phase of test S-FS-7.

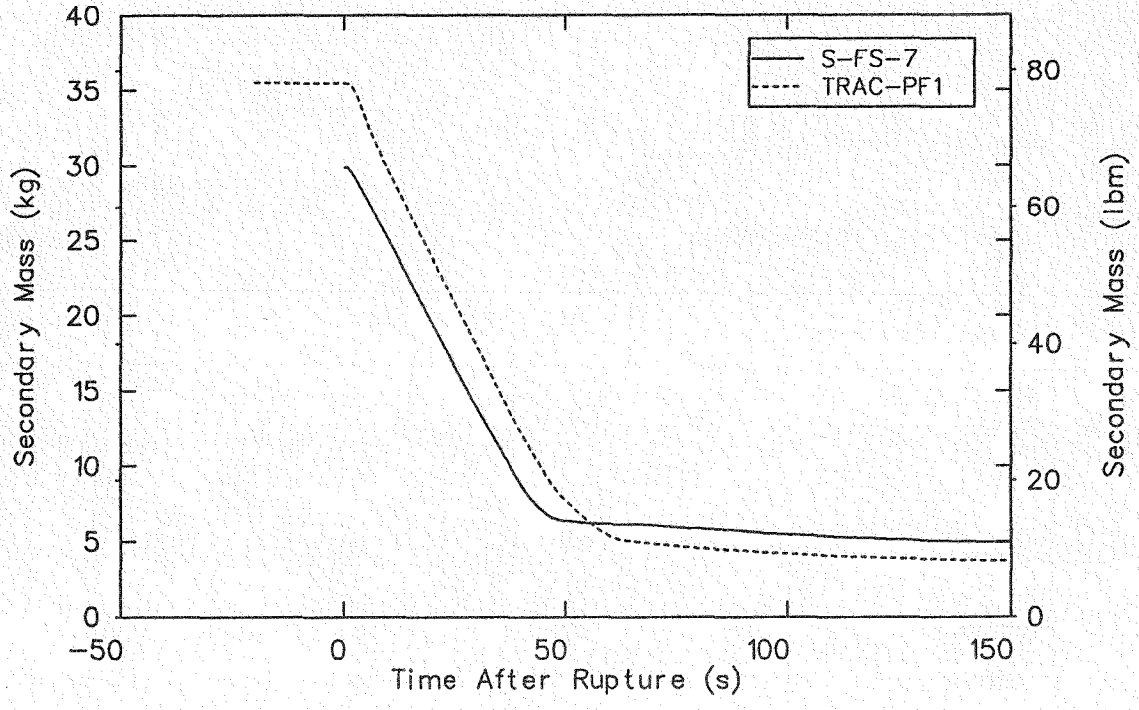

Figure 61. Comparison of measured and calculated broken loop steam generator secondary mass during the early part of the blowdown phase of test S-FS-7.

the transient conditions caused by the simulated 14.3% bottom feedwater line break has shown mixed results, similar to those that were observed for S-FS-6B. The calculated primary side heat transfer coefficients were bounded by, and had the same characteristics as, the measured coefficients at all times during the period when the coefficients decreased from their initial to negligible values. The calculated secondary side heat transfer coefficients exhibited some of the proper trends during the transient, and probably would have agreed better with the data if the initial secondary mass agreed better with the test value. The initial values of the calculated coefficients at the lower elevations agreed reasonably well with the measured values, but the calculated and measured values at the upper elevations were very different, and the variations of the upside coefficients with elevation for the two sets of data were opposite each other. The calculated primary heat fluxes agreed reasonably well with the measured data before transient initiation, but exhibited significant differences during the transient. Again, correction of the initial secondary mass would have improved the results. The calculated energy removal rate through the steam generator was in reasonable agreement with the measured data during the loss of heat removal capability, although the calculated rates did not decrease as rapidly. The calculated reduction in heat transfer rate versus secondary mass inventory did agree reasonably well with the measured data in spite of differences between the calculated and measured energy removal rate and secondary mass histories.

8. S-FS-11 TRANSIENT SIMULATION RESULTS

This section presents the results of the S-FS-11 (50% feedwater line break) transient calculation. Separate subsections compare the results of the TRAC-PF1/MOD1 simulation to the data measured during the test. Subsection 8.1 discusses the general response of the system during the blowdown phase of the test. Subsection 8.2 discusses the response of the broken loop steam generator until the energy removal capability was negligible. Subsection 8.3 discusses the general response of the system during the subsequent stabilization phase of the simulation.

8.1 General System Response During the Blowdown Phase

This subsection discusses the ability of TRAC-PF1/MOD1 to calculate the response of a system following a 50% break in a bottom feedwater line. Selected parameters from the calculation are compared to measured parameters in both the primary and secondary systems up to the end of the blowdown phase of the transient. The discussion generally coincides with the simulated automatic actions of the plant protection system.

The events influencing the response of the system during the test were the bottom feedwater line break and the automated actions of the plant protection system. Following the initiation of the break, feedwater to both of the steam generators was terminated. This event caused the primary coolant system to pressurize due to the reduced energy removal capacity of the steam generators. The primary pressure eventually reached the pressurizer high pressure trip set point, which caused the main steam control valves to close, the primary coolant pumps to begin coasting down, and the reactor to SCRAM. Associated delays with all automatic actions were simulated concurrent with an assumed simultaneous loss of offsite power.

Figure 62 contains the measured and calculated parameters associated with these automatic actions. Table 6 compares the time these automatic actions occurred during the test[9] relative to the TRAC-PF1/MOD1 calculations. In general, the simulation was more responsive than the test. The break caused the calculated pressurizer pressure to rise faster than the test and initiate the high pressurizer pressure trip 4.7 s early. Thereafter, the pressurizer pressure is adequately simulated.

The steam generator secondary pressure is also more responsive following the SCRAM signal. Both of the calculated steam generator pressures initially rise above, then decay back to, the test pressures. This appears to be caused by an error in modeling the steam generator secondary volumes. Subsequent to completing the calculations, Semiscale personnel indicated that a section of the steam piping from the crossover line junction to the steam control valves on both steam generators was not included in the model. Inclusion of this 1 ft^3 volume would have increased the total secondary volume by 13% and minimized the response of the pressure.

The pump coast down and the core power decay were adequately simulated in the calculation, allowing for the early SCRAM signal. The total calculated energy removal rate of the steam generators was lower than the test for the first 35 s; thereafter, it was higher than the test. Nevertheless, it appears to represent the test adequately and differences between the measured and calculated energy removal rates are within the tolerances of the measured data.

Following the high pressurizer pressure trip, the steam generator secondary pressures peak, decaying thereafter. When the broken loop secondary pressure decayed to 4.47 MPa (648.2 psia), the next automatic action occurred. A Safety Injection System (SIS) signal closed the crossover line valve and initiated auxiliary feedwater flow to both steam generators. This event prevented a further loss of secondary mass in the intact loop steam generator and heat removal capability. The auxiliary feedwater flow rates matched those of the test, but were initiated 18 s too early, a direct result of the early SIS signal.

Following closure of the crossover line valve, the intact loop secondary pressure increased due to the increasing energy content of the secondary. Before the crossover line valve closure, the energy transferred from the primary system exited through the crossover line. Closure of this flow path bottled up the energy transferred from the primary system, resulting in an increasing pressure. Conversely, the broken loop secondary pressure decrease accelerated, due to mass and energy no longer being supplied from the intact loop secondary through the crossover line. In addition, mass and energy were still being lost out the break.

Because the broken loop steam generator had effectively no mass and could no longer contribute to the removal of energy from the primary, the intact loop steam generator was the only component available to remove energy from the primary. Thus, the net energy balance across the intact loop steam generator controlled the response of the system until the end of the blowdown. This balance included energy from the decay heat of the core, energy removed by the steam generators, energy transferred to or from the metal in

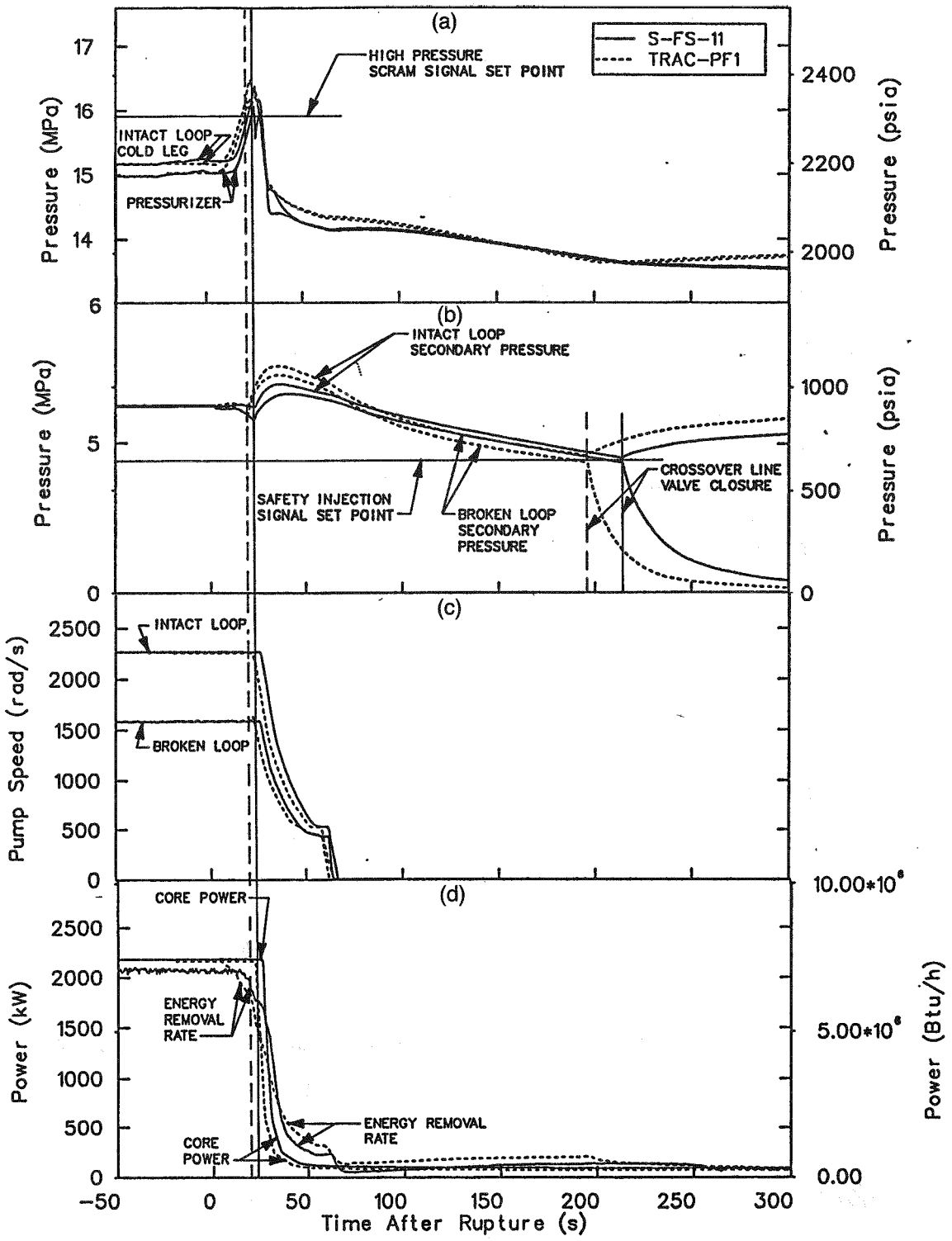

Figure 62. Composite of measured and calculated parameter histories showing the results of simulated automatic actions during the early part of the blowdown phase of test S-FS-11.

Table 6. Sequence of events for test S-FS-11

	Time (s)	
	Data	TRAC
Broken loop steam generator main feedwater line break		
Initiated	0.0	0.0
Fully open	0.7	0.7
Steam generator main feedwater isolated		
Intact loop	1.0	4.0
Broken loop	2.0	4.0
SCRAM at P_{pzr} = 15.86 MPa (2300 psia)	23.0	18.3
Main coolant pump begins coast down		
Intact loop	25.0	20.6
Broken loop	25.0	20.6
Core power decay initiated	26.0	20.8
Main steam flow control valve closed		
Intact loop	26.5	22.3
Broken loop	26.5	22.3
Power to main coolant pump tripped off		
Intact loop	61.0	56.6
Broken loop	61.0	56.6
Safety injection signal		
Broken loop secondary pressure at 4.47 MPa (648.2 psia)	209.0	187.0
High pressure injection flow available		
Intact loop	209.0	187.0
Broken loop	209.0	187.0
Auxiliary feedwater flow initiated		
Intact loop	211.0	192.7
Broken loop	211.0	192.7
Crossover line valve closed	214.0	195.2
Blowdown phase of transient completed	600.0	600.0
Initiate operator recovery actions	600.0	600.0
Auxiliary feedwater flow terminated		
Broken loop	610.0	610.0
Maintain the subcooled margin with the pressurizer heaters		
Heaters on	731.0	731.3
Heaters off	1053.0	1024.3
Stabilization phase of transient completed	4055.0	4100.0

the system, and energy lost due to the loss of primary and secondary fluid. Based on this energy balance, the trend of the primary and secondary pressures were correct. However, the calculated intact loop secondary pressure was too high once the crossover line valve closed; primarily due to the early isolation of the intact loop steam generator and also to the steam piping from the crossover line junction to the steam control valves on both steam generators not being included in the model. Inclusion of this 1 ft^3 volume for each steam generator would have reduced the rate of pressure decrease in the secondary.

Figure 63 shows a comparison between the measured and calculated crossover line flow. Although the calculated flow appears reasonable, the broken loop steam generator pressure decayed too rapidly. This result was due to either a mismatch between energy removed out the break relative to energy input to the unit, or to the secondary volume of each steam generator that was not modeled. The energy input was primarily from the crossover line and the primary coolant system. Consequently, energy transfer from either the primary system or the crossover line must be too small, because the additional secondary volume was necessary to allow the pressure to decay slower; or else the simulation was too simplistic, and effects such as the ambient heat losses and the steam generator secondary metal mass must be included.

Figure 64 compares the measured and calculated primary system pressure during the blowdown phase. The pressure trends were in good agreement until about 200 s. Thereafter, the calculated pressures began an almost linear increase. The pressure increased as a result of a net energy addition to the primary coolant system, evidently due to the intact loop steam generator not removing enough energy from the primary system. During the initial blowdown of the broken loop steam generator, the pressure decayed too quickly, causing an early SIS trip. Consequently, the steam generators were isolated too quickly and the resulting intact loop steam generator energy content and temperature were too high. This diminished the driving potential between the primary and secondary and by the end of the blowdown phase, the calculated primary system pressure was 0.68 MPa (100 psi) higher than the measured pressure.

Ideally, differences between the calculated and measured primary and secondary pressure histories could be explained by the differences in the calculated and measured energy balances. Comparisons of calculated and measured pressurizer pressure, intact and broken loop secondary pressures, core power, and total energy removal rate (sum of the primary-to-secondary heat transfer in both generators) are given in Figure 62. Both of the calculated secondary pressures decreased too rapidly, resulting in an early

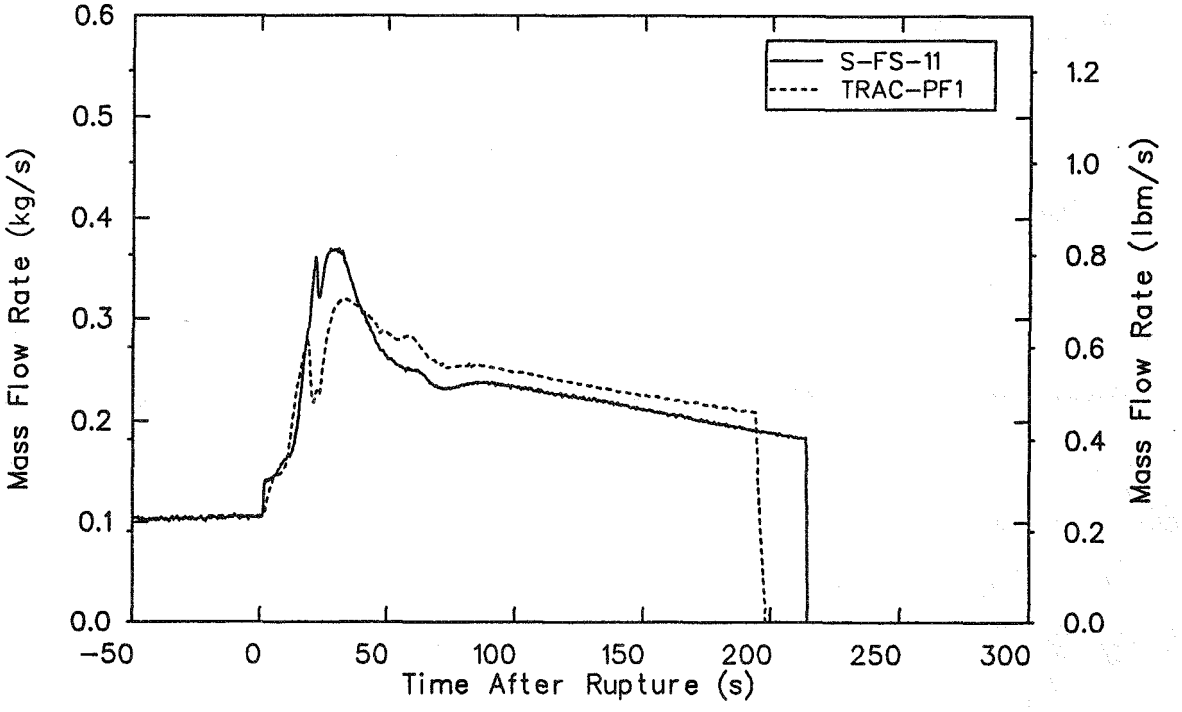

Figure 63. Comparison of measured and calculated crossover line flow rate during the early part of the blowdown phase of test S-FS-11.

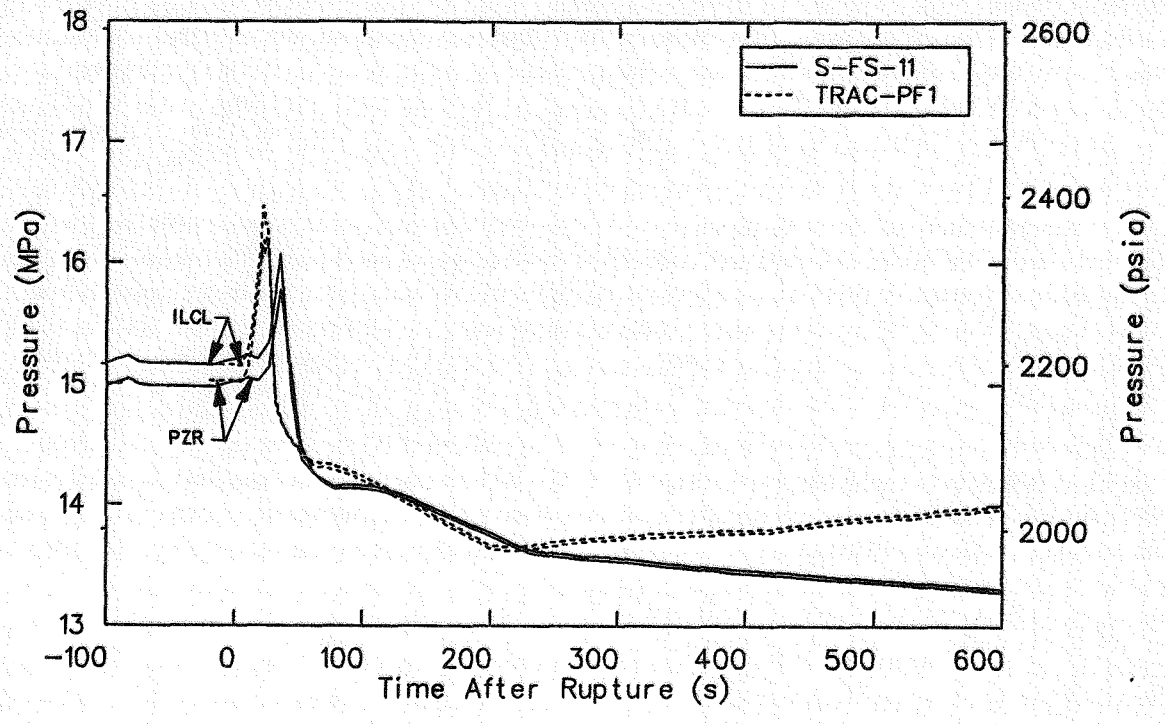

Figure 64. Comparison of measured and calculated pressurizer (PZR) and intact loop cold leg (ILCL) pressures during the blowdown phase of test S-FS-11.

SIS signal. Figure 62 illustrates again that the calculated total energy removal rate was larger than the corresponding measured data during the period when both of the secondary pressures were decreasing, and does not explain the difference between the calculated and measured data. Differences between the calculated and measured core power and total energy removal rate do explain the differences between the calculated and measured primary pressure histories. After simulating the primary pressure accurately out to about 200 s, the calculated primary pressure began an almost linear increase. Figure 62 shows that this corresponded to the time the calculated energy removal rate decreased below the core power, resulting in a net energy input to the primary fluid. Accounting for the metal-to-fluid energy input could make the times of the energy crossover point and the change in the pressurization rate coincide exactly.

At about the same time, an abrupt change in the slope of the calculated intact loop secondary pressure history was noticed. Just before the calculated total energy removal rate decreased below the core power, the energy removal rate exhibits an abrupt change in slope. An extensive review of calculated parameters associated with the intact loop steam generator failed to show any clear reason for the abrupt decrease in energy removal capability and change in pressurization of the secondary. However, they may be related to a change in heat transfer mode at locations within the intact loop steam generator.

Even without the abrupt decrease in the energy removal rate, the rate would have fallen below the core power. The measured energy removal rate was larger than the core power and remained larger until the end of the blowdown phase. A review of the component and heat transfer modeling associated with the intact loop steam generator is indicated. However, unlike the broken loop steam generator, extensive localized heat transfer data for the intact loop steam generator is not available. The Semiscale intact loop steam generator contains six U-tubes that were modeled as a single tube. The model also contains riser and downcomer filler pieces that were lumped into the riser shell. These simplifications may have caused the heat transfer areas and flow resistances to become distorted, adversely affecting the accuracy of the steam generator simulation.

Figures 65 and 66 compare, respectively, the broken loop and intact loop primary coolant temperatures during the blowdown phase. In general, the temperatures, exhibit similar trends, although the calculated broken loop temperatures were too high. This again was the result of the net energy in the system during the simulation being greater than that observed during the test. Note that following the SCRAM, the apparent broken loop cold leg temperature was hotter than the hot leg temperature in both the measured and calculated data.

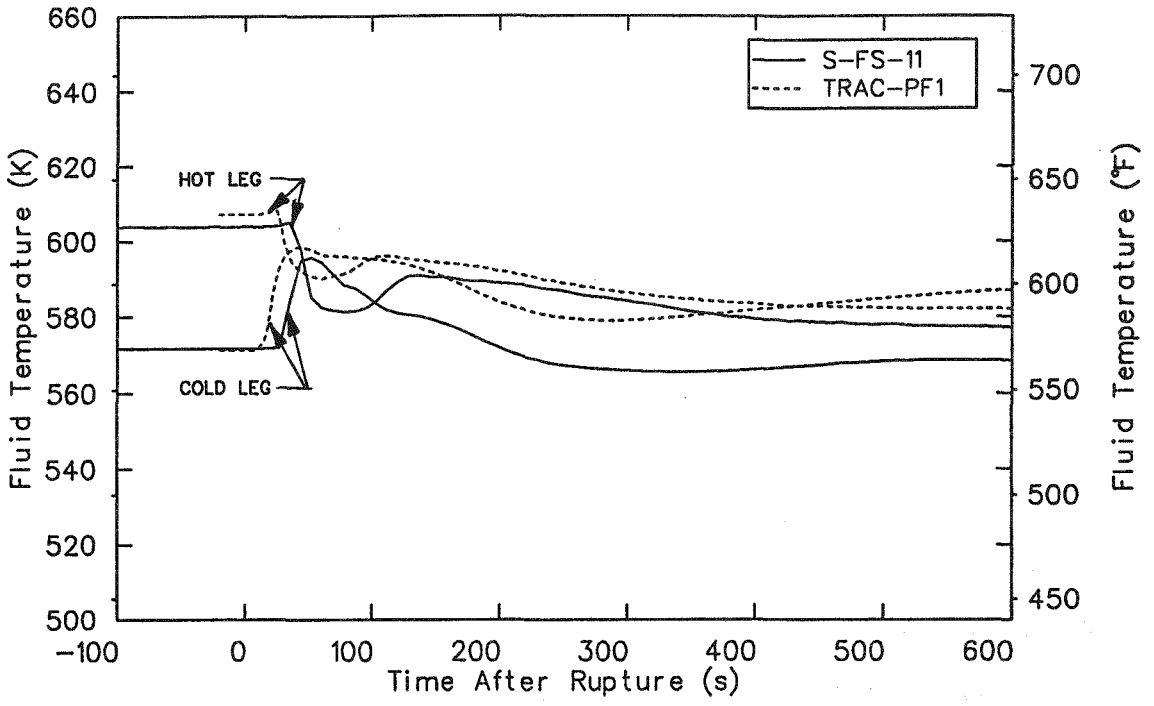

Figure 65. Comparison of measured and calculated broken loop hot and cold leg fluid temperatures during the blowdown phase of test S-FS-11.

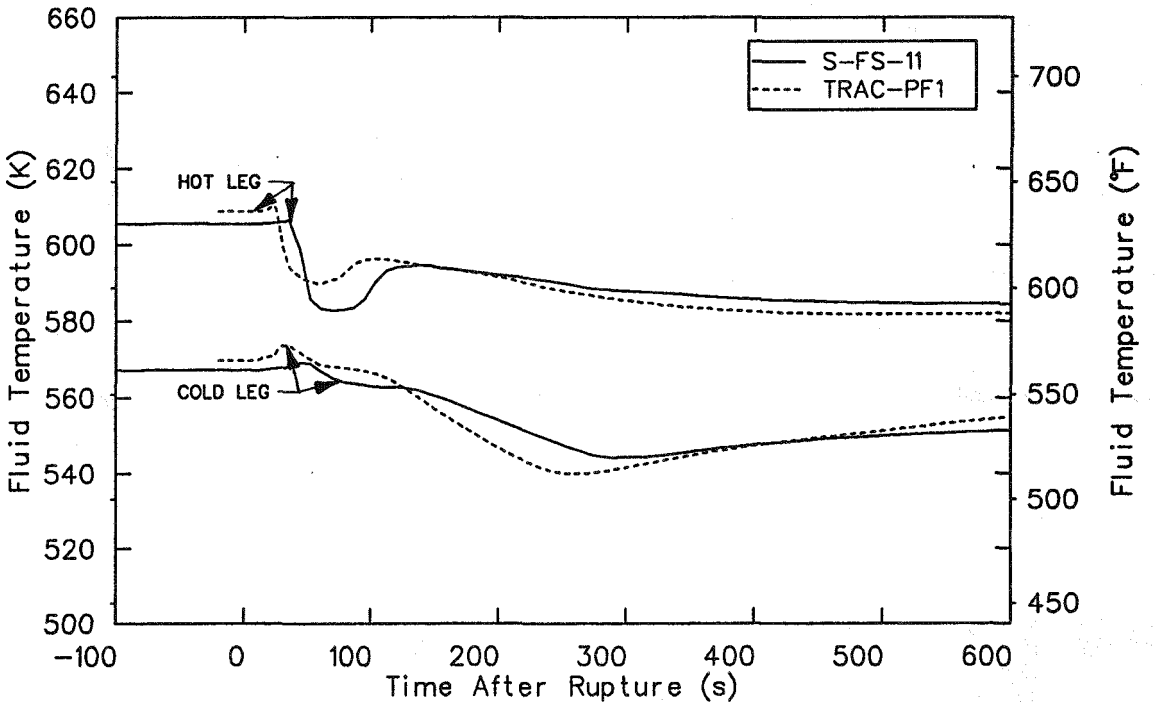

Figure 66. Comparison of measured and calculated intact loop hot and cold leg fluid temperatures during the blowdown phase of test S-FS-11.

This occurred for two reasons. First, the cold leg temperature increased due to the degraded energy removal capability of the steam generator. Second, the hot leg temperature decreased due to the decreasing energy addition from the core, a direct result of the SCRAM. Also, the temperatures as noted at the thermocouple locations shift relative to each other, due to the pump coast down, the resulting decrease in loop flow, and the longer loop transit time.

By the end of the blowdown phase, the temperatures are more representative of conditions in the system. However, the calculated broken loop hot and cold leg temperatures were 5 K (9°F) and 19 K (34°F), respectively, higher than those measured. The higher calculated temperatures are indicative of the heating on the primary side that occurred for two reasons. First, the steam generator was removing less energy from the primary coolant in the calculation than during the test. Second, heat losses in excess of the 22 kW augmented core power were not included in the simulation, which would affect the calculated temperatures.

Conversely, the calculated temperatures in the intact loop, as shown in Figure 66, were much closer to the measured results, 2 K (4°F) lower in the hot leg and 4 K (7°F) higher in the cold leg. The lower calculated hot-to-cold leg temperature difference is indicative of the lower energy transfer to the intact loop steam generator relative to the test. Energy losses to the ambient will not affect the results in the intact loop as much as the broken loop because of higher natural circulation mass flow rates.

In summary, most of the trends in the calculated parameters relative to Semiscale feedwater line break test S-FS-11 were correct. The results were in good agreement for the first 18 s, then the steam control valves closed. Thereafter, the results were in fair agreement until the SIS signal occurred and the crossover line valve closed at approximately 195 s. From then until the end of the blowdown phase, the results showed significant differences from the measured data. As will be shown later, these differences impacted the recovery phase of the calculation.

Three areas have been identified that could improve the simulation. The first is the primary-to-secondary heat transfer in the intact loop steam generator. During the early portions of the transient, the energy removal rate was too high; later, the energy removal rate was too low. This was responsible, in part, for the differences observed in the primary pressure, and that ultimately caused the uncontrollable increase in pressure by the end of the blowdown. The intact loop steam generator contains six U-tubes, and the broken loop steam generator contains two U-tubes. Although the geometry of the tubes in each steam generator are different, they were modeled as a single tube. This simplification may have distorted the effective heat transfer area as well as the fluid conditions affecting the heat transfer.

Second, the steam piping between the crossover line junction and the steam control valves on both steam generators should be included. This piping was identified by the Semiscale project after the conclusion of the calculations. Inclusion of this 1 ft^3 volume in both steam generators would have increased the total secondary volume by 13% and minimized the responsiveness of the secondary pressure.

Third, improving the secondary fluid to structure energy transfer within the steam generators is needed. The riser and downcomer filler pieces were modeled as part of the steam generator shell in the calculation. This simplification may have distorted the secondary fluid-to-metal heat transfer area and storage masses and adversely affected the accuracy of the energy removal rate. The differences noted in the magnitude and timing of the secondary pressure history cannot be fully explained with primary-to-secondary heat transfer or with an increase in the secondary volume.

8.2 Broken Loop Steam Generator Response

This subsection discusses the ability of TRAC-PF1/MOD1 to calculate the response of the broken loop steam generator secondary following a 50% break in a bottom feedwater line. The broken loop steam generator reacts to both a loss of feedwater and to a loss of mass, both a direct result of the break. Selected parameters from the calculation are also compared to measured parameters in the broken loop steam generator. The discussion begins with the parameters associated with the feedwater line break flow, discusses the secondary side flow rates and inventory distribution, the primary and secondary temperatures, and concludes with local and total heat transfer.

The principal boundary condition affecting the broken loop steam generator was a simulated 50% break in the bottom feedwater line. Figure 67 provides a composite of measured and calculated parameters associated with flow out the break. In general, the calculated results were in good agreement with the measured data. Notable similarities include the peak break flow and the decay in break flow as the secondary pressure decreased. Note, however, that before the start of the transient, the calculated subcooling upstream of the break was much less than that measured. The duration of this difference was very short. Consequently, only the initial peak flow rate would be affected, not the break flow rate in general.

The measured and calculated void fraction histories are shown in Figure 67. This indicates that the early

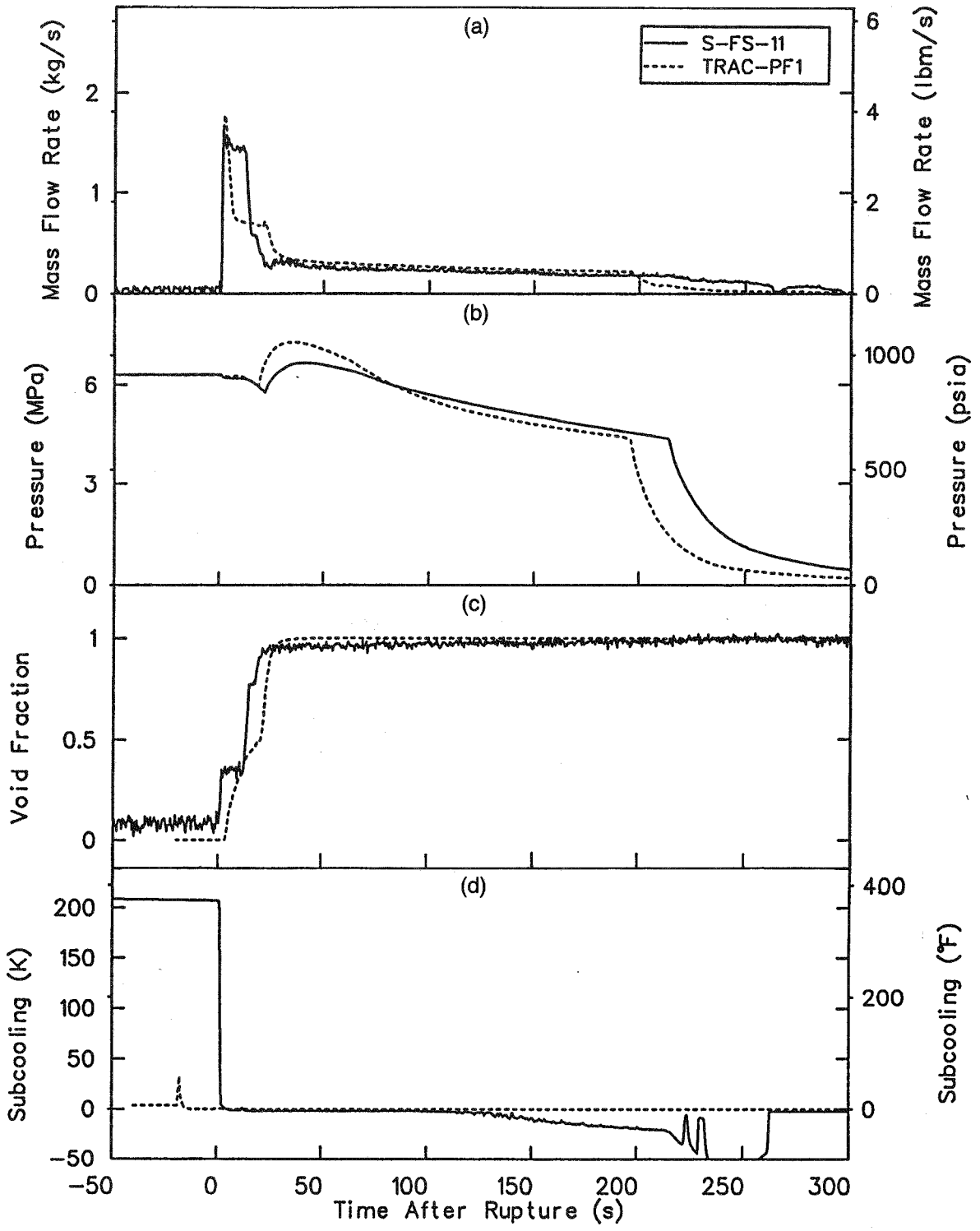

Figure 67. Composite of measured and calculated parameter histories associated with feedwater line break flow during the early part of the blowdown phase of test S-FS-11.

discrepancies in the break flow rate are the result of the calculated void fraction differing from the measured void fraction. This may have been due to slight differences in the initial secondary mass in the steam generator. However, it was more likely the result of flow resistances in the secondary being too low and allowing water to reach the break location too easily. Increasing the secondary resistances would cause more secondary fluid to flash as it approached the break location.

Figures 68 and 69 present, respectively, calculated and measured flow rates associated with the broken loop steam generator. Initially, the calculated riser flow equaled the sum of the downcomer and steam flow exiting the steam generator. The riser and steam flows decreased once the break opened and eventually reversed direction. After the steam valves closed, the crossover line supplied all the flow to the broken loop steam generator. Thus, the steam flow equaled the crossover flow and was split between the riser and the downcomer. Note that after the steam valves closed, a positive crossover flow became a negative steam flow. This relationship was maintained until the crossover line valve closed, then all flows went to zero. These trends were expected during the blowdown phase and the magnitudes are consistent at the various locations.

The measured steam generator flow rates in Figure 69 initially indicate a similar relationship between the riser, downcomer, and steam flows. However, the measured riser and downcomer flows were smaller than the calculated values. Once the break opened, the riser and steam flows decreased. As before, after the steam valve closed, the steam flow reversed. Because the steam flow instrumentation could not monitor reverse flow accurately, the data became unreliable. Aside from the steam flow, the measured and calculated results were not at all consistent. The riser and downcomer flows were approximately equal and of the same magnitude, indicating that flow continued up the riser instead of reversing and that all of the flow passed into the downcomer. The existing data does not incidate where the flow from the crossover line was going. Such significant differences between the calculated and measured flows with respect to a steam dome mass balance lead to the conclusion that the measured mass flow rates are questionable, or may simply be due to measurement errors.

Heat transfer in the steam generator is partially dependent upon the level and distribution of liquid in the secondary. Figures 70 and 71 contain the measured and calculated collapsed liquid levels in the broken loop steam generator downcomer and riser, respectively. Both the measured and calculated collapsed liquid levels indicated that the downcomer and the riser

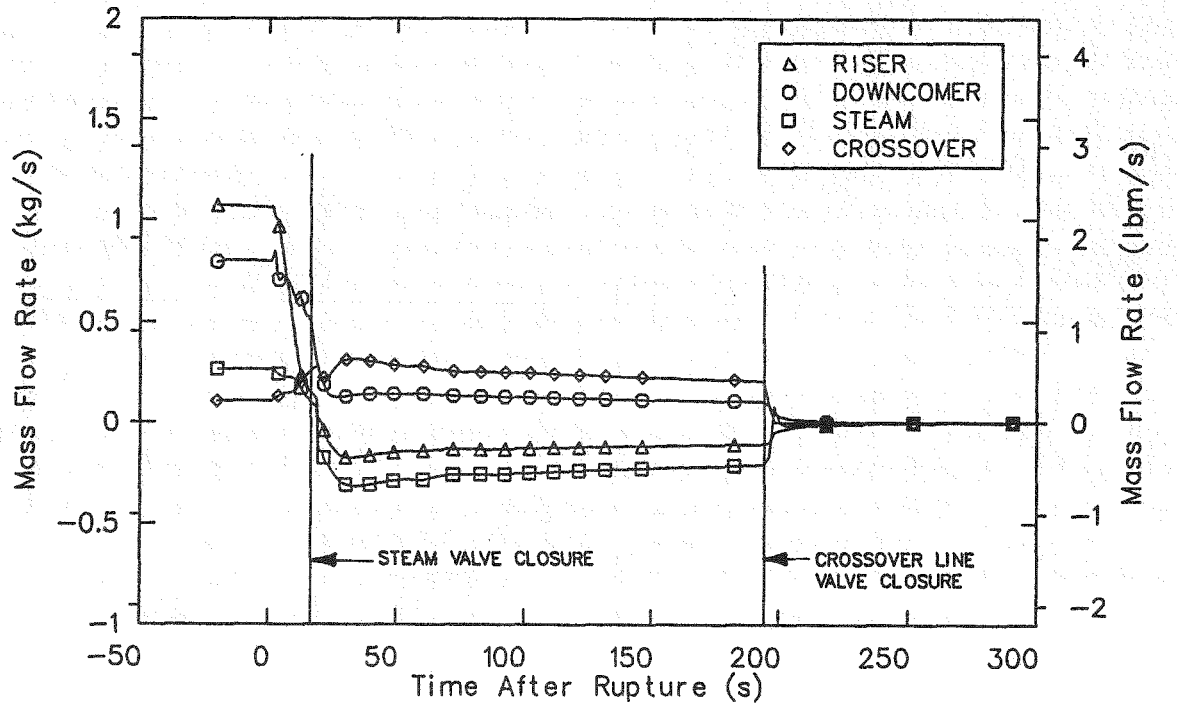

Figure 68. Calculated broken loop steam generator external and internal flow rates during the early part of the blowdown phase of test S-FS-11.

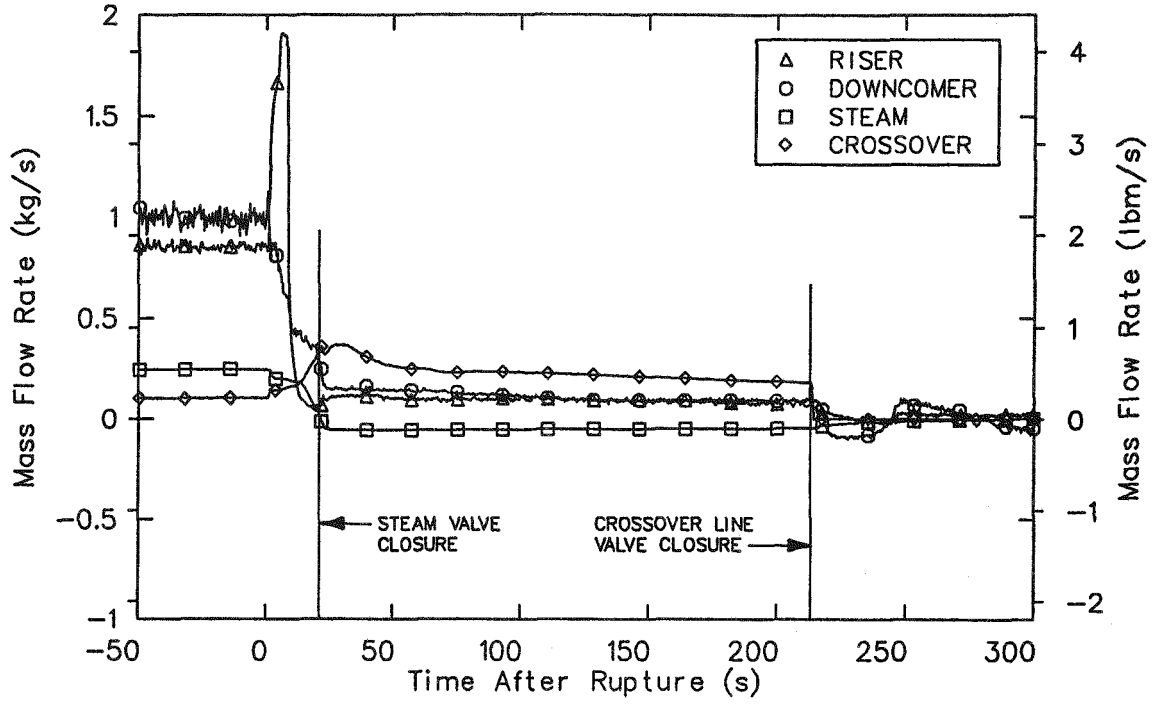

Figure 69. Measured broken loop steam generator external and internal flow rates during the early part of the blowdown phase of test S-FS-11.

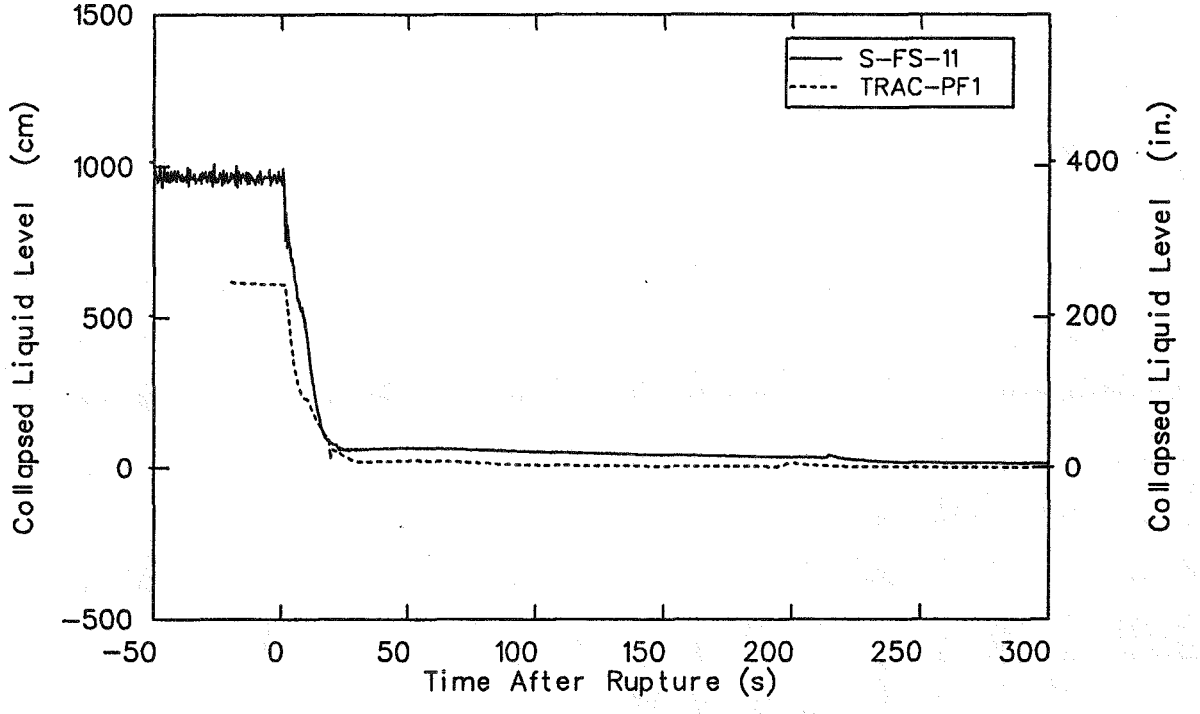

Figure 70. Comparison of measured and calculated broken loop steam generator riser collapsed liquid level during the early part of the blowdown phase of test S-FS-11.

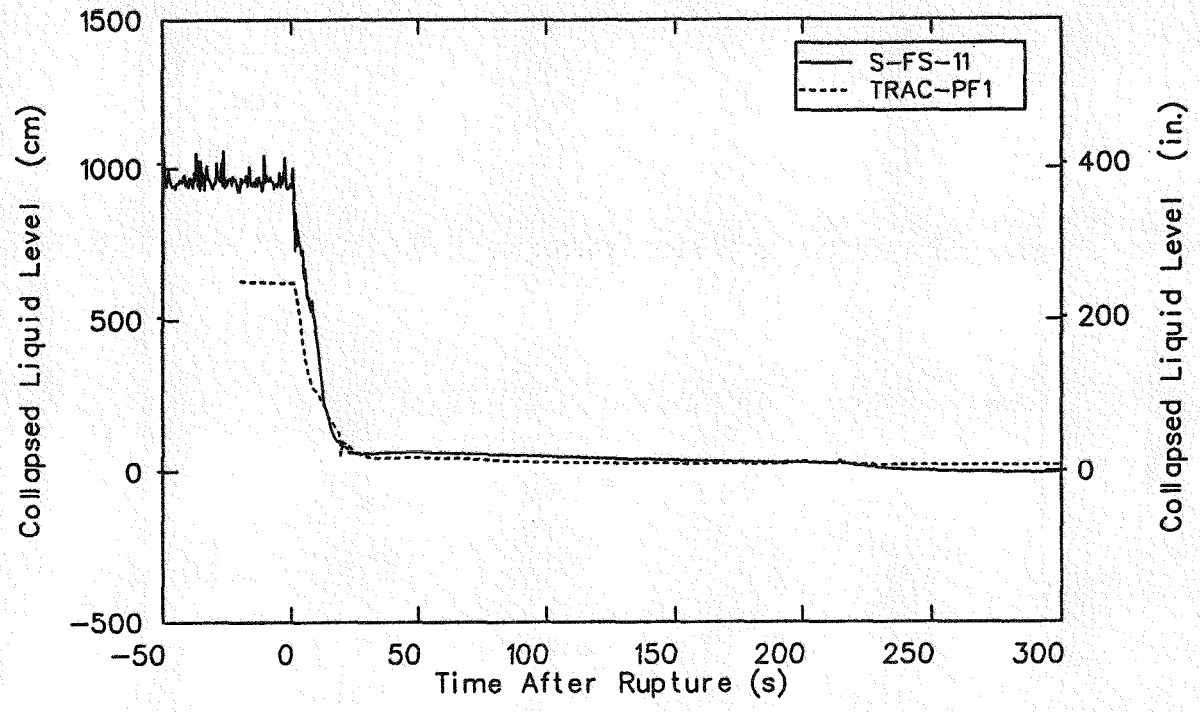

Figure 71. Comparison of measured and calculated broken loop steam generator downcomer collapsed liquid level during the early part of the blowdown phase of test S-FS-11.

drained uniformly. In general, the calculated trends were in good agreement with the measured data. The principal difference was the initial levels. The indicated levels were based on differential pressures in the steam generator. The initial mass in the steam generator was close to the initial mass before the start of the test. Therefore, adjusting resistances internal to the steam generator would alter the differential pressures inside the steam generator and, consequently, the indicated liquid levels.

Figures 72 and 73 compare the measured and calculated void distribution in the lower and upper portions of the riser, respectively. These figures indicate that the void fraction began to rise immediately after the break opened as a result of vaporization in the system due to a decrease in the secondary pressure and termination of the feedwater. The measured data also indicated that the void fraction increased rapidly at all elevations. The calculated void fractions indicate a response very similar to the data.

Figures 74 and 75 compare the primary and secondary fluid temperatures across the broken loop steam generator U-tube. Figure 74 compares these temperatures on the hot side of the U-tube; Figure 75 on the cold side. The calculated primary temperatures are liquid temperatures. The calculated secondary temperatures are vapor temperatures. These temperatures are most representative of the fluid conditions that existed at these locations during the transient. Calculated secondary liquid temperature is also included in Figures 74 and 75 for comparison. In general, the measured and calculated temperatures are either in good agreement or exhibit similar trends. The dip in the secondary temperatures around 200 s resulted from closure of the crossover line valve. The difference in the timing of the dip reflects the offset in the measured versus calculated time of the SIS signal. Proper timing of the SIS signal in the calculation would have resulted in a better agreement between the calculated and riser fluid temperatures.

The ability of TRAC-PF1/MOD1 to calculate local heat transfer under transient conditions was evaluated next. Calculated heat transfer coefficients and heat fluxes were compared with heat transfer data obtained from the test data. This data included primary and secondary fluid temperatures and wall temperatures at a common elevation. Calculated and measured primary side heat transfer coefficients are presented in Figures 76 through 78. These include, respectively, the lower elevations on the upside of the tube, upper elevations on the upside of the tube, and the full range of elevations on the downside of the tube. The measured data includes both the long and the short tubes in the Semiscale broken loop steam generator. In general, the calculated heat transfer coefficients are bound by the measured data, but more representative

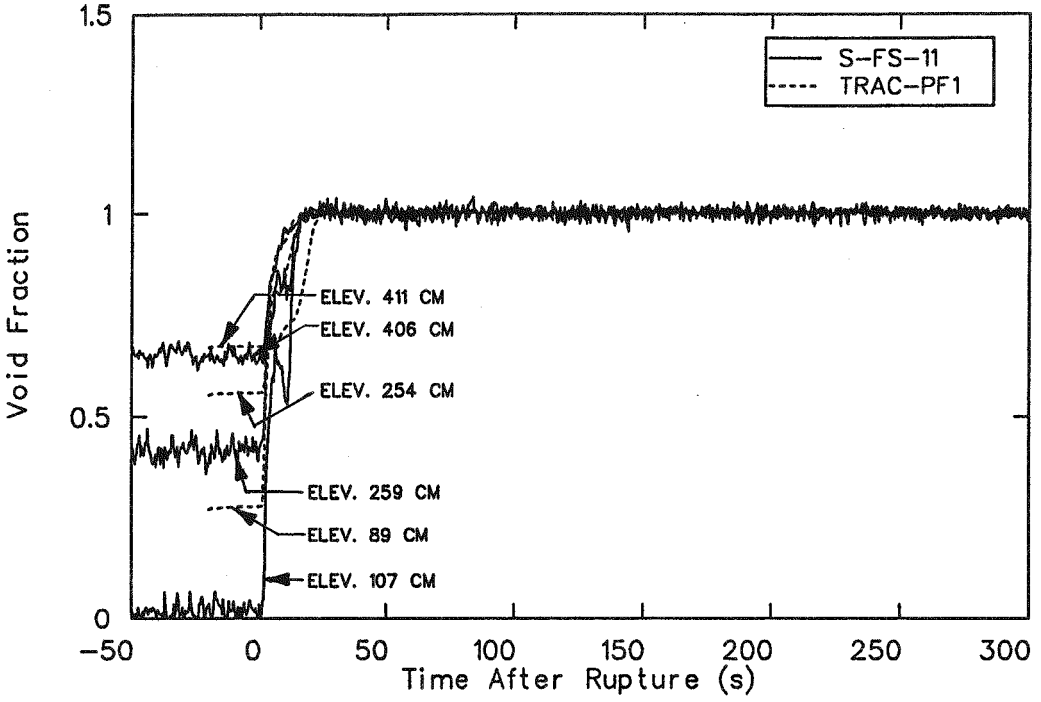

Figure 72. Comparison of measured and calculated lower riser void distribution during the early part of the blowdown phase of test S-FS-11.

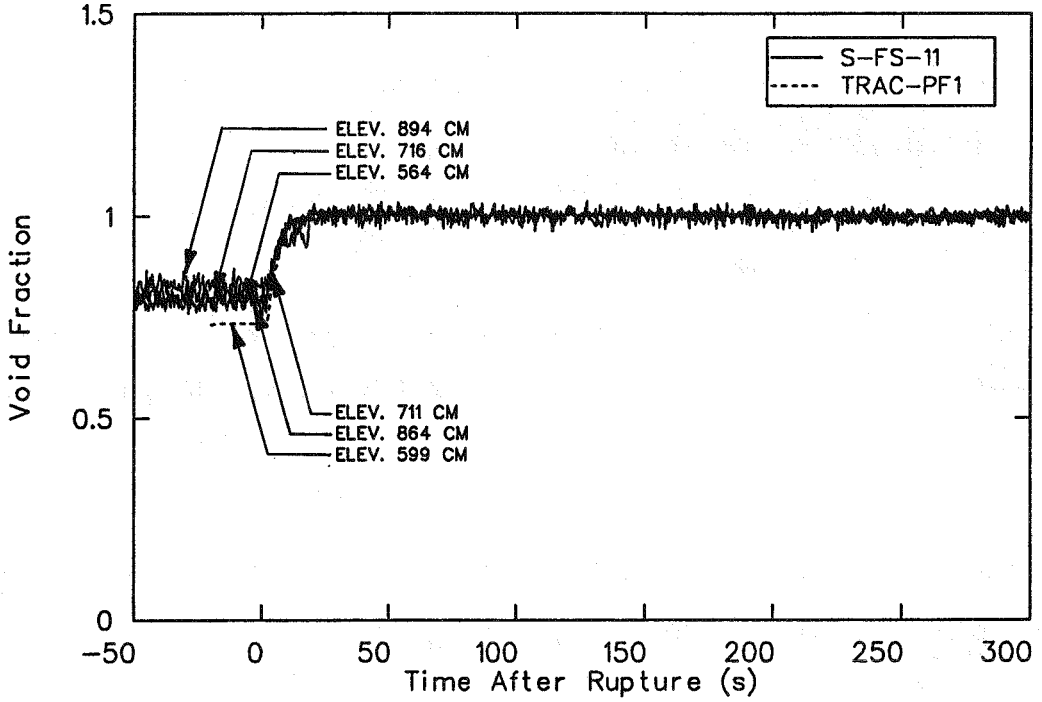

Figure 73. Comparison of measured and calculated upper riser void distribution during the early part of the blowdown phase of test S-FS-11.

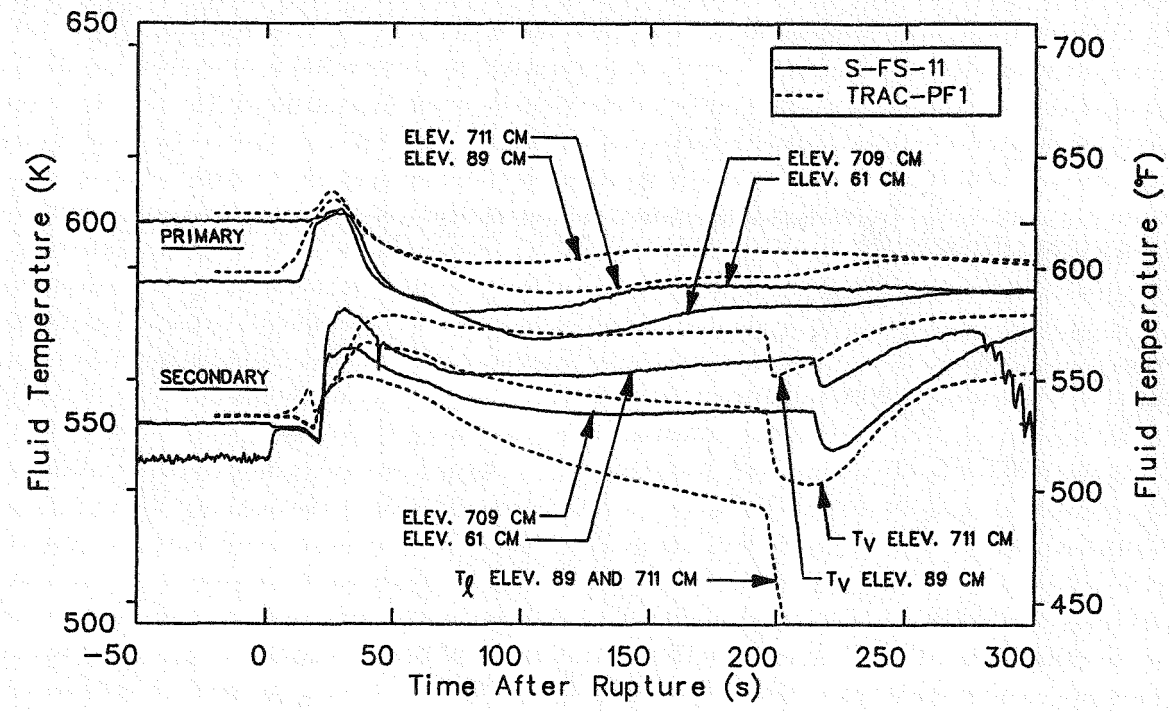

Figure 74. Comparison of measured and calculated primary upside and secondary temperatures at U-tube upper and lower elevations during the early part of the blowdown phase of test S-FS-11.

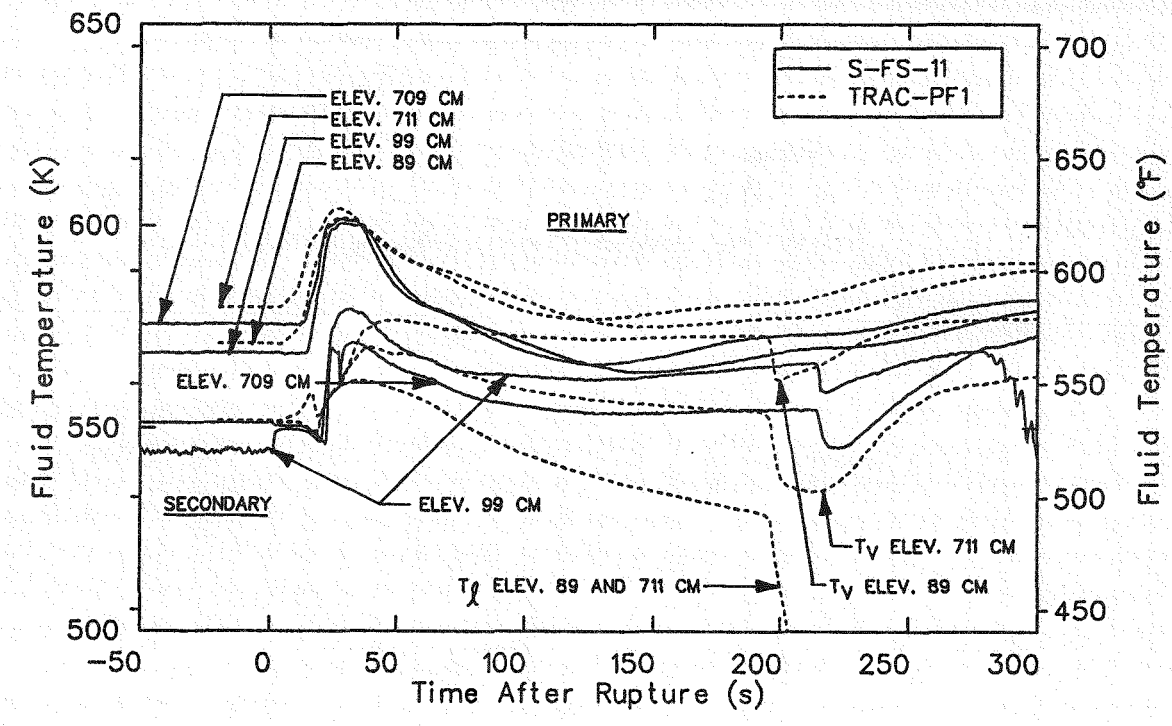

Figure 75. Comparison of measured and calculated primary downside and secondary temperatures at U-tube upper and lower elevations during the early part of the blowdown phase of test S-FS-11.

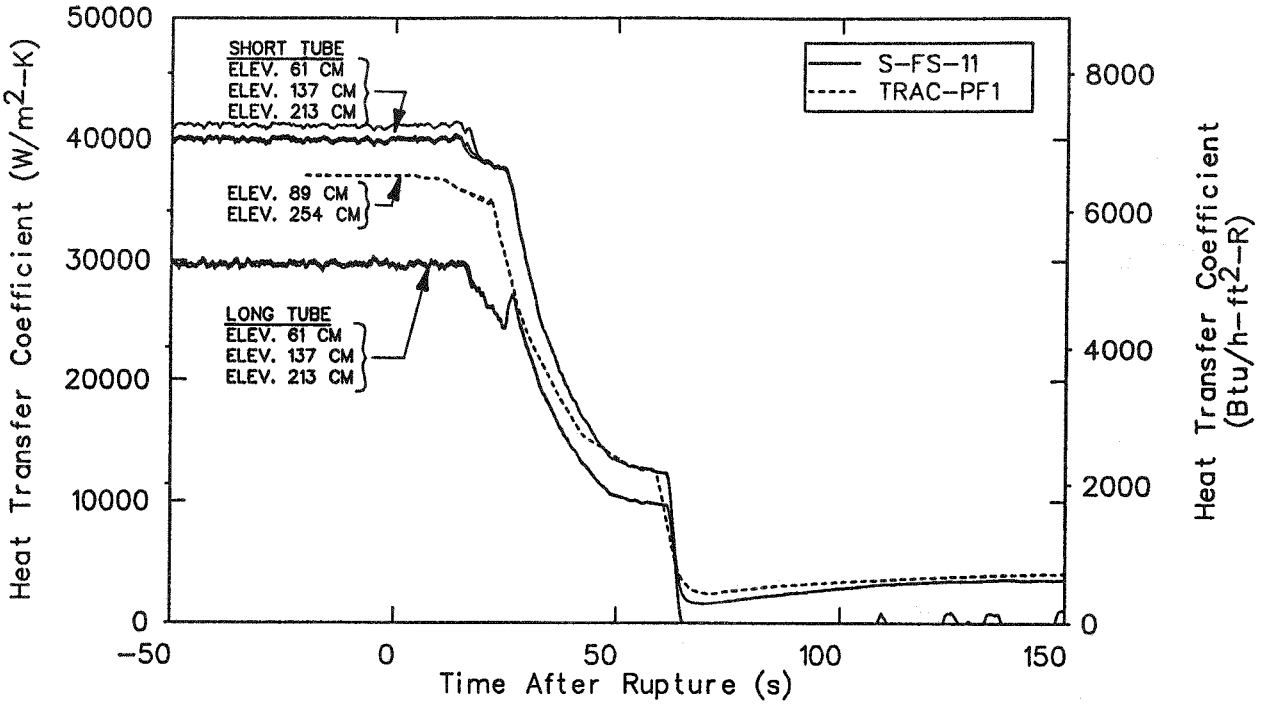

Figure 76. Comparison of measured and calculated primary upside heat transfer coefficients at the lower elevations during the early part of the blowdown phase of test S-FS-11.

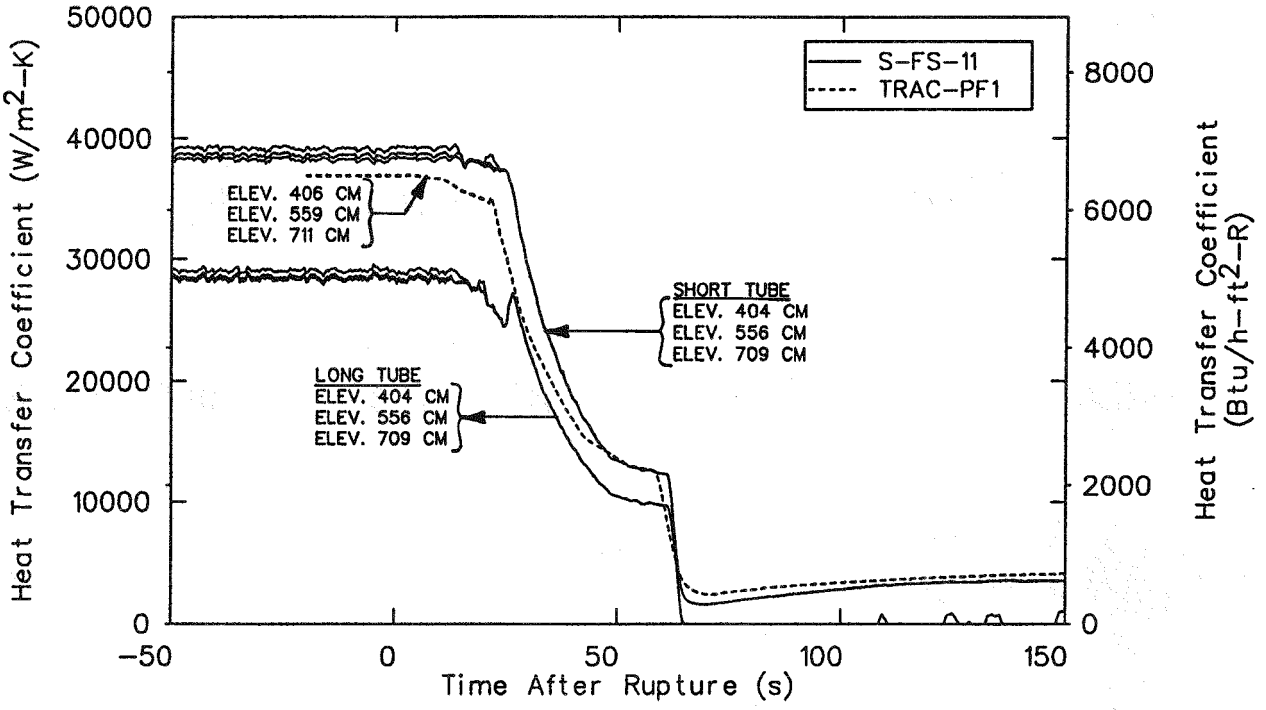

Figure 77. Comparison of measured and calculated primary upside heat transfer coefficients at the upper elevations during the early part of the blowdown phase of test S-FS-11.

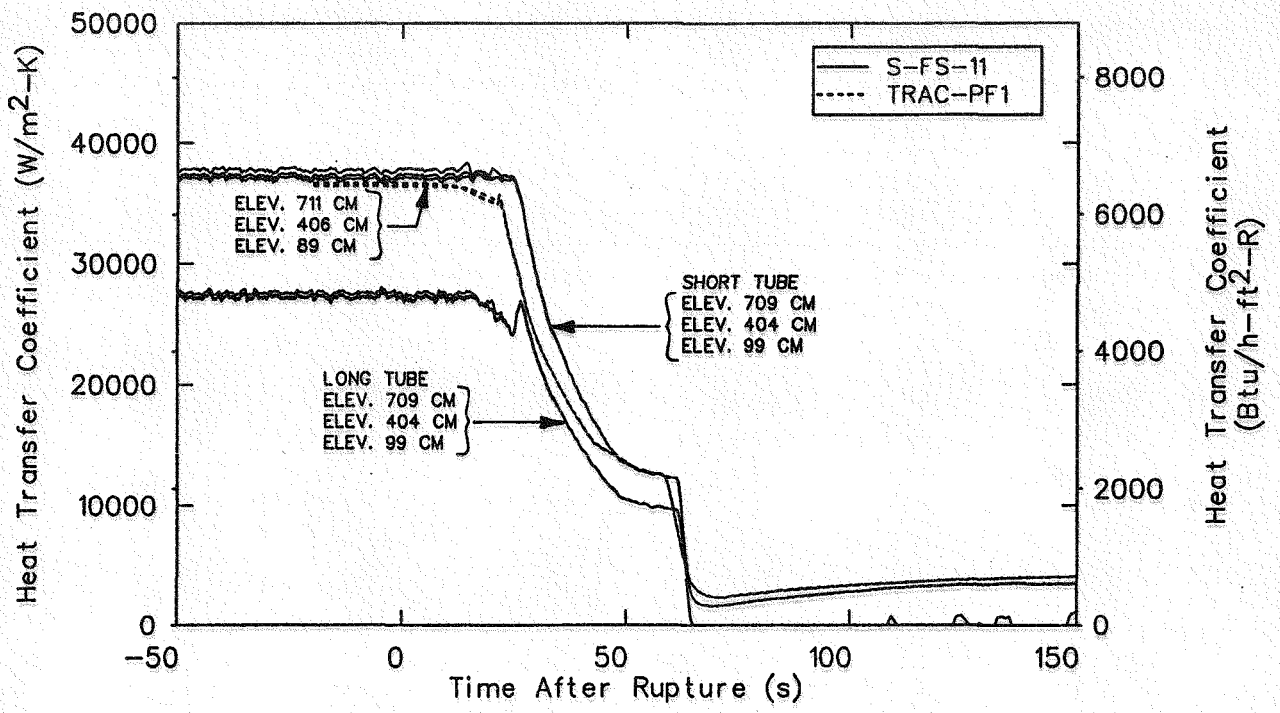

Figure 78. Comparison of measured and calculated primary downside heat transfer coefficients during the early part of the blowdown phase of test S-FS-11.

of the short tube than the long tube. Conversely, the steady-state heat fluxes indicated that the calculated heat fluxes were in better agreement with the long tube than with the short tube.

Calculated and measured secondary side heat transfer coefficients on the upside and downside of the U-tubes are presented in Figures 79 and 80, respectively. The data in both figures show significant differences between the calculated and measured results. The measured data in Figure 79 indicates that before the start of the transient, the heat transfer coefficient increased with increasing elevation. The measured data also shows that the heat transfer coefficient for the short tube was larger than that of the long tube at the same elevation. Conversely, the calculated heat transfer coefficients decrease with increasing elevation and indicate a much smaller variation from the bottom to the top of the tube. The calculated heat transfer coefficient at the lowest elevation was in reasonable agreement with the measured data at that location. In spite of the large differences between the measured and calculated data, the calculated heat transfer coefficients in Figure 79 do exhibit some of the same behavior as the measured data. Shortly after the transient was initiated, the coefficients at the lowest elevation rose immediately, whereas coefficients at the upper elevation began to decrease. The measured coefficients, in general, are more responsive than the calculated coefficients, possibly due somewhat to differences in the initial secondary mass of the steam generator. However, the modeling of the tubes and the resulting fluid conditions in the secondary may be more responsible.

The downside heat transfer coefficients shown in Figure 80 exhibit better agreement between the calculated and measured results. The variation of the measured heat transfer coefficients with elevation was duplicated in the calculation; however, the variation was much smaller. As with the upside, the calculated heat transfer coefficient at the lowest elevation is in reasonable agreement with its measured counterparts. The calculated coefficients also exhibit the same trends during the transient. The calculated coefficient at the lowest elevation increased shortly after the start of the transient; whereas the calculated coefficient at the highest elevation did not. This was consistent with the measured results. The calculated results also began to decrease at the same time as the measured data. As with the upside, the measured data was more responsive than the calculated data. This may be due somewhat to differences in the initial secondary mass of the steam generator. However, the modeling of the tubes and the resulting fluid conditions in the secondary may be more responsible.

Calculated and measured primary side heat fluxes for the upside and downside are compared in Figures 81 and 82, respectively. These comparisons

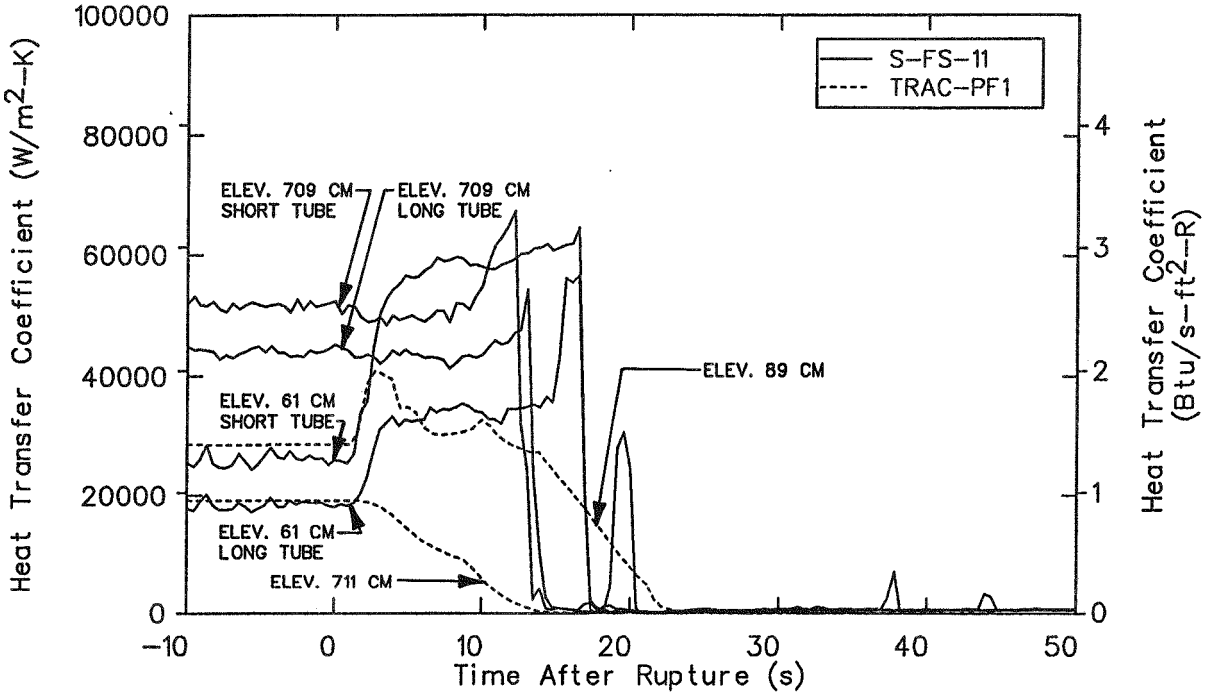

Figure 79. Comparison of measured and calculated secondary upside heat transfer coefficients during the early part of the blowdown phase of test S-FS-11.

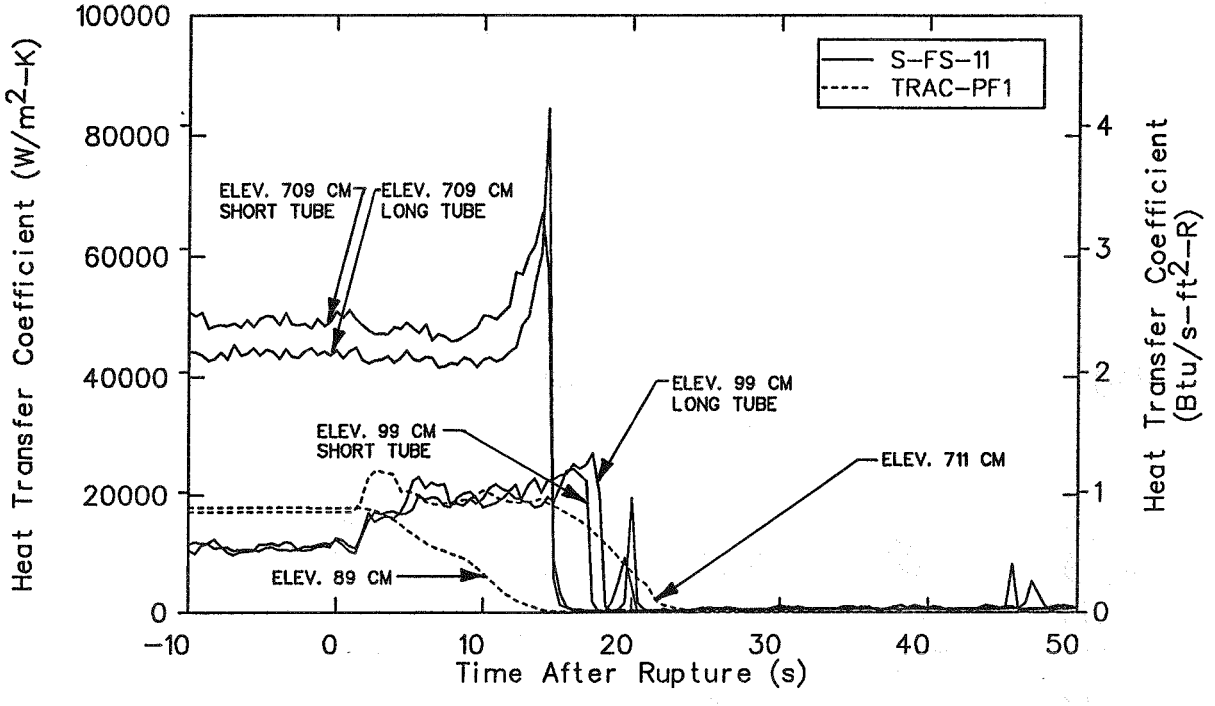

Figure 80. Comparison of measured and calculated secondary downside heat transfer coefficients during the early part of the blowdown phase of test S-FS-11.

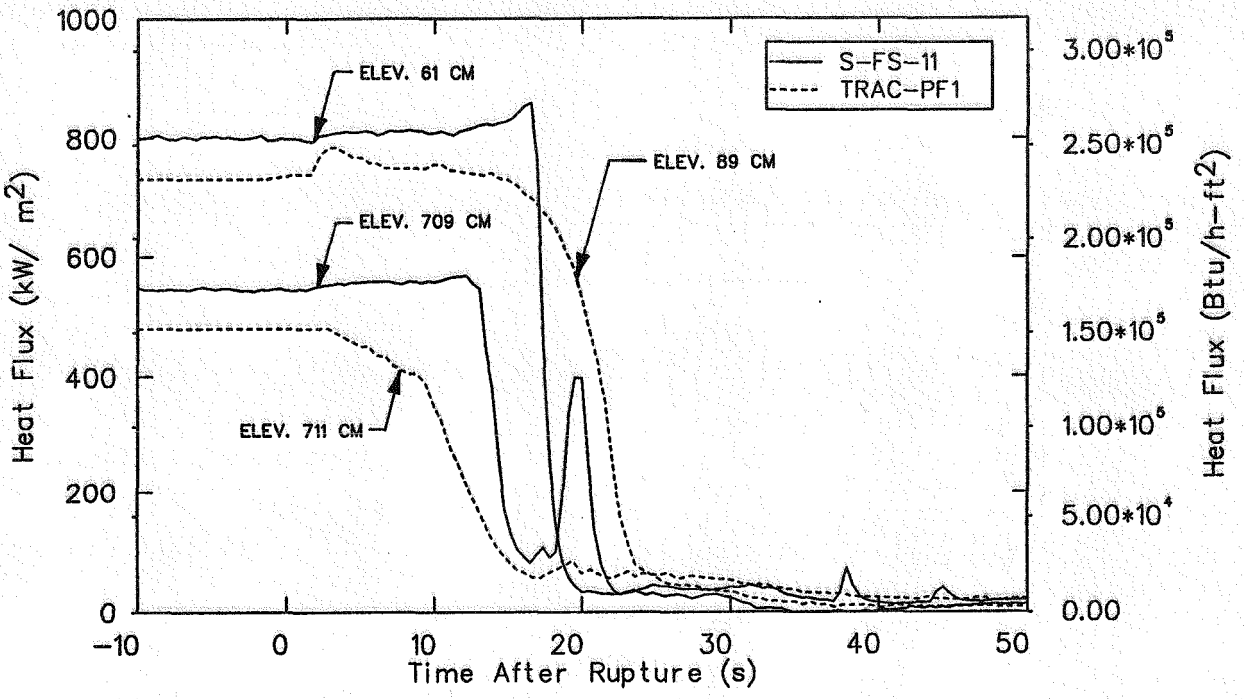

Figure 81. Comparison of measured and calculated primary upside heat fluxes during the early part of the blowdown phase of test S-FS-11.

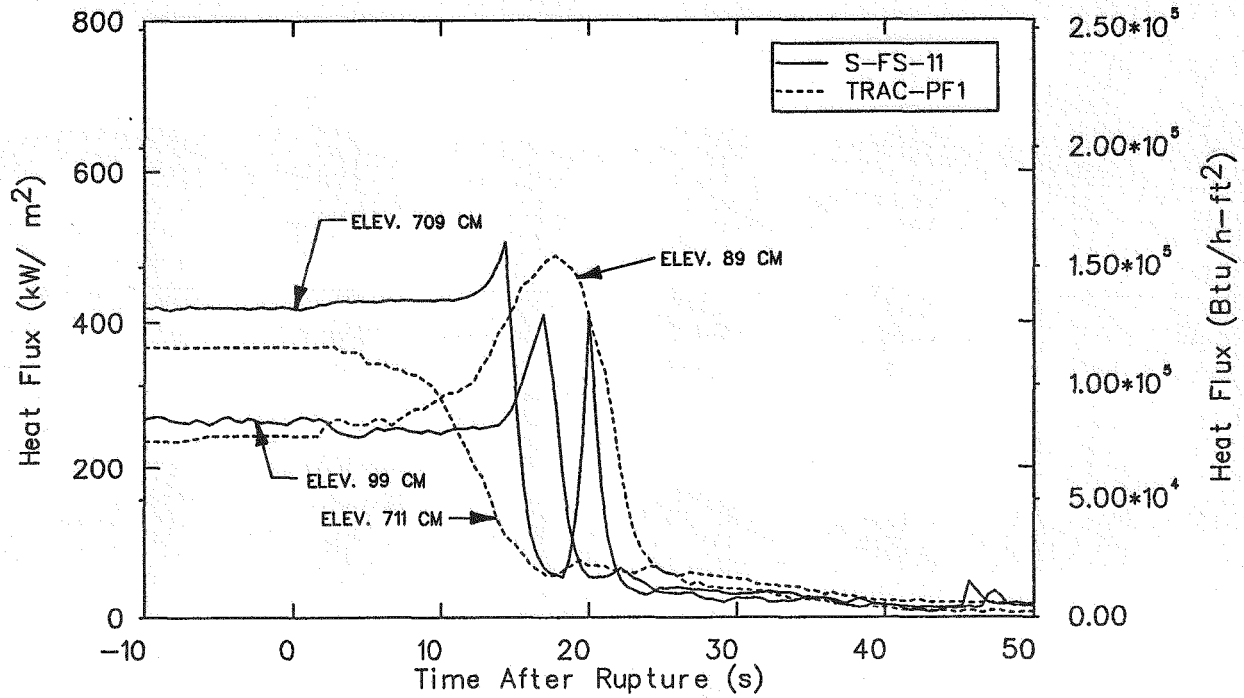

Figure 82. Comparison of measured and calculated primary downside heat fluxes during the early part of the blowdown phase of test S-FS-11.

show, in general, the same results. The initial calculated heat fluxes were in fair agreement with, but lower than, the data measured at approximately the same elevation. The calculated heat fluxes, in general, do not agree well with the measured data during the transient. Also, the calculated data does not show the same resurgence in the heat flux at the upper elevations as the measured data. Correcting the initial secondary mass and revising the modeling of the U-tubes may well increase the agreement.

Figure 83 shows the integrated effect of the local heat transfer conditions. The calculated primary-to-secondary energy removal rate is compared to the corresponding experimental data. This comparison shows that the decay in the calculated energy removal coincides with the decay in the test data. The initial difference was the result of measurement uncertainties in the experimental data used to determine the energy removal rate. As an alternative, the energy removal rate can also be considered a function of secondary mass. Figure 84 compares the calculated and measured data in this form. Although the calculated energy removal rate agrees well with the experimental data as a function of time, significant differences are evident when viewed as a function of secondary mass. The difference in behavior is the result of slight differences in the calculated and measured secondary mass during the blowdown. Figure 85 highlights these differences. Although the initial secondary masses are similar, the two differ beginning at 20 s as a result of the break flow rate differences. These mass differences produced the results in Figure 84.

In general, the calculated response of the broken loop steam generator during a 50% bottom feedwater line break must be considered fair. The code typically calculated correct trends in nearly all of the parameters. The differences between calculated and measured broken loop steam generator data is due generally to the early SIS signal and subsequent early crossover line valve closure. The early SIS signal and crossover line valve closure was a result of the broken loop steam generator secondary pressure decreasing too rapidly. This result may also be indicative of the problems noted in the intact loop steam generator.

An evaluation of the ability of TRAC-PF1/MOD1 to calculate localized heat transfer coefficients under the transient conditions of a simulated 50% feedwater line break has shown mixed results. The calculated primary side heat transfer coefficients were bounded by, and had the same characteristics as, the measured coefficients. The calculated secondary side heat transfer coefficients exhibited some of the correct trends during the transient; however, they would have agreed better with the data with better modeling of the initial secondary mass and of the U-tubes. The calculated coefficients at the lower elevations initially agreed with

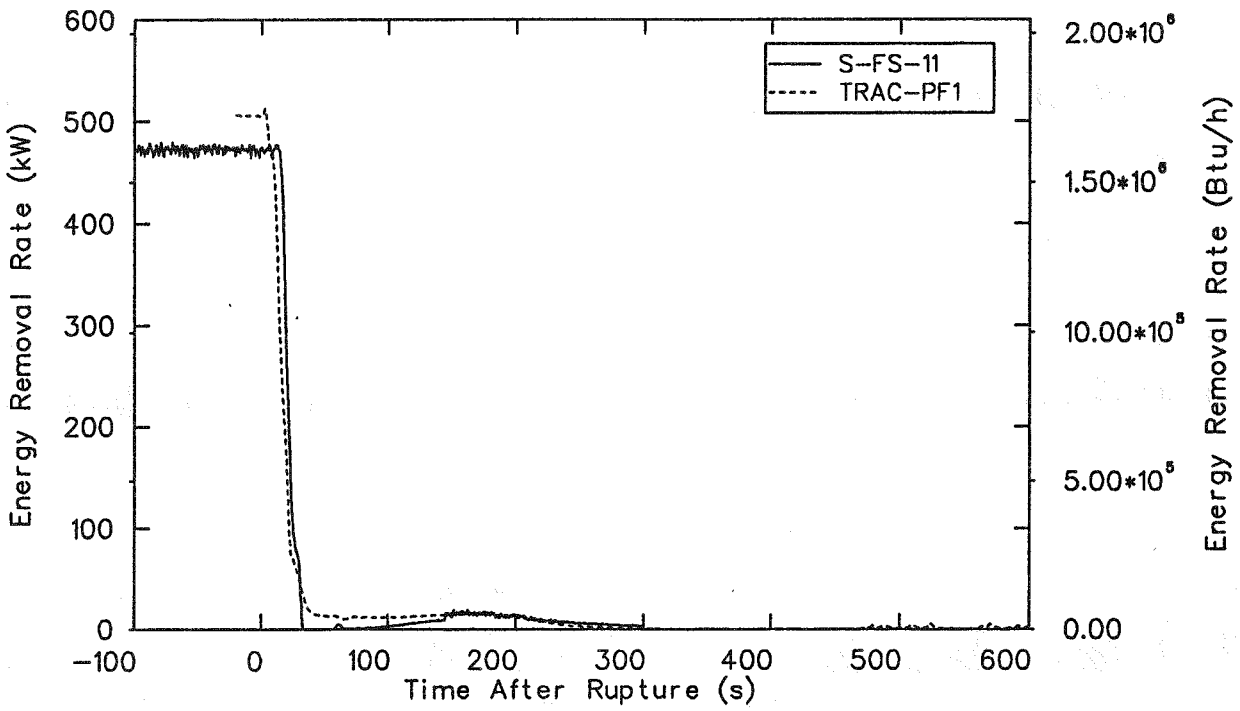

Figure 83. Comparison of measured and calculated broken loop primary-to-secondary heat transfer rate during the early part of the blowdown phase of test S-FS-11.

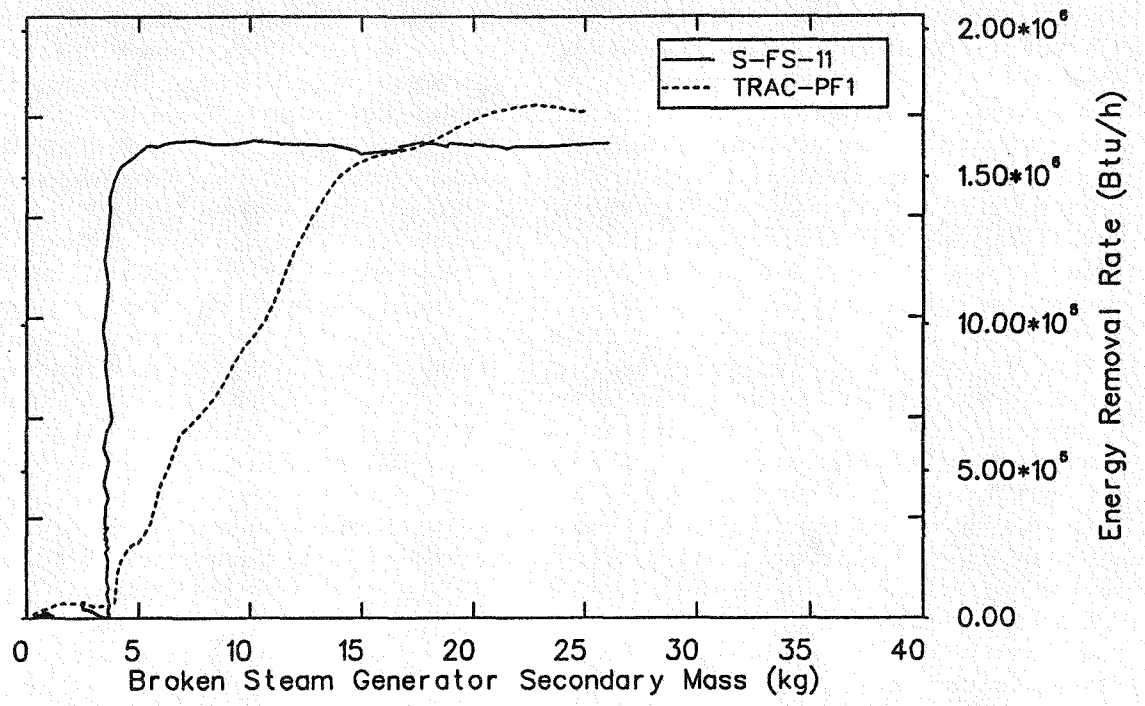

Comparison of measured and calculated broken loop steam generator energy removal rate as a function of total secondary mass during the early part of the blowdown phase of test S-FS-11.

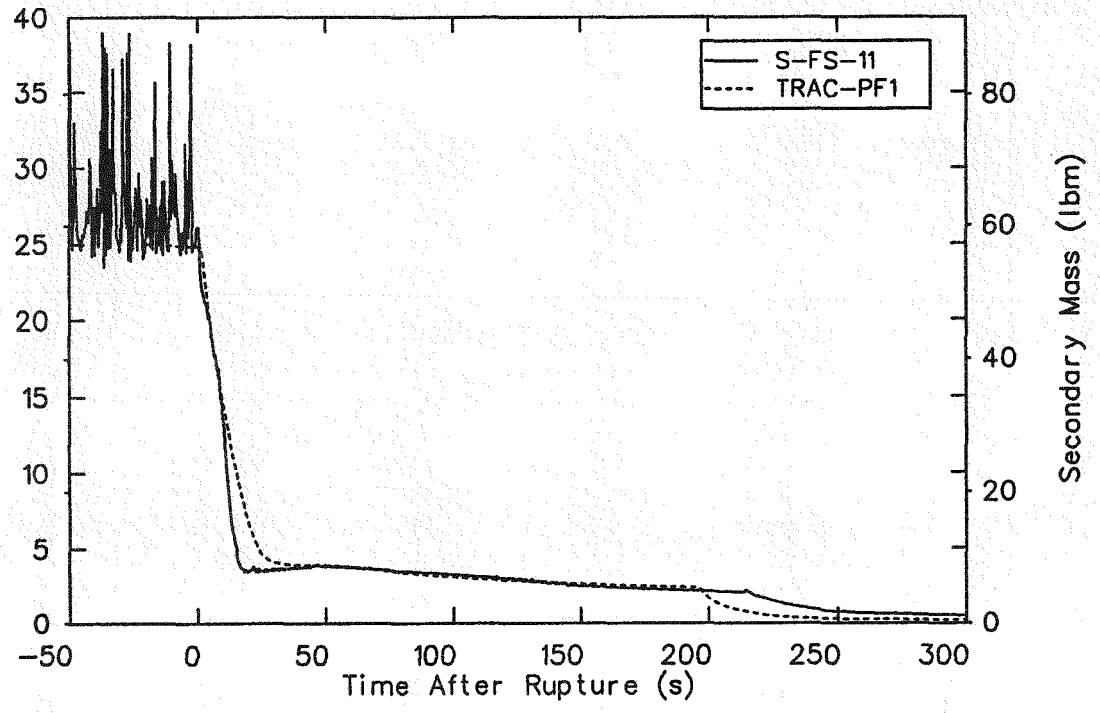

Comparison of measured and calculated broken loop steam generator secondary mass during the early part of the blowdown phase of test S-FS-11.

the measured data, whereas the calculated and measured values at the upper elevations were very different.

The calculated primary heat fluxes agreed reasonably well with the data before the start of the transient; during the transient, they exhibited significant differences. Again, correcting the initial secondary mass and improving the modeling of the U-tubes would have improved the results. The total energy removal rate through the steam generator agreed reasonably well with the measured data, although the calculated heat transfer versus secondary mass did not agree with the data. Better agreement with the data might have been obtained by modeling each of the two U-tubes separately instead of combining them into one U-tube model; a more accurate simulation of the break flow, as discussed earlier; or including ambient heat losses.

8.3 General System Response During The Recovery Phase

This subsection discusses the ability of TRAC-PF1/MOD1 to calculate the response of a system during the plant stabilization phase of the transient. At this time, the broken loop steam generator was empty, the break was still open, and the intact loop steam generator provided the only heat sink for the system. The blowdown was allowed to continue until a plant operator could identify that a feedwater line break had occurred and what steam generator it had occurred in. This time was simulated as 600 s, the plant stabilization phase beginning thereafter. The system was stabilized in accordance with the guidance provided in the Waterford Unit No. 3 (a Combustion Engineering System 80 Plant) Emergency Operating Procedures (EOPs) for recovery from a secondary transient.

At the conclusion of the blowdown phase, the operator terminated the auxiliary feedwater flow to the affected loop steam generator and monitored the primary system subcooling. This subcooling was the temperature difference between the pressurizer and the intact loop hot leg. To reestablish and maintain the primary system subcooling between 27.8 K (50°F) and 33.3 K (60°F), the pressurizer warmup heaters were energized at half their rated power (7.10 kW) for a total of 322 s. The pressurizer heaters were not energized until 120 s after termination of the auxiliary feedwater to the affected loop steam generator. At 900 s, the availability of the High Pressure Safety Injection System (HPIS) flow was terminated because the subcooling was above 27.8 K (50°F) and the pressurizer level was above 235 cm (92.5 in.). The primary system pressure remained above the HPIS shutoff head of 12.32 MPa (1786 psia) during the entire test. Consequently, no HPIS injection occurred before termination of the flow.

Beginning at 1062 s, charging flow maintained the pressurizer level above 235 cm (92.5 in.). A total of 10 charging cycles occurred during the stabilization phase of the transient. Auxiliary feedwater flow was then used to reestablish and maintain the unaffected loop steam generator secondary level between 910 and 1000 cm (358.3 and 393.7 in.). Although it was not used, the unaffected loop steam generator simulated atmospheric dump valve (ADV) was available to maintain the secondary pressure below 6.98 MPa (1012 psia). The plant was stabilized at 4055 s when the unaffected loop steam generator level reached 910 cm (358.3 in.) and all stabilization criteria was satisfied. No primary system voiding was evident during the stabilization phase of the test.

The TRAC-PF1/MOD1 simulation of S-FS-11 attempted to duplicate the sequences and responses noted during the test. Thus, the affected loop steam generator auxiliary feedwater flow was terminated at 600 s. To reestablish and maintain the primary system subcooling between 27.8 K (50°F) and 33.3 K (60°F), the pressurizer warmup heaters were energized. The heaters were not energized until 120 s after termination of the auxiliary feedwater to the affected loop steam generator. The heaters were energized for a total of 293 s, slightly less than the 322 s required during the test. Termination of the availability of HPIS, like the test, resulted in no flow injection to the system.

Unlike the test, the primary system subcooling dropped below 27.8 K (50°F) later in the simulation, which caused the pressurizer heaters to reenergize at 2158 s to regain the primary system subcooling. The heaters remained reenergized until the termination of the calculation but were unsuccessful in regaining the subcooling. The subcooling could not be regained because the primary coolant was continuing to heat up and the relief valve limited the pressurizer temperature to the set point saturation temperature. Figure 86 indicates that the pressurizer pressure eventually reached the relief valve set point at 2337 s and the relief valve chattered during the remainder of the simulation. The heatup of the primary coolant system was the result of the energy imbalance noted during the blowdown phase. As before, it was the result of the inability of the steam generators to remove the decay heat of the core. This imbalance is shown in Figure 87 and indicates that the heat input to the primary system was greater than the losses after 420 s.

The stabilization phase of the transient was rerun with the pressurizer heaters prohibited from reenergizing after the initial recovery of subcooling. Figure 88 indicates that the results of this simulation were more characteristic of the test even though the subcooling still decayed. As before, Figure 89 indicates that the heat input to the primary coolant system

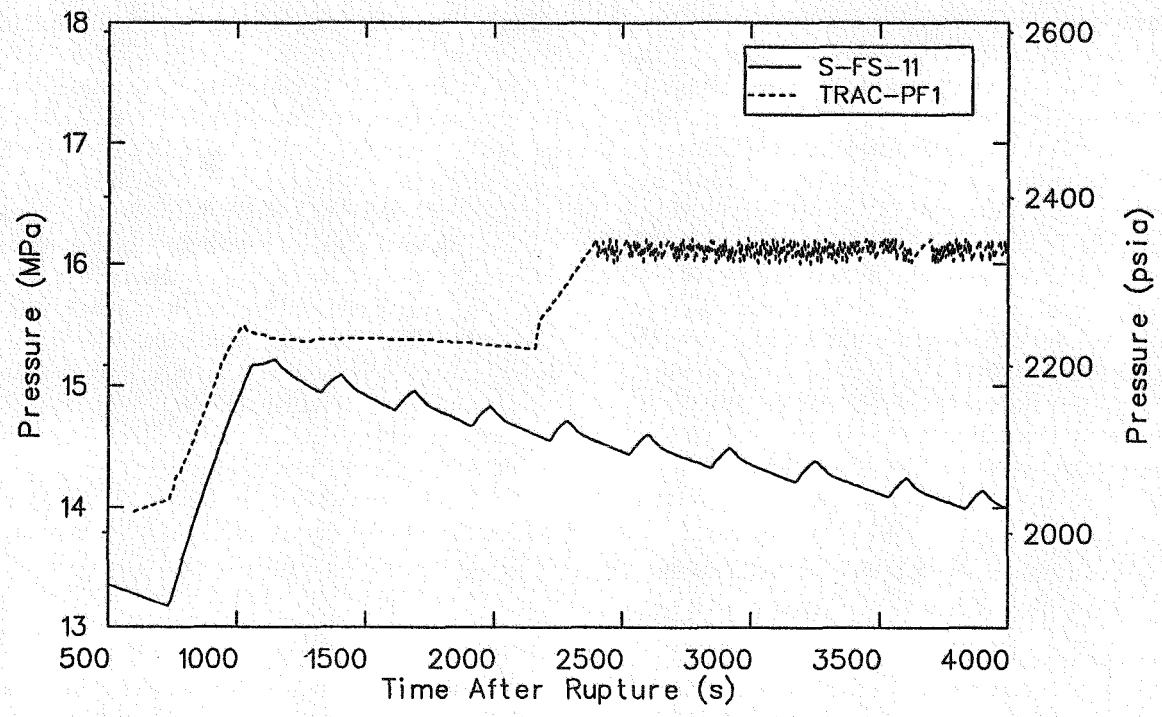

Figure 86. Comparison of measured and calculated pressurizer pressure during the recovery phase of test S-FS-11; pressurizer heaters reenergized.

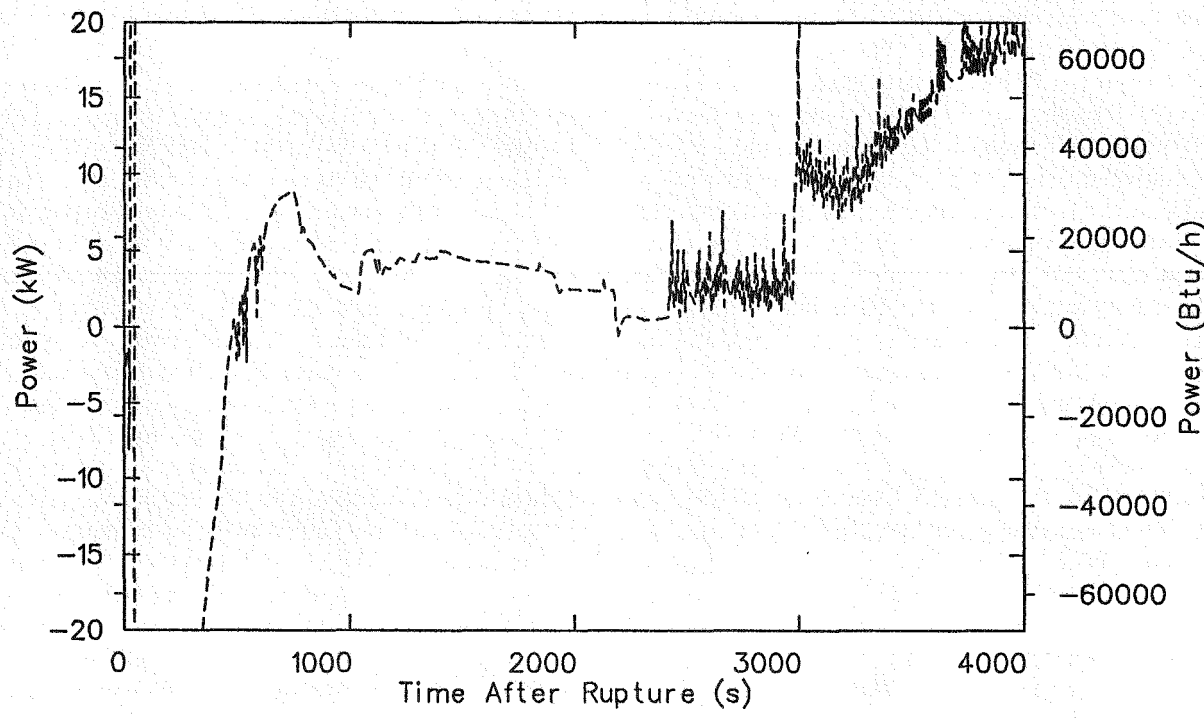

Figure 87. Calculated primary cooling system net energy balance during test S-FS-11; pressurizer heaters reenergized.

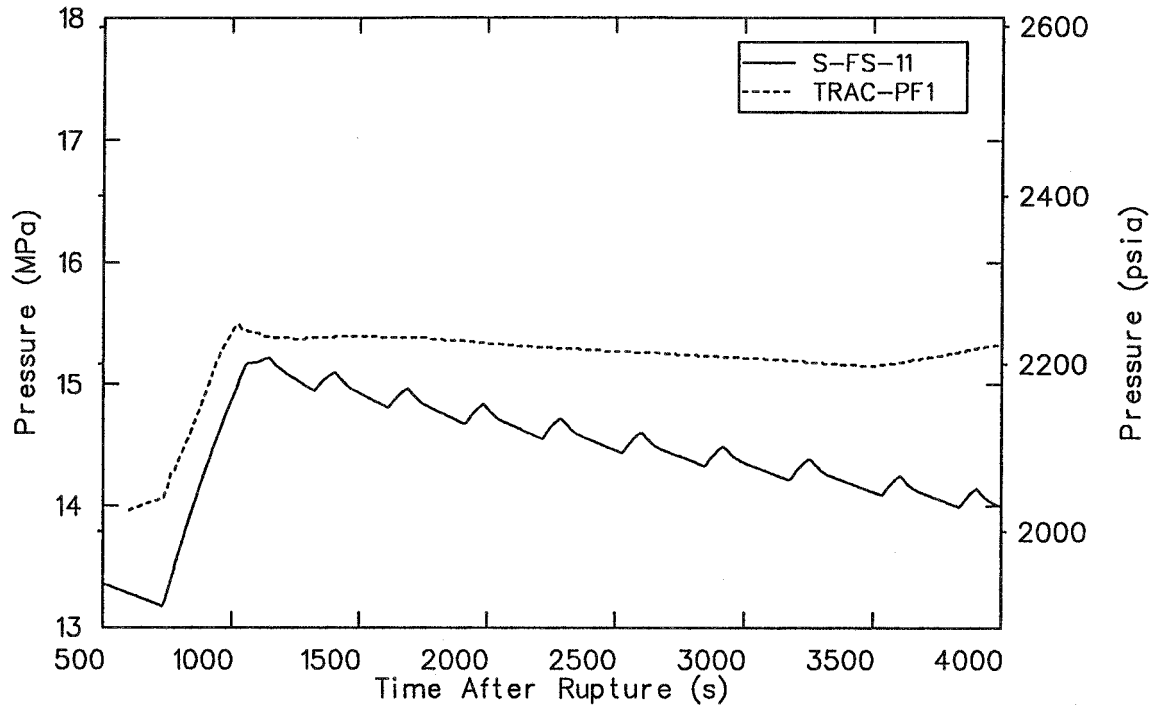

Figure 88. Comparison of measured and calculated pressurizer pressure during the recovery phase of test S-FS-11; pressurizer heaters not reenergized.

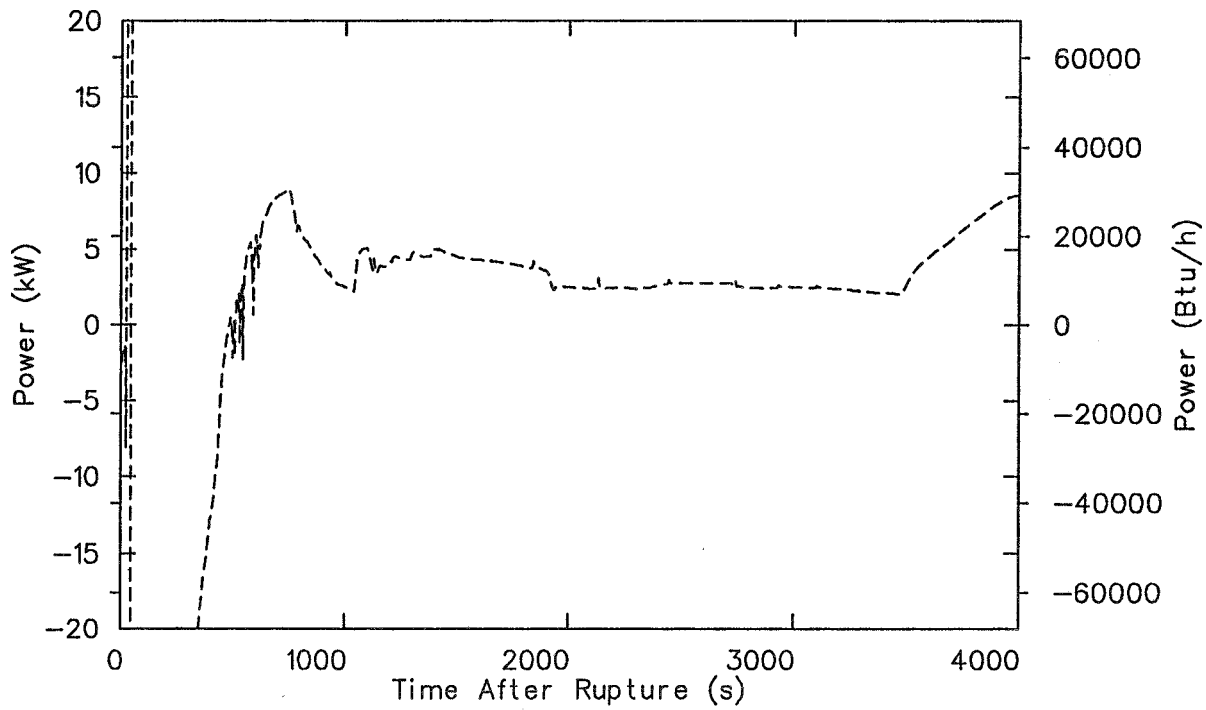

Figure 89. Calculated primary cooling system net energy balance during test S-FS-11; pressurizer heaters not reenergized.

was larger than the heat losses. Figures 90 and 91 indicate that this heat imbalance caused an uncontrolled heatup of the intact and broken loop, respectively. Because the primary coolant was heating up, Figure 92 indicates that the pressurizer level did not decrease like the test. Consequently, no charging operations were necessary during the stabilization phase of this simulation. The heat imbalance that affected the primary system also affected the secondary system. Figure 93 indicates that the secondary pressure was perturbed and rose well above that noted during the test. Figure 94 also indicates that the intact loop secondary temperature increased well above that measured during the test. During the test, the unaffected loop steam generator ADV was available to keep the secondary pressure below 6.98 MPa (1012 psia). The ADV was not used during the test. Therefore, the ADV was not used in the calculation to control the secondary pressure because this would not have produced a meaningful simulation of the test.

The conditions at the end of the stabilization phase were much different than those noted during the test. The primary and intact loop steam generator secondary pressures are 1.44 MPa (209 psia) and 3.03 MPa (439 psia) higher than the test. The intact loop hot and cold leg temperatures were 15 K (27°F) and 23 K (42°F) higher than the test. Likewise, the broken loop hot and cold leg temperatures were 24 K (44°F) and 32 K (57°F) higher than the test. The pressurizer level had not dropped and makeup coolant from the charging system was not needed. Finally, heat losses from the primary coolant system were less than the heat input from the core. This trend has existed since approximately 420 s and resulted in an uncontrolled heatup of the primary coolant system. Collectively, the plant conditions were much different than the test. Corrections to the model to better simulate the test are discussed extensively in the preceding sections. These corrections should first be factored into the model and a reevaluation of the results performed before continuing the calculations. Consequently, continuing the transient on into the recovery phase did not seem productive and the simulation was terminated at 4100 s.

In summary, the calculation exhibited the results of an uncontrolled heatup. The primary and secondary pressures and temperatures were well above the values noted during the test. In fact, the results were so different that the actual transient was no longer being meaningfully simulated. Consequently, the simulation was terminated at the conclusion of the stabilization phase of the transient. Before this transient can be successfully simulated, the modifications to the model discussed earlier must be incorporated and the results reevaluated to determine if the primary system energy imbalance has been corrected.

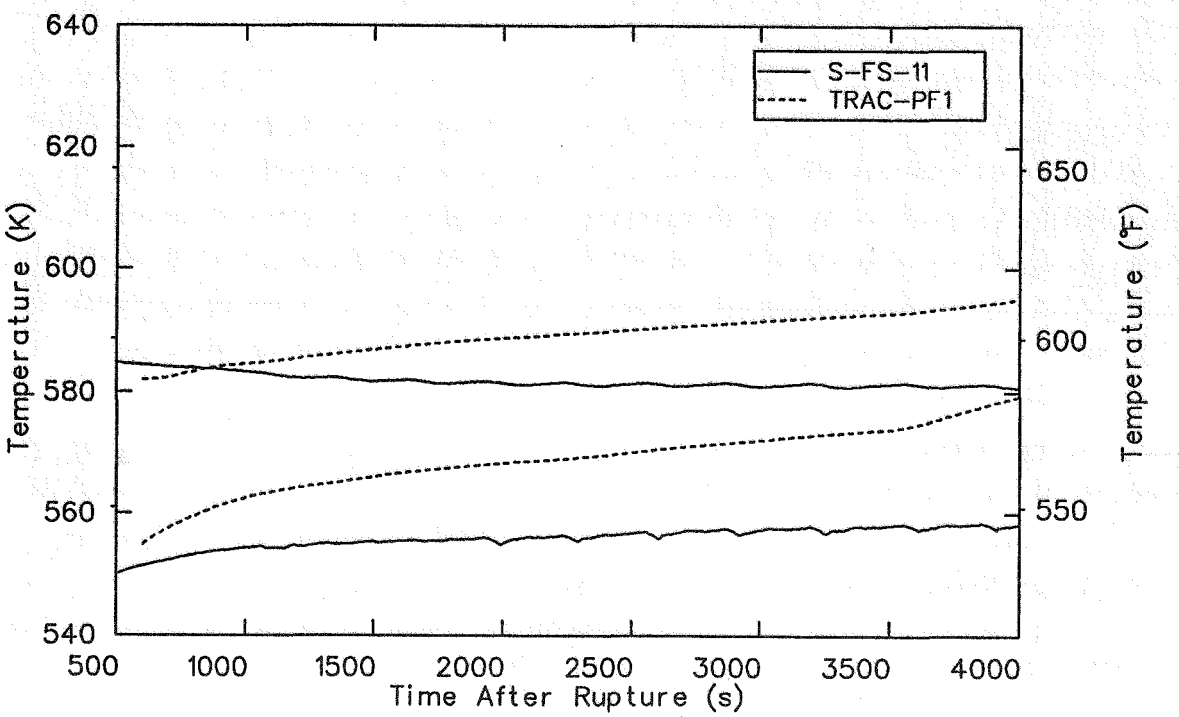

Figure 90. Comparison of measured and calculated intact loop hot and cold leg fluid temperatures during the recovery phase of test S-FS-11; pressurizer heaters not reenergized.

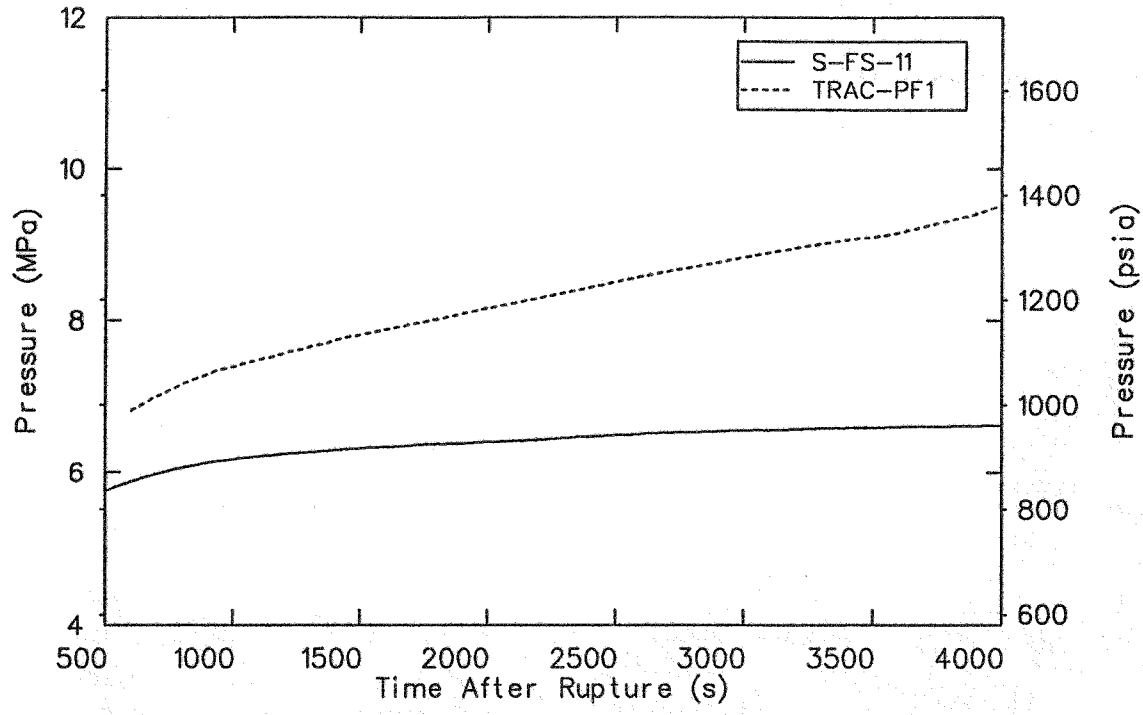

Figure 93. Comparison of measured and calculated intact loop secondary pressure during the recovery phase of test S-FS-11; pressurizer heaters not reenergized.

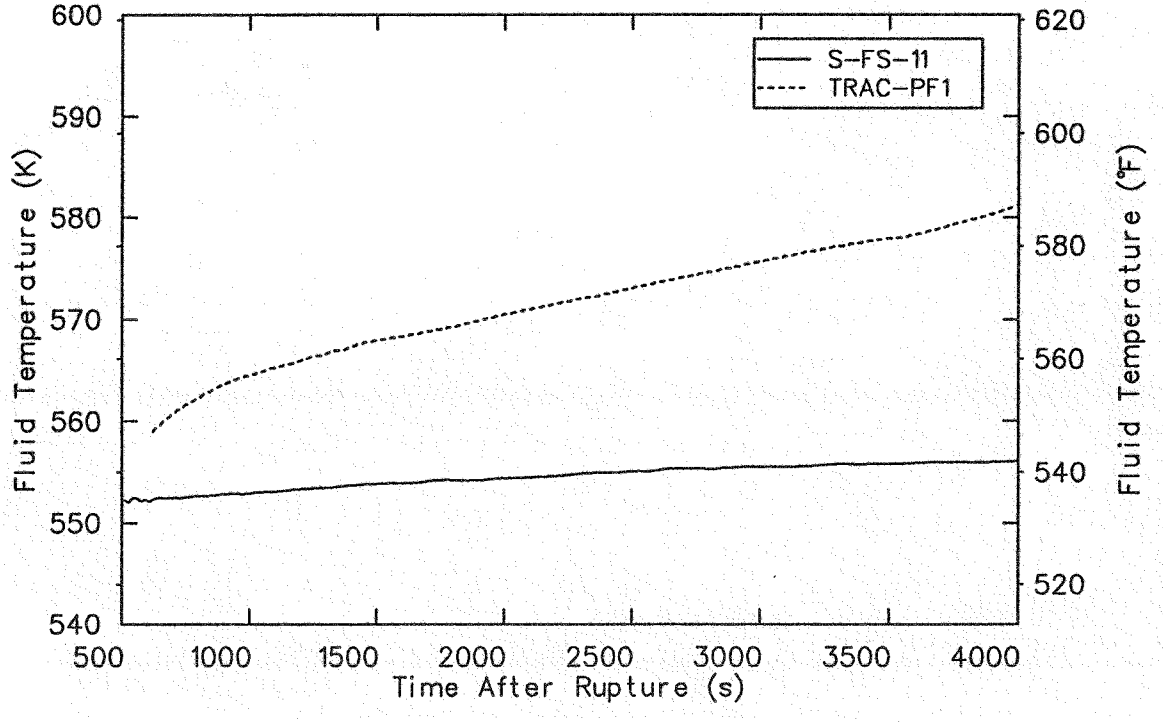

Figure 94. Comparison of measured and calculated intact loop secondary temperature during the recovery phase of test S-FS-11; pressurizer heaters not reenergized.

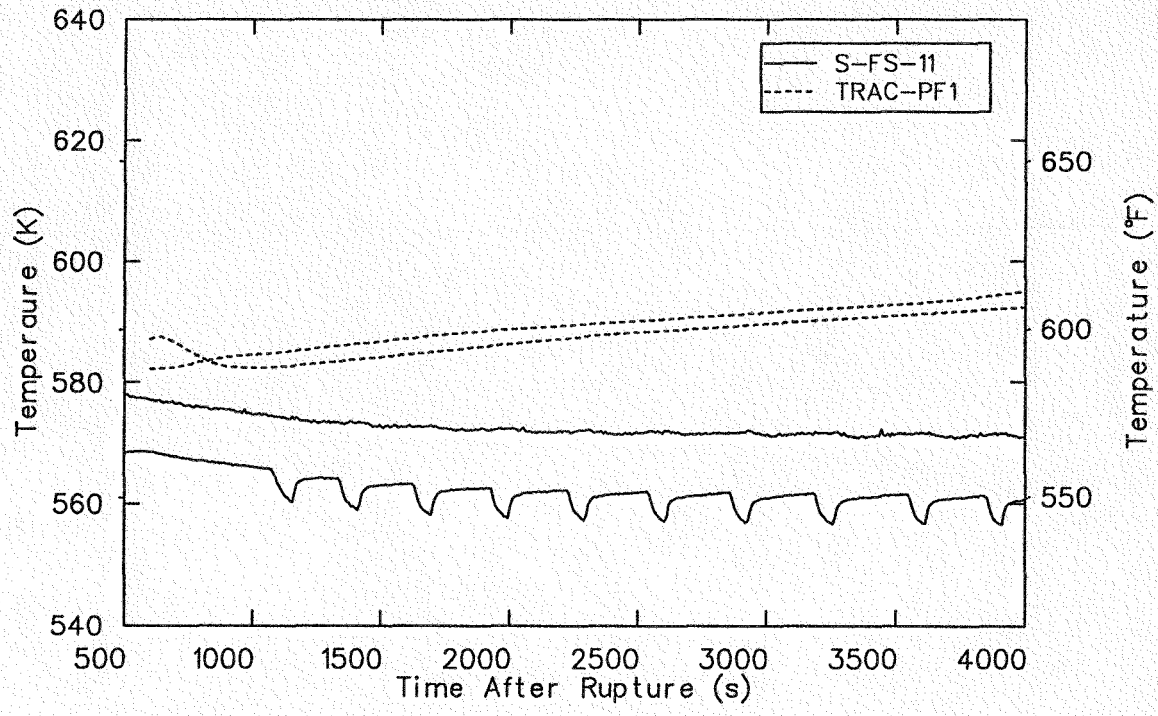

Figure 91. Comparison of measured and calculated broken loop hot and cold leg fluid temperatures during the recovery phase of test S-FS-11; pressurizer heaters not reenergized.

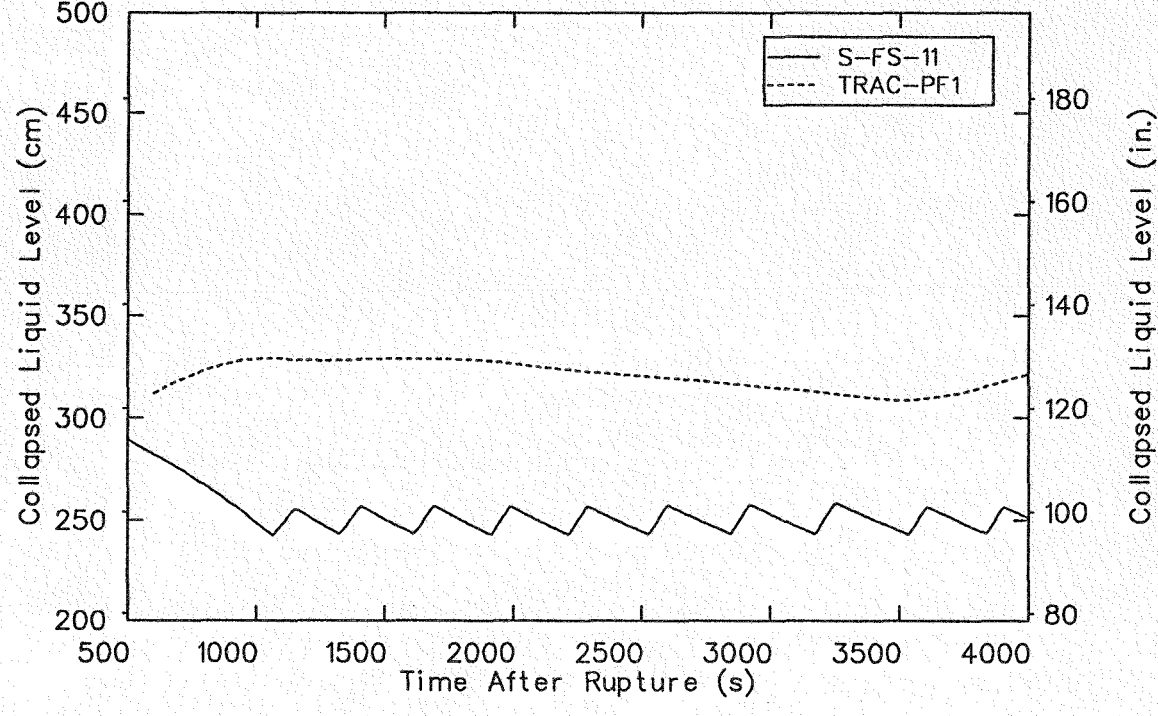

Figure 92. Comparison of measured and calculated pressurizer collapsed liquid level during the recovery phase of test S-FS-11; pressurizer heaters not reenergized.

9. TRAC-PF1/MOD1 COMPUTATIONAL PERFORMANCE AND USER EXPERIENCE

This section provides information on the computational performance of TRAC-PF1/MOD1 during the simulations of parts of three Semiscale bottom feedwater line break tests, and users experiences with the code while making the simulations. Computational performance is presented in the form of statistics related to simulated time and histories of time step size, computer central processing unit (CPU) time, and CPU time per second of simulated time. The variations in the latter three parameters are related to events that are occurring in the simulation. The user experience given in the second part of this section is primarily a discussion of improvements to features of the code that would have made the simulations easier.

9.1 Computational Performance

The computer simulations of Semiscale tests S-FS-6B, S-FS-7, and S-FS-11 using the TRAC-PF1/MOD1 code were performed using the Cray computer at Kirtland Air Force Base in Albuquerque, New Mexico. The frozen version of the code (12.1) was used with correction sets 12.2 through 12.5. The code's computational performance during the simulations of the blowdown phases of the three tests and part of the recovery phase of S-FS-11 are summarized in Table 7. The statistics indicate the increasing difficulty of the calculations as the break size was increased from 14.3% (S-FS-7) to 100% (S-FS-6B). The computational performance, even for the most difficult transient, S-FS-6B, was good with a CPU time-to-simulated time ratio of 5.4 and a cost of $700.

"Histories" of the calculations are shown in Figures 95 through 102. Alternate figures show time step size, cumulative CPU time, and the rate of change of CPU time with simulated transient time as a function of simulated transient time. The figures cover the blowdown phase of the three tests and part of the recovery phase of S-FS-11.

The calculational histories for the two larger feedwater break transients, S-FS-6B (100% break) and S-FS-11 (50% break), have similar characteristics, as shown in Figures 95 through 98. Figures 95 and 97 show that the calculation used small time steps,

Table 7. Run time statistics for the S-FS-6B, S-FS-7, and S-FS-11 TRAC-PF1/MOD1 calculations

	S-FS-6B Blowdown	S-FS-7 Blowdown	S-FS-11 Blowdown	S-FS-11 Recovery
Break size (%)	100.0	14.3	50.0	50.0
Simulated time (s)	620.1	770.5	621.0	3501.2
CPU time (s)	3363.7	1066.2	1931.8	772.5
Number of time steps	11597	3845	6508	2791
Average time step size (ms)	53.5	200.4	95.4	1254.5
Minimum time step size (ms)	0.1	0.1	0.1	41.2
Maximum time step size (ms)	1345.0	1329.0	1535.0	1879.0
Ratio of CPU time-to-simulated time	5.42	1.38	3.11	0.22
Average CPU time-to-second of simulated time	3.85	3.56	3.32	0.23
Cost of calculation (dollars)[a]	699.50	235.15	411.30	162.82

a. Costs based on $500/h of CRAY time and includes CPU, I/O, and MEMORY time.

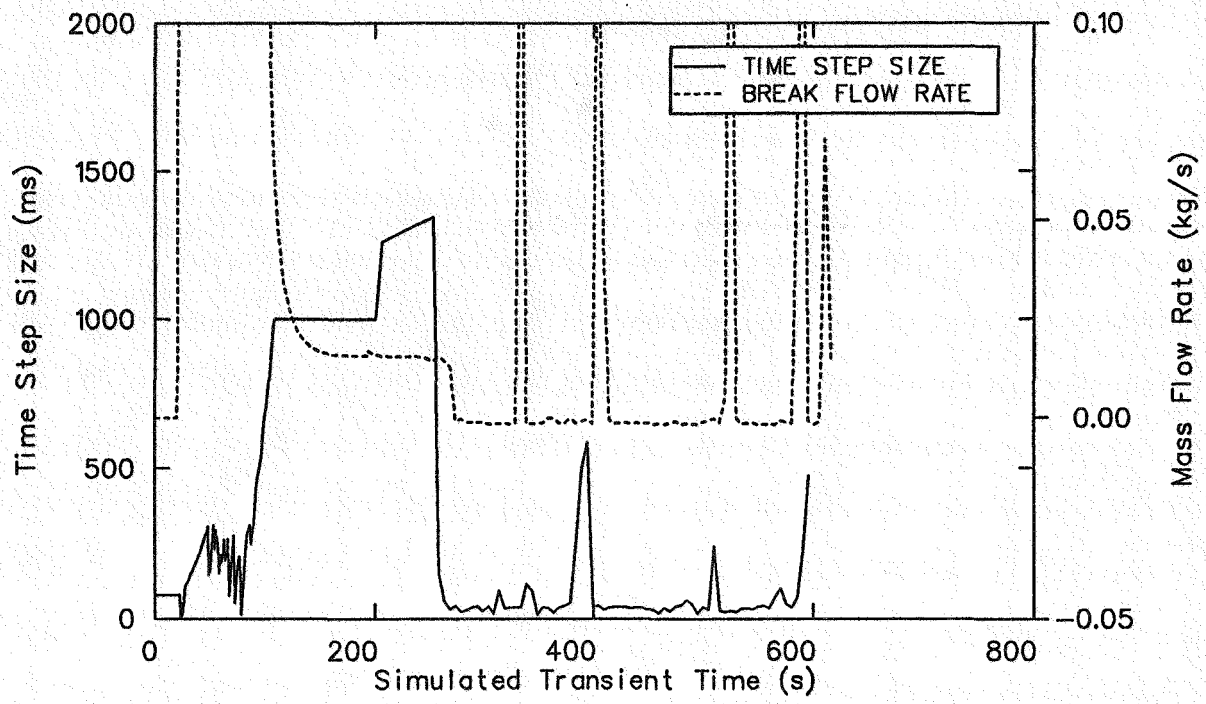

Figure 95. Time step size and break mass flow rate as a function of simulated time during the S-FS-6B calculation.

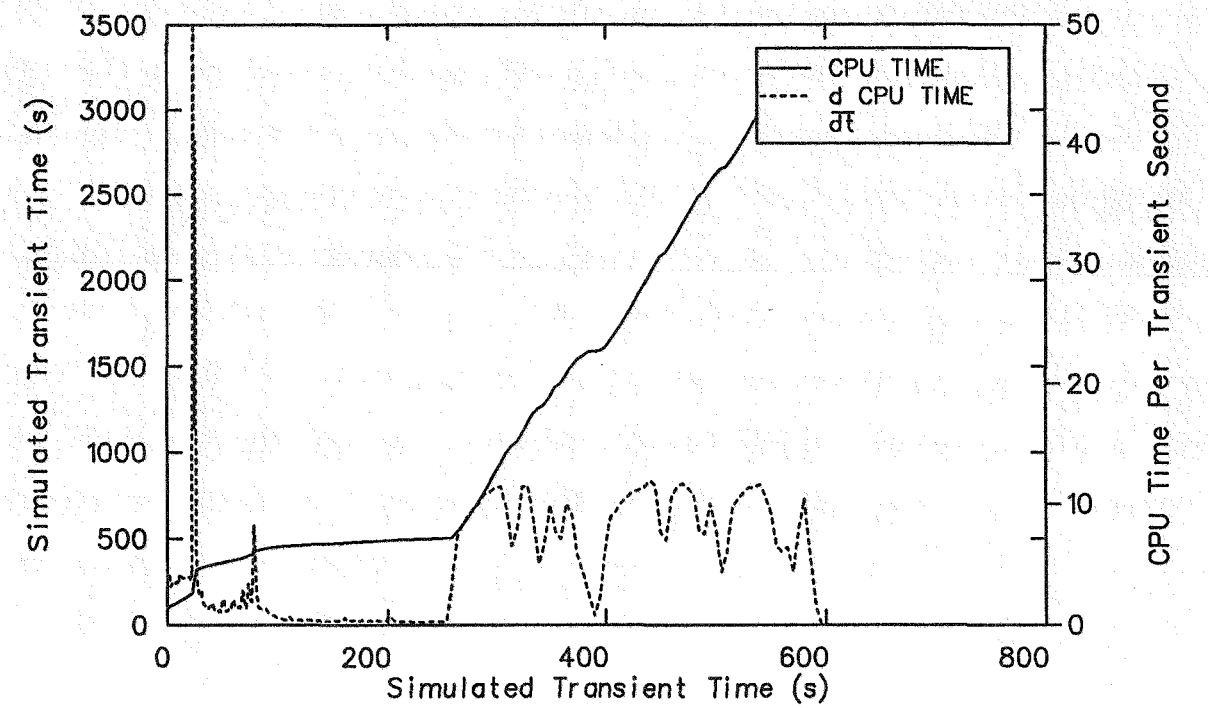

Figure 96. CPU time and CPU time increment per simulated second as a function of simulated time during the S-FS-6B calculation.

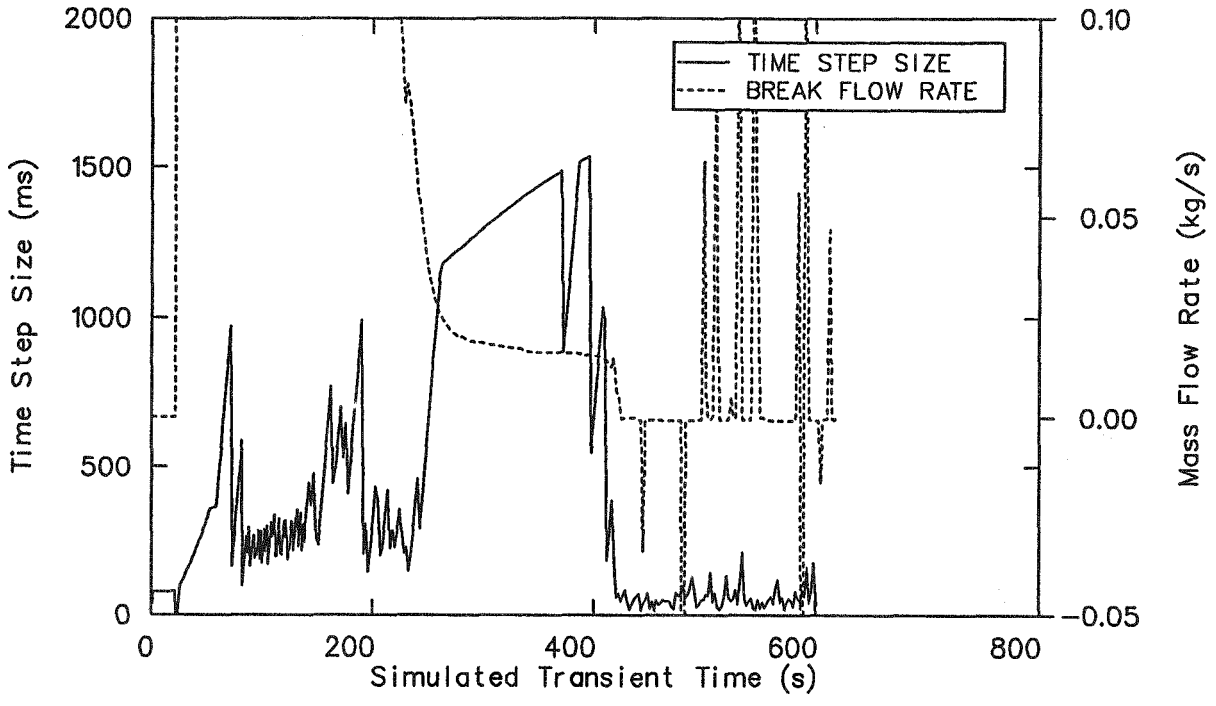

Figure 97. Time step size and break mass flow rate as a function of simulated time during the S-FS-11 blowdown calculation.

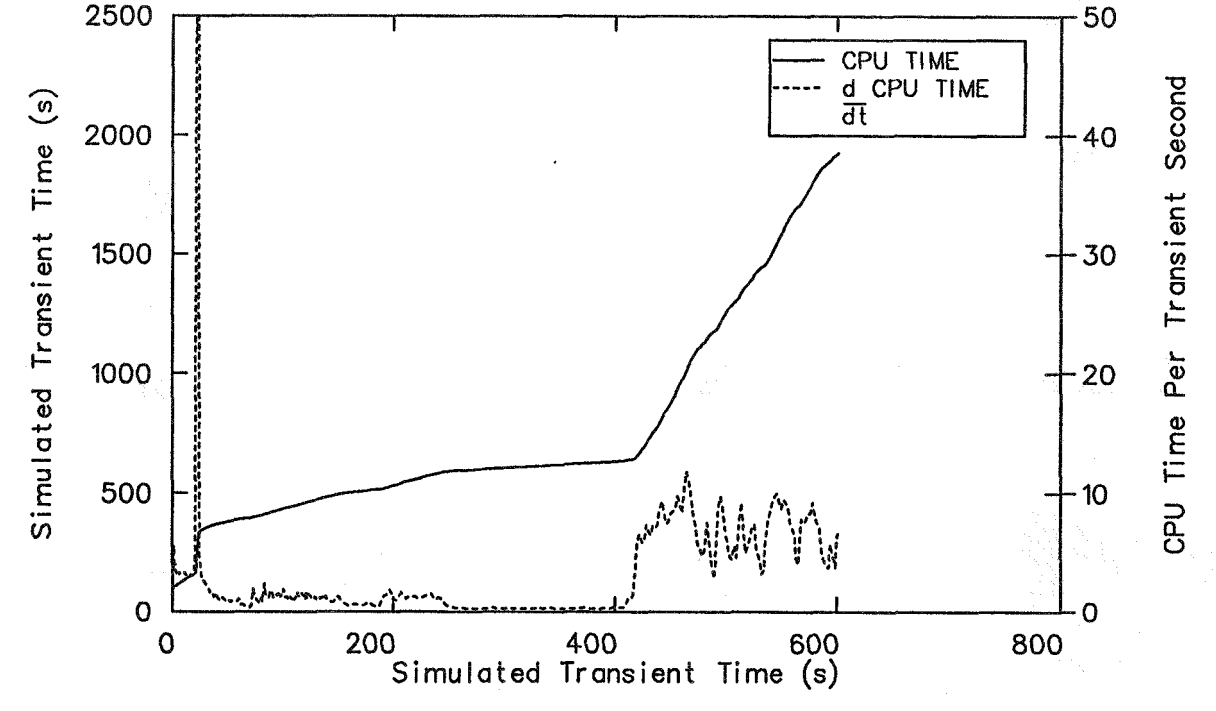

Figure 98. CPU time and CPU time increment per simulated second as a function of simulated time during the S-FS-11 blowdown calculation.

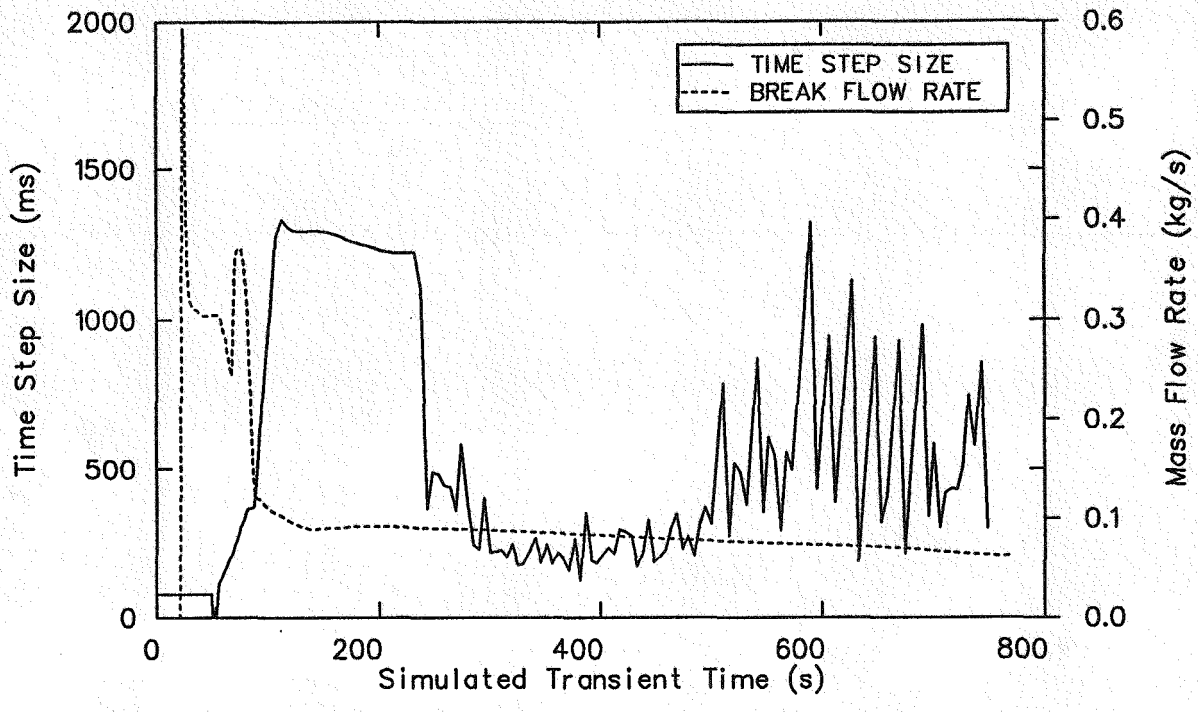

Figure 99. Time step size as a function of simulated time during the S-FS-7 blowdown calculation.

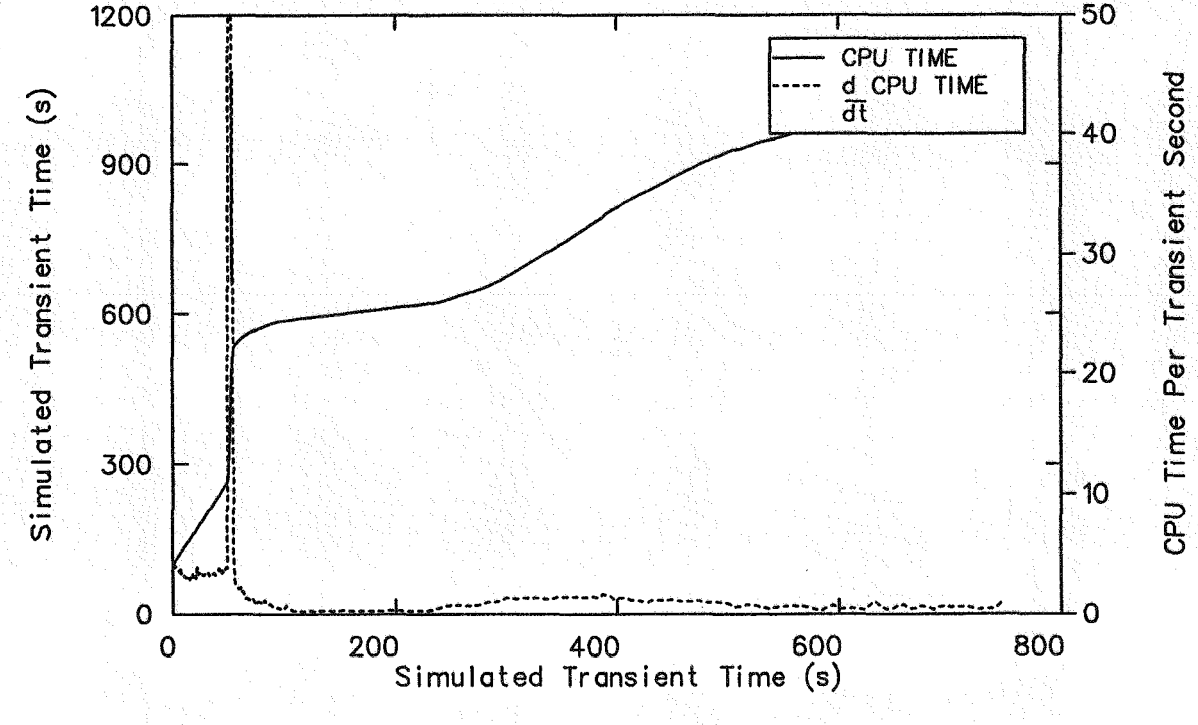

Figure 100. CPU and CPU time increment per simulated second as a function of simulated time during the S-FS-7 blowdown calculation.

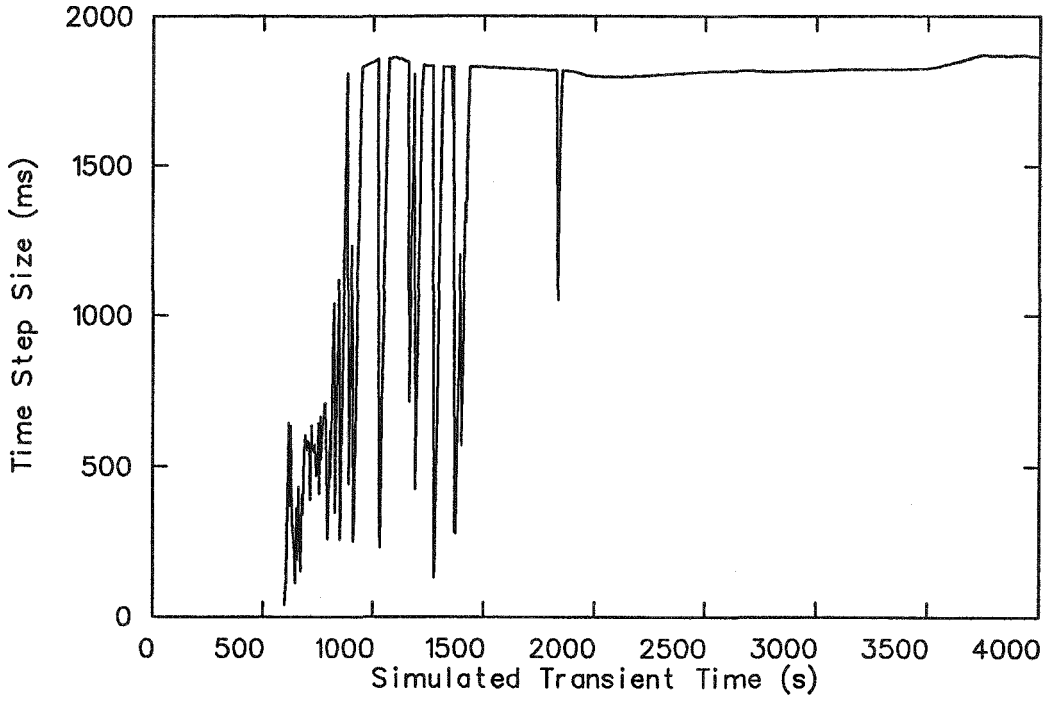

Figure 101. Time step size as a function of simulated time during the S-FS-11 recovery calculation.

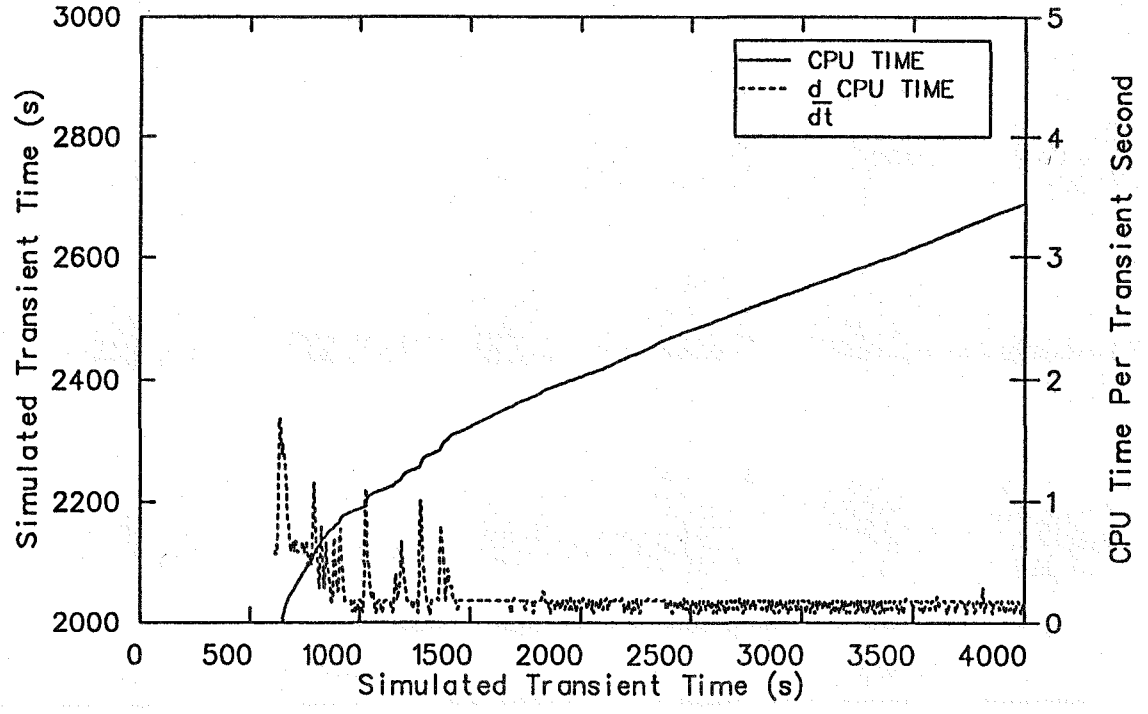

Figure 102. CPU time and CPU time increment per simulated second of simulated time during the S-FS-11 recovery calculation.

approaching the minimum value, for a short period starting when the core power trip occurred (22.9 s in S-FS-6B and 20.8 s in S-FS-11). Thereafter, moderate-sized time steps were used while SCRAM-related actions were simulated and the break flow rate decayed to a nearly constant value. Once the break flow decayed to a nearly constant value and the crossover line valve was closed, the system was in a condition that allowed the time step to rise to large values approaching the maximum specified. This condition continued until the broken loop steam generator secondary pressure decayed to atmospheric pressure, at which time the break flow went to zero. This marks the beginning of a period that lasted until the end of the calculation, during which the time step size was controlled by the break assembly valve component in the model. Small time steps were taken as the break flow varied about zero, as shown in Figures 95 and 97.

The small time step size caused by the near zero break flows greatly increased the calculation time over what might have been necessary if use of the large time steps could have continued, as shown in Figures 96 and 98. The time step was reduced to calculate a phenomena that was not significant in the real transients. Calculational time could have been saved without adversely affecting the simulation by not initiating the auxiliary feedwater to the broken loop steam generator, and closing the break valve component when the flow rate went to zero because the auxiliary feedwater simply exited through the break during the test.

The blowdown portion of the S-FS-7 transient calculation was similar to the other two calculations during the early part of the calculation. The time step reduced to nearly the minimum value when the core power trip occurred at 47 s. The time step increased to large values once the break flow decayed to a point after which it slowly decreased, as shown in Figure 99. The break flow rate did not go to zero as in the other two calculations. After approximately the initial 200 s of simulated time, the time step size was controlled by events in the intact loop steam generator. These events did result in the time step decreasing to moderate, but still relatively large, values. The fact that small time steps were not needed, due to the break flow going to zero, resulted in the S-FS-7 calculation having the best CPU time-to-simulated time ratio during the blowdown phase, as shown in Figure 100.

Most of the recovery phase of the S-FS-11 calculation was made with time steps approaching the maximum specified, as shown in Figure 101. This resulted in a very efficient calculation with local and overall CPU time to transient time ratios less than unity, as shown in Figure 102.

9.2 User Experience

It is generally easier for code users to enumerate aspects of using a code that are troublesome than it is to list attractive or useful features of a code. The following discussion is admittedly rather one-sided in this regard, but is warranted perhaps from a code improvement point of view. The suggestions for improving the ease of using the code fall into four categories: model input data, code output data, input checking, and restarting.

There are several areas for possible improvement in the model input data, which include the following:

- The code purports to allow "free-formatted" input, which is clearly true relative to the early requirement that input data be in specific fields. However, TRAC-PF1/MOD1 input is not free-formatted to the extent that one usually expects. No more than five data entries can be made on a single line and the field length of individual entries is limited.
- The requirement to enter an "S" to continue data entry and an "E" to end data entry for a load-type variable does not seem to have any significant value from a user's point of view. This is particularly true because the user inputs the dimensions of variables.
- While it may have some value in detecting input errors, it is inconvenient to have to count and input the total number of components, junctions, signal variables, control blocks, and trips.
- The code allows comments to be intermixed with the input data by the use of beginning and ending asterisks, which can cause trouble if a line containing an embedded comment is commented out, such as when commenting out an entire component. A global comment character to be placed in column one would eliminate this possible source of error.
- We were impressed by the power and flexibility that the trips and control blocks offer. It is an unfortunate result of the input format for the control blocks that the evaluation of a polynomial of a single variable or an algebraic sum of more than three variables is cumbersome.

Several items were also identified that could make the output more useful or easy to use. These include the following:

- The inclusion of mass flow rates at all junctions in the printed output and as variables that can be plotted would be very helpful.

- A consistent means of identifying steam generator variables would also be helpful. Specifically, when specifying signal variables, the secondary component numbers are used. When specifying plot variables, all of the variables are numbered with the primary component number. Use of the secondary component numbers in specifying plot variables would be helpful.
- Having to account for "phantom" cells between the parts of the steam generator component and in tees seems unnecessary and is a possible source of error when specifying plot variables.
- The use of heat structure numbers introduces a third numbering system when specifying steam generator plot variables. Either allowing the user to specify the numbering of heat structures or using the number of the component the heat structure is attached to could eliminate some confusion.

A major source of aggravation and inefficiency in using the code was encountered during input checking. Often, a single input error would trigger a large number of inappropriate input errors because of the code's misinterpretation of subsequent input data. Thus, it was necessary to correct input errors one at a time with intervening input checking code runs to discover all of the input errors. It would seem that more errors could be noted and then overlooked to allow checking of the rest of the input in a single pass. Many, if not all, of the input errors could, therefore, be corrected in a single pass.

A problem was encountered in restarting the code when renodalization had been performed. The code requires that the junction properties specified in the renodalized component match very precisely those of the adjacent components. The values listed in the printed output were not sufficiently accurate to avoid input errors when the restart was attempted. The restart input data required modifying, using values output from the failed restart run. Relaxation of the boundary value input checking on restart could mitigate the problem. TRAC NEWS has indicated that an EXTRACT program will soon be available that could also solve the problem by making part or all of an input deck available at the conditions at which a restart is to be initiated.

We were favorably impressed both by the results of the simulations reported in Sections 6 through 8 of this report and by the computational performance of the code reported in the first part of this section. The results of the simulations indicate that the modeling of thermal-hydraulic phenomena is basically sound. Modifications to the model and the initial conditions, in light of our findings during analysis of the results of the simulations that have been performed, would probably confirm these indications.

10. CONCLUSIONS

An evaluation of the TRAC-PF1/MOD1 reactor safety analysis code performance during posttest simulations of three Semiscale bottom feedwater line break tests has been performed. Comparisons of calculated histories of a general selection of system parameters, with measured counterparts, have shown that the code is capable of modeling the basic system responses that occurred during a major part of the blowdown phase of the feedwater line break transients.

The simulations were divided into three periods on the basis of accuracy. During the first period, from the beginning of the transient until the SCRAM signal occurred, the results coincided closely with the measured data. During the second period, which occurred between the times of the SCRAM and SIS signals, the simulation results paralleled the measured results, but were quantitatively different. During the third period, from the time of the SIS signal until the end of the blowdown phase, the simulation results exhibited significant differences from the measured data. The simulations accurately predicted both the time and magnitude of the peak in the pressurization of the primary system and the amount of overpressurization beyond the pressurizer pressure. The code adequately simulated the response of the system to automated actions of the plant protection system associated with a high system pressure scram signal, loss of offsite power, and a safety injection system (SIS) actuation signal caused by low steam generator pressure. Although the SIS signal occurred early in all three of the simulations, the primary and secondary system responses were similar to those in the test data until that time. After the occurrence of the SIS signal in the calculations, the simulations deviated significantly from the measured results. Reasons for the differences between the results of the simulations and the test data have been identified.

The accuracy of the simulations could be improved by modifications to the TRAC-PF1/MOD1 model of the Semiscale Mod-2C system and in the S-FS-6B and S-FS-7 simulations to the initial broken loop secondary mass. Differences in the system responses between the time of the SCRAM and SIS signals are traceable to several factors including primary-to-secondary heat transfer, particularly in the intact loop steam generator due to modeling simplifications, incorrect initial broken loop secondary masses, errors in the secondary volumes due to the omission of a portion of the steam line connected to each steam generator, and modeling inaccuracies in the resistance and minimum area of the crossover line connecting the steam generators. Improvements in these areas would improve the accuracy of simulated primary and secondary responses, which would result in closer agreement of the calculated and measured times of occurrence of the SIS signal. The timing of all subsequent simulated events would be improved.

The discrepancies in system response that occurred after the SIS signal in the simulations are traceable to primary-to-secondary heat transfer in the intact loop steam generator, and possibly to the modeling of energy transfer between the fluid and the primary system structures and the need to model heat losses to the environment. Modifications in these areas would probably improve the primary pressure response between the time of the SIS signal and the end of the blowdown phase of the transient. The repressurization of the primary system that occurred in the S-FS-6B and S-FS-11 simulations and that in the case of the S-FS-11 simulation, prevented simulation of the recovery phase of the transient, would also be corrected.

Evaluation of the ability of TRAC-PF1/MOD1 to simulate the responses of a steam generator during a loss of secondary inventory were inclusive, partially due to problems in simulating events in other parts of the system that influenced the broken loop steam generator response. The primary-to-secondary heat transfer rates, and primary and secondary temperatures were generally in good agreement with the measured data at steady-state conditions. The histories of the primary side local heat transfer coefficients, primary-to-secondary heat transfer rate, and the break flow rates were in reasonable agreement with the data during the transient simulations. On the other hand, histories of local secondary side heat transfer coefficients and local primary side heat fluxes show significant differences from the measured data.

The code was found to be capable of performing feedwater line break transients with computational efficiency and at reasonable cost. The most difficult of the simulations from a computational point of view was performed with a total central processing unit (CPU) time-to-simulated time ratio of 5.42 and at a cost of about $700 for a 620 s transient when executed on a Cray computer costing $500 per hour.

The TRAC-PF1/MOD1 code was also evaluated with regard to ease of use during the course of modifying the input model; performing input checks, steady-state calculations, and transient simulations; and using the code output in evaluating simulation results. Suggested improvements have been noted in the areas of model input data, code output data, input checking, and code restarting.

11. RECOMMENDATIONS

During the course of analyzing the results of the simulations that were performed, several modeling deficiencies were identified and others were indicated by the comparisons to the test data. These deficiencies need to be corrected in order to get a clearer picture of the simulation accuracy the code is capable of. The known deficiencies include:

- Errors in the volumes of the steam generator secondaries due to part of the steam lines not being modeled
- Incorrect initial broken loop steam generator secondary masses being used as a result of re-evaluations that produced different values than were reported in the Semiscale Quick Look Reports
- Initial fluid conditions upstream of the break. (This error would only effect the peak break flow and would not have a major effect on the results due to the short duration of the peak break flow rate.)

Other deficiencies that are indicated by the comparisons to the test data, but not confirmed include:

- Primary-to-secondary heat transfer, particularly in the intact loop steam generator (Simplifications such as combining U-tubes into a single tube, which was done in both steam generator models, and lumping riser and downcomer filler pieces with other parts on the component model, in the case of the intact loop steam generator, may have compromised the results.)
- Modeling of the crossover line flow path, including the crossover line resistance and the minimum flow area
- Possible need to model environment heat losses associated with the primary and secondary systems
- Possible need to modify internal flow resistances in the steam generators
- Possible errors in modeling energy transfer between system structures and fluid in the primary and secondary systems.

A more accurate evaluation of the ability of TRAC-PF1/MOD1 to calculate steam generator response, and particularly localized heat transfer under loss of secondary inventory conditions, should be made by performing separate effects calculations using the broken loop steam generator model driven with measured boundary conditions. This approach would eliminate the influence of boundary conditions imposed by other parts of the system that are not simulated with acceptable accuracy.

To the extent possible, the code improvements enumerated in Section 9 should be implemented to increase user efficiency in performing simulations with TRAC-PF1/MOD1 and performing analyses using the results produced by the code.

12. REFERENCES

1. *TRAC-PF1/MOD1: An Advanced Best-Estimate Computer Program for Pressurized Water Reactor Thermal-Hydraulic Analysis*, NUREG/CR-3858 (LA-10157-MS), July 1986.

2. *CESSAR-80 Final Safety Analysis Report, Appendix 15*, Combustion Engineering Company.

3. T. J. Boucher and J. R. Wolf, *Preliminary Experiment Operating Specification for Semiscale Mod-2C Feedwater and Steam Line Break Experiment Series*, EGG-SEMI-6551, March 1984.

4. T. J. Boucher and W. A. Owca, *Appendix S-FS-6 and 7 of the Experimental Operating Specification for the Semiscale Mod-2C Feedwater and Steam Line Break Experiment Series*, EGG-SEMI-6871, May 1985.

5. T. J. Boucher and W. A. Owca, *Appendix S-FS-11 of the Experiment Operating Specification for the Semiscale Mod-2C Feedwater and Steam Line Break Experiment Series*, EGG-SEMI-6909, June 1985.

6. D. Dobranich, *TRAC-PF1/MOD1 Independent Assessment: Semiscale MOD-2A Feedwater-Line Break (S-SF-3) and Steam-Line Break (S-SF-5) Tests*, NUREG/CR-4189 (SAND85-0576), November 1985.

7. T. J. Boucher and D. G. Hall, *Quick Look Report for Semiscale Mod-2C Test S-FS-6*, EGG-SEMI-7022, September 1985.

8. D. G. Hall, *Quick Look Report for Semiscale Mod-2C Test S-FS-7*, EGG-RTH-7072, October 1985.

9. M. P. Plessinger, *Quick Look Report of Semiscale Mod-2C Test S-FS-11*, EGG-RTH-7103, November 1985.

APPENDIX A

LISTING OF TRAC-PF1/MOD1 INPUT TO MODEL THE SEMISCALE MOD-2C SYSTEM

(Appendix A is on microfiche attached to the inside back cover.)